TECHNICAL REPORT STANDARD TITLE PAGE

1. Report No.	2. Government Accession No.	3. Recipient's Catalog No.
FHWA/TX-86/69+382-2F		

4. Title and Subtitle	5. Report Date
RESPONSE OF HIGHWAY BARRIERS TO REPEATED IMPACT LOADING: CONCRETE BARRIERS	November 1985
	6. Performing Organization Code
7. Author(s)	8. Performing Organization Report No.
M. A. Steves, R. E. Klingner, and K. S. Armstrong	Research Report 382-2F
9. Performing Organization Name and Address	10. Work Unit No.
Center for Transportation Research The University of Texas at Austin Austin, Texas 78712-1075	11. Contract or Grant No. Research Study 3-5-84-382
	13. Type of Report and Period Covered
12. Sponsoring Agency Name and Address Texas State Department of Highways and Public Transportation; Transportation Planning Division P. O. Box 5051 Austin, Texas 78763	Final
	14. Sponsoring Agency Code

15. Supplementary Notes

Study conducted in cooperation with the U. S. Department of Transportation, Federal Highway Administration.

Research Study Title: "Resistance of Anchor Bolts to Repeated Impact Loading"

16. Abstract

The purpose of this study was to investigate the behavior of proposed anchorage designs for two Texas SDHPT T5 concrete traffic barriers, subjected to static and dynamic loads. It was believed that the current design, which specifies the use of 1-in.-diameter A193, Grade B7 anchor bolts, spaced at 50 in., lacked sufficient ductility. Therefore, an anchorage system consisting of 1-in.-diameter, A36 bolts, spaced at 25 in., was proposed. Larger spacings of the proposed anchor bolts were also investigated. Two barriers were constructed and tested: a cast-in-place barrier, capable of accommodating a variety of anchor bolt patterns. A 10-in. test slab, representing a typical Texas SDHPT slab overhang, was also constructed and used in all tests. Four tests were conducted: three static tests, and one series of impact tests to increasing maximum loads. Brittle behavior was observed in the three static tests. Loading was discontinued during these tests, due to the development of a localized flexural-torsional failure mechanism in the slab, located near the point of load application. Excessive slab cracking, which initiated the development of this mechanism, was sustained by the slab during the first static test. Somewhat greater ductility was observed in the dynamic test (MPACT1). Failure was achieved through fracture of the anchor bolts. However, anchor bolt failure was accompanied by a brittle shearing failure of the corner of the slab.

In general, the tests indicated that the current and proposed concrete barrier anchorage designs have insufficient ductility. A possible solution is the use of smaller and/or lower strength anchor bolts requiring a smaller spacing of the bolts.

17. Key Words	18. Distribution Statement
concrete highway barriers, anchor bolts, impact loading, repeated, static, dynamic, ductility, spacing	No restrictions. This document is available to the public through the National Technical Information Service, Springfield, Virginia 22161.

19. Security Classif. (of this report)	20. Security Classif. (of this page)	21. No. of Pages	22. Price
Unclassified	Unclassified	120	

Form DOT F 1700.7 (8-69)

RESPONSE OF HIGHWAY BARRIERS TO REPEATED IMPACT LOADING: CONCRETE BARRIERS

by

M. A. Steves
R. E. Klingner
K. S. Armstrong

Research Report Number 382-2F

Resistance of Anchor Bolts to Repeated Impact Loading

Research Project 3-5-84-382

conducted for

Texas
State Department of Highways and Public Transportation

in cooperation with the
U. S. Department of Transportation
Federal Highway Administration

by the

CENTER FOR TRANSPORTATION RESEARCH
BUREAU OF ENGINEERING RESEARCH
THE UNIVERSITY OF TEXAS AT AUSTIN

November 1985

The contents of this report reflect the views of the authors, who are responsible for the facts and the accuracy of the data presented herein. The contents do not necessarily reflect the official views or policies of the Federal Highway Administration. This report does not constitute a standard, specification, or regulation.

There was no invention or discovery conceived or first actually reduced to practice in the course of or under this contract, including any art, method, process, machine, manufacture, design or composition of matter, or any new and useful improvement thereof, or any variety of plant which is or may be patentable under the patent laws of the United States of America or any foreign country.

P R E F A C E

Parapet-style concrete traffic barriers are a common feature along most major elevated roadways. The most prominent of these is the so-called "New Jersey" or "safety shape" barrier, which is the focus of this study. Of particular interest is the anchorage system which connects the barrier to the roadway. The safety shape barrier is generally connected to the roadway with either steel reinforcing bars or steel anchor bolts. This report is limited to the consideration of bolted connections.

The main objective of this research project is to design, construct, and test a more ductile anchorage system for the Type T5 (safety shape) traffic barrier now being used by the Texas State Department of Highways and Public Transportation. A standard Texas SDHPT slab reinforcement scheme and 1.5 in. barrier edge distance were used in an effort to reproduce field conditions. However, the test barriers were overreinforced in order to force a failure into the anchorage zone.

This study is part of a research project sponsored by the Texas State Department of Highways and Public Transportation, and administered by the Center for Transportation Research at The University of Texas at Austin.

S U M M A R Y

The purpose of this study was to investigate the behavior of proposed anchorage designs for two Texas SDHPT T5 concrete traffic barriers, subjected to static and dynamic loads. It was believed that the current design, which specifies the use of 1-in. diameter A193, Grade B7 anchor bolts, spaced at 50 in., lacked sufficient ductility. Therefore, an anchorage system consisting of 1-in. diameter, A36 bolts, spaced at 25 in., was proposed. Larger spacings of the proposed anchor bolts were also investigated.

Two barriers were constructed and tested: a cast-in-place barrier, with six 1-in. diameter A36 anchor bolts, spaced at 25 in.; and a precast barrier, capable of accommodating a variety of anchor bolt patterns. A 10-in. test slab, representing a typical Texas SDHPT slab overhang, was also constructed and used in all tests.

Four tests were conducted: three static tests, and one series of impact tests to increasing maximum loads. Brittle behavior was observed in the three static tests. Loading was discontinued during these tests, due to the development of a localized flexural-torsional failure mechanism in the slab, located near the point of load application. Excessive slab cracking, which initiated the development of this mechanism, was sustained by the slab during the first static test. Somewhat greater ductility was observed in the dynamic test (MPACT1). Failure was achieved through fracture of the anchor bolts. However, anchor bolt failure was accompanied by a brittle shearing failure of the corner of the slab.

In general, the tests indicated that the current and proposed concrete barrier anchorage designs have insufficient ductility. A possible solution is the use of smaller and/or lower strength anchor bolts. A smaller spacing of the bolts would then be required to avoid a loss of barrier system load capacity.

I M P L E M E N T A T I O N

Further research to develop a more ductile anchorage system for the safety shape concrete traffic barrier is recommended. Because the current Texas SDHPT slab reinforcement scheme does not adequately resist the development of flexural-torsional and shearing failure mechanisms in the slab, anchor bolt strengths must be lowered. Therefore, any subsequent investigations should include the use of smaller and/or lower strength anchor bolts. A variety of anchor bolt spacings should also be investigated, in order to determine the effect of bolt spacing on overall barrier system capacity (assuming that a ductile failure mode can be obtained). It is believed that a decreased spacing of lower strength anchor bolts could prevent a loss of barrier capacity, while also providing the desired level of ductility.

TABLE OF CONTENTS

Chapter Page

C H A P T E R 1

INTRODUCTION

1.1 General

Parapet-style concrete traffic barriers are a common feature along most major elevated roadways. The most prominent of these is the so-called "New Jersey" or "safety shape" barrier, which is the focus of this study. Of particular interest is the anchorage system which connects the barrier to the roadway. The safety shape barrier is generally connected to the roadway with either steel reinforcing bars or steel anchor bolts. This report is limited to the consideration of bolted connections.

As is the case with other types of roadway appurtenances, anchor bolts play a major role in determining the strength and behavior of traffic barrier systems. These characteristics are greatly affected by the strength, size, shape and spacing of the bolts. The behavior of the system is also influenced to a smaller degree by the rate of load application to the barrier.

Although thousands of miles of safety shape barriers currently exist, AASHTO Specifications governing their design are minimal. Conclusive test results are also limited in both scope and number. Some static tests [1] have been performed on barriers with reinforcing bar connections. However, more research is needed to observe the performance of safety shape barriers with varying bolted anchorage details, subjected to both static and dynamic loads.

1.2 Objectives and Scope

The main objective of this research project is to design, construct, and test a more ductile anchorage system for the Type T5 (safety shape) traffic barrier now being used by the Texas State Department of Highways and Public Transportation. A standard Texas SDHPT slab reinforcement scheme and 1.5 in. barrier edge distance were used in an effort to reproduce field conditions. However, the test barriers were overreinforced in order to force a failure into the anchorage zone.

Tests were conducted on two Texas SDHPT T5 barriers: first, a cast-in-place barrier; and second, a precast barrier. A static test

was performed on the cast-in-place barrier using a proposed anchorage design. The precast barrier was subjected to both static and dynamic loads. A proposed anchorage design was also used in the precast barrier tests.

CHAPTER 2

BACKGROUND

2.1 Analytical Background

The analysis and design of a safety shape barrier involves the study of various potential failure modes. The behavioral characteristics of the governing failure mode determine the ultimate performance of the barrier system. It is therefore desirable to have some control in determining the governing failure mode. The primary barrier failure mechanisms are illustrated in Fig. 2.1 and include: (1) tensile fracture of the anchor bolt; (2) tensile failure of the slab; (3) shearing failure of the slab; (4) flexural failure of the slab; and (5) flexural/shear failure of the barrier. Each of these mechanisms is subsequently discussed in detail. But first, a description of the load response behavior of the barrier system is in order.

With the application of a lateral load, the barrier anchorage is subjected to an applied shear and moment (Fig. 2.2). The shear is equal to the applied load, P, and the moment is equal to P x H, where H is the height above the slab at which the load is applied. The applied moment produces tension in the anchor bolts, and compression over an area near the back edge of the barrier. For analytical purposes, the compression zone is assumed to take the form of a Whitney rectangular stress block. The resulting tensile force, T, and effective compressive force (C = T) form an internal resisting couple which is equal to T x A, where A is the distance between the bolts and the center of the compressive stress block. To satisfy rotational equilibrium, the internal resisting couple must be equal to the applied external moment, or P x H = T x A. This equation is fundamental in the analysis and design of the barrier anchorage system.

When the above equation is expressed in the form

$$P=TA/H, \qquad (2.1)$$

it can be seen that the capacity of the barrier, P, for a given loading position is dependent upon the values of T and, to a lesser extent, A. The term T represents the force component of the internal couple and is limited to the smallest of the following values: the tensile capacity of the anchor bolts; the tensile capacity of the concrete; and the shearing capacity of the concrete. These values correspond to the first three failure modes shown in Fig. 2.1. The

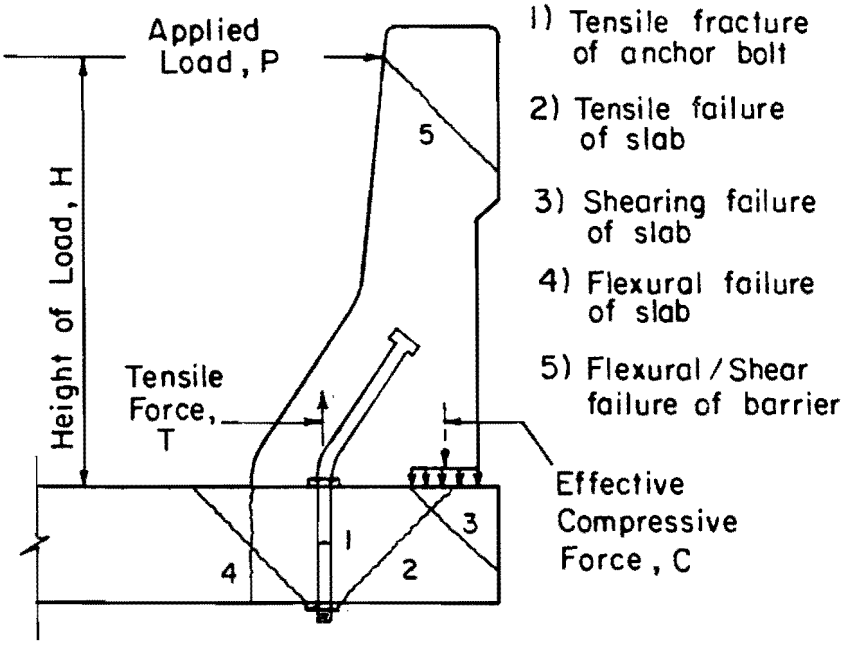

Fig. 2.1 Basic failure mechanisms of Texas SDHPT cast-in-place T5 (safety shape) barrier subjected to lateral load

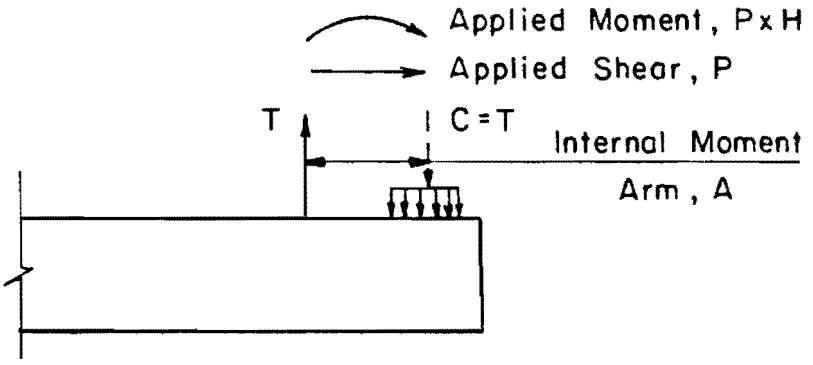

Fig. 2.2 Forces acting on barrier anchorage zone

designer can control these values and thus determine the ultimate strength and behavior of the barrier system.

The means of controlling the value of the internal force component, T, are generally simple and applicable. The tensile capacity of the anchor bolts can be altered by changing the strength, size, or spacing of the bolts. The tensile and shearing capacity of the concrete can be affected by varying the thickness of the slab or the strength of the concrete. However, since barrier anchorages are not the primary consideration in the design of bridge decks, it may not be feasible to alter the strength or thickness of the slab. A more effective method of increasing the shearing capacity of the slab is to increase the edge distance of the barrier. These methods are discussed in greater detail in the following section.

The capacity of the barrier can also be influenced by an increase in the length of the internal moment arm, A. If an average stress of $0.85f'_c$ acting on the compressive stress block is assumed (based on Eq. 10.2.7.1 of Ref. 2), the equation of vertical equilibrium for the anchorage zone can be expressed as follows:

$$T = 0.85f'_c\, b\beta_1 c \qquad (2.2)$$

where b = width of stress block

$\beta_1 c$ = depth of stress block

If the distance between the anchor bolt and the far edge of the stress block is denoted by Z, the length of the internal moment arm may be expressed as follows:

$$A = Z - \beta_1 c/2 \qquad (2.3)$$

From the two above equations, it can be seen that the depth of the stress block, $\beta_1 c$, decreases as the compressive strength of the concrete, f'_c, increases. This results in a longer internal lever arm and, consequently, greater barrier capacity. However, the methods used to alter the value of T are more effective in controlling the capacity of the barrier system.

In addition to the applied moment, the barrier anchorage must also resist the applied shear, P (Fig. 2.2). The anchor bolts will undoubtedly resist a portion of the shear force. However, it is assumed for design purposes that all of the applied shear is resisted by frictional forces acting in the compression zone of the anchorage, parallel and opposite to the direction of the applied shear. Because of this assumption, shear is not considered in the design of the anchor bolts themselves.

2.1.1 Failure Modes

Tensile Fracture of Anchor Bolts

Tensile fracture of the anchor bolts occurs when the stress in the bolts reaches the ultimate tensile stress of the bolt material. In this case, the value of T at failure is equal to $A_b f_{ult}$, where A_b represents the total cross-sectional area of the anchor bolts and f_{ult} is equal to the ultimate tensile strength of the bolt material. Since the bolted connections under consideration are unbonded, A_b represents an effective bolt area which is reduced to account for the threads.

By setting $T = A_b f_{ult}$ and combining Eqs. 2.1, 2.2, and 2.3, the following expression for barrier capacity based on tensile fracture of the anchor bolts can be derived:

$$P = \frac{A_b f_{ult}}{H}\left[Z - \frac{A_b f_{ult}}{1.7 f'_c b}\right] \qquad (2.4)$$

The most effective and practical method of controlling the value of P in the above equation is to choose the value of A_b and//or f_{ult}. This is done by selecting the appropriate size, spacing, and strength of the anchor bolt.

Tensile Failure of the Slab

Several studies and reports [3,4,5,6] dealing with steel anchorages embedded in concrete have been produced in recent years. It has been found that a steel anchor bolt embedded in or through concrete and subjected to tension will cause a tensile cone pullout failure of the concrete (Fig. 2.3), assuming no tensile fracture of the bolt. The pullout cone (or trapezoidal prism, in the case of a rectangular anchor head) is formed by failure surfaces which project from the bearing edges of the anchor head toward the surface at roughly a 45 degree angle. The tensile stress can be considered as acting on an effective stress area defined by the projected area of the cone. Since failure begins at the edges of the anchor head, the area of the anchor head does not affect the pullout load, and is subtracted from the total projected area. The effective stress area is also reduced in the case of overlapping cones or an intersection of a cone and a free surface. However, neither of these two cases occurs in the barrier anchorages under consideration.

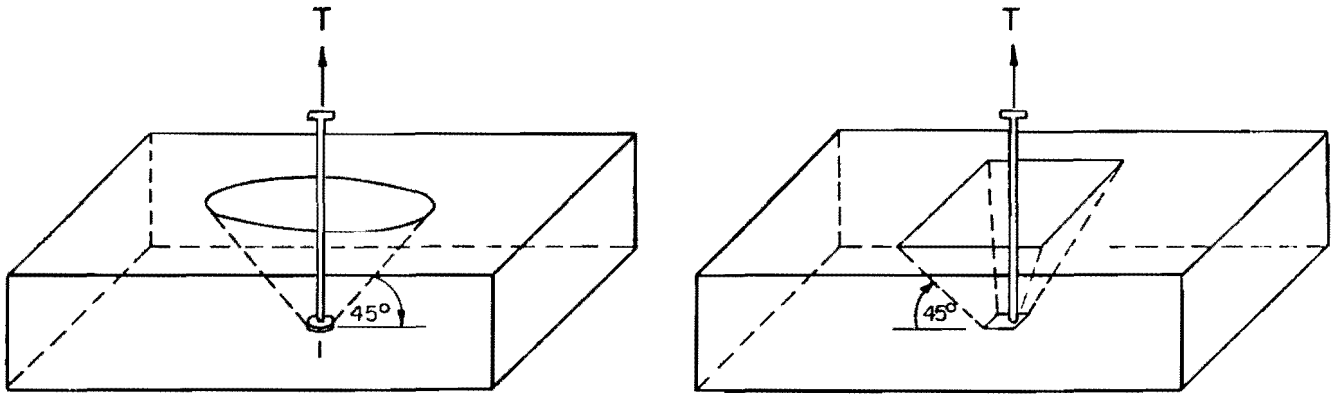

a. Circular Anchor Head

b. Rectangular Anchor Head

Fig. 2.3 Tensile cone pullout failure of slab

The tensile stress acting on the projected area varies from a maximum value at the bearing edges of the anchor head to a value of zero at the surface of the cocrete. The resulting average tensile resistance of the concrete has been found to equal approximately $4\sqrt{f'_c}$. Therefore, in the event of a pullout failure, the value of T at failure is equal to $4\sqrt{f'_c}A_c$, where A_c represents the total effective concrete stress area for all bolt locations. By setting $T = 4\sqrt{f'_c}A_c$ and combining Eqs. 2.1, 2.2, and 2.3, the following expression for barrier capacity based on tensile cone pullout failure of the slab can be derived:

$$P = \frac{4\sqrt{f'_c}\,A_c}{H}\left[Z - \frac{2.35\sqrt{f'_c}\,A_c}{f'_c b}\right] \qquad (2.5)$$

Barrier capacity is most easily affected in this case by controlling the value of A_c. The total effective tensile stress area can be increased by increasing the embedment length of the bolts and/or the area of the anchor heads. Because the bolts used in the safety shape barrier are anchored completely through the slab, the only means of increasing embedment length is to increase the slab thickness. It is, therefore, more practical to alter pullout capacity by changing the anchor head area.

Shearing Failure of the Slab

Excessive compressive forces acting in the rectangular stress block of the barrier anchorage can result in a local shearing failure of the slab. This type of failure is characterized by a shearing crack which propagates from the inside edge of the compressive stress block toward the free edge of the slab at approximately a 45 degree angle (Fig. 2.4). The vertical compressive force acting on the failure mechanism is resisted by a shear-friction force μN which acts on the failure surface, and a normal force N which acts perpendicular to the failure surface (Fig. 2.5). In order to satisfy horizontal equilibrium, these two forces must be equal and, thus, the coefficient of friction, μ, must equal unity.

In solving the equation of vertical equilibrium, it is found that the shear friction force is equal to C/2 sin 45°. Since the effective compressive force, C, is equal to the tensile component of the internal couple, T, the value of μN may also be expressed as T/1.414. The value of T in this case is equal to that which corresponds with the governing failure mode. Once the controlling failure mode is determined and the values of T and β_{1c} at failure are known, the maximum value of the shear-friction stress acting on the potential failure surface can be computed. Based on the assumed 45

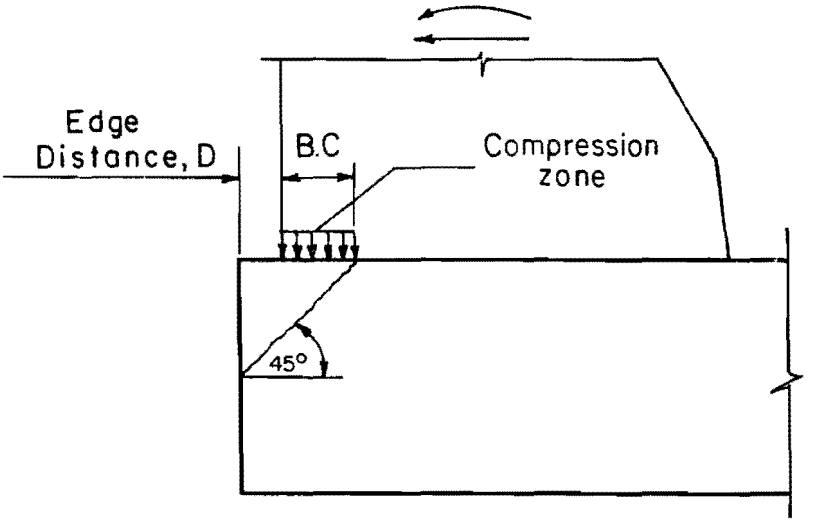

Fig. 2.4 Shearing failure of slab

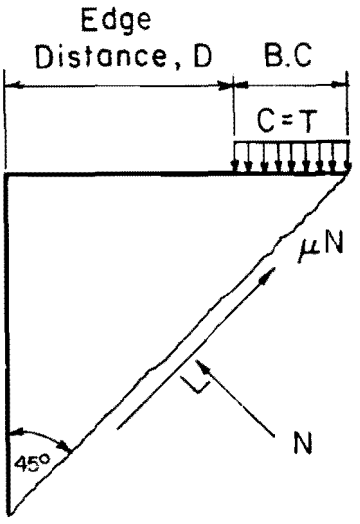

Fig. 2.5 Forces acting on shearing failure mechanism

degree failure angle, the area of the shearing surface is found to equal $b\sqrt{2}(D + \beta_1 c)$, where D represents the barrier edge distance. If the shearing surface area is denoted by A_v, the maximum value of the shear-friction stress can be expressed in the following form:

$$\frac{\mu N}{A_v} = \frac{T}{2b(D+\beta_1 c)} \qquad (2.6)$$

According to Section 11.7.5 of Ref. 2, the design shear resistance offered by the concrete should not be taken greater than $0.2f'_c$ nor 800 psi. During analysis and design of a barrier anchorage system, these values should be checked against the value computed in Eq. 2.6 to ensure that they are not exceeded. It should be noted that the most efficient method of increasing slab shearing capacity is to increase the barrier edge distance. However, edge distance is usually minimized for spatial and economic considerations.

Flexural Failure of the Slab

Flexural failure of the slab occurs when the transverse tensile reinforcement in the slab yields. Although most bridge decks, inccluding the one considered in this study, contain both top and bottom transverse reinforcement, the compressive (bottom) reinforcement has little effect on ultimate flexural strength and is neglected during analysis. Therefore, the slab is treated as a singly reinforced concrete beam (Fig. 2.6).

According to the Commentary to Section 10.3.1(A) of Ref. 2, the flexural strength of a singly reinforced concrete section is expressed as follows:

$$M_n = A_s f_y (d - \beta_1 c/2)$$

where A_s = total area of tensile steel

f_y = yield stress of reinforcement

d = distance from extreme compression fibber to centroid of tension reinforcement

and

$$\beta_1 c = A_s f_y / 0.85 f'_c b$$

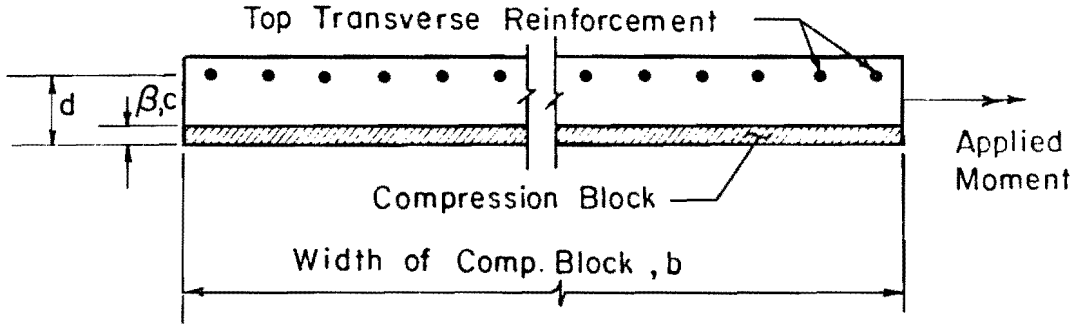

Fig. 2.6 Transverse section of roadway slab

Flexural failure of the slab occurs when the moment applied to the barrier anchorage reaches the flexural capacity of the slab, or $P \times H = M_n$. By a combination of this expression with the above equation, the following expression for barrier capacity based on flexural failure of the slab can be derived:

$$P = \frac{A_s f_y}{H}\left[d - \frac{A_s f_y}{1.7 f'_c b}\right] \qquad (2.7)$$

It is evident that the flexural strength of the roadway slab is highly dependent upon the strength, placement and total area of the transverse tensile reinforcement, as well as the effective slab depth, d. As mentioned previously, however, it may not be practical to alter the slab design in order to improve barrier system behavior.

Flexural/Shear Failure of the Barrier

Because of the variable thickness of the barrier and the wide range of possible loading conditions, it is difficult to assess the desirable and available levels of flexural and shear resistance inherent in the safety shape barrier. However, as mentioned previously, the primary objective of this project is to study the behavior of the barrier anchorage. To accomplish this, tests were conducted using barriers which were heavily reinforced in order to prevent barrier failures. Since the barriers possessed much greater strength and stiffness than the test slab to which they were anchored, the possibility of a barrier failure was virtually eliminated. A flexural and shear analysis of the barriers themselves was therefore of little consequence.

2.1.2 Ductile vs. Brittle Failure. In addition to resisting high impact loads, traffic barriers must also possess energy absorption capabilities. When a vehicle strikes a barrier, a great amount of kinetic energy is imparted to the barrier over a very short time span. In order to absorb this energy and prevent a sudden, brittle failure, the barrier system must possess a high degree of ductility. Of greatest importance is the ductility of the barrier anchorage, where failure is most likely to occur.

In the Addition to Commentary on Code Requirements for Nuclear Safety Related Structures [3], ACI Committee 349 proposes design requirements which are "intended to result in an embedment design which will exhibit ductile behavior in the case of unexpected overload." To achieve ductility, the committee requires yielding of the steel anchorage prior to brittle failure. More specifically, the calculated pullout strength of the concrete should exceed the minimum

specified tensile strength of the steel. By selecting the appropriate size, strength and spacing of the anchor bolts, the designer can produce an anchorage system which can resist high impact loading and which possesses the ductility required to ensure safety and minimal slab damage.

2.1.3 Static vs. Dynamic Response. As is discussed in detail in later sections of this report, the barrier test specimens were subjected to static and impact loads. In assessing the response of the barrier to impact loads of a duration close to the fundamental period of vibration of the slab-barrier system, it is usually necessary to include the effects of inertial forces. In this case, however, the periods of vibrtion of the slab-barrier system were much shorter than the duration of the impact load, and the response of the barrier was therefore treated as static.

CHAPTER 3

TEST PROGRAM

3.1 Test Specimen

The specimen used in this series of tests consists of two Texas SDHPT T5 traffic barriers and a test slab. Each is discussed in detail in the following sections.

3.1.1 Cast-in-Place vs. Precast Barriers. Cast-in-place and precast T5 barriers are geometrically identical, and have similar reinforcement details. The major differences between the two types of barriers are the method of fabrication and the shape of the anchor bolts. The cast-in-place barrier (Fig. 3.1) is anchored to the deck with bent anchor bolts, inserted through predrilled holes in the deck and held in place by jam nuts at the slab surface. The reinforcing cage is then lowered into place over the bolts, the steel forms are positioned around the cage, and the concrete barrier is cast directly on the deck surface.

The precast barrier is attached to the roadway with straight anchor bolts. Anchor bolt packets and holes are formed in the barrier during casting (Fig. 3.2). Upon arrival at the site, the barrier is anchored to the bridge slab by inserting the straight bolts through the formed holes and predrilled holes in the slab. The precast barrier must be placed on a grout pad to ensure a good contact surface between the barrier and the slab.

3.1.2 Geometry. The dimensions of the cast-in-place and precast Texas SDHPT T5 barriers used in testing are shown in Figs. 3.1 and 3.2, respectively. The two barriers are dimensionally identical. The minimum specified length of a precast barrier section is 12 ft, 6 in. Because of this specification, and partly because of formwork availability, both barriers and the test slab were cast in 12 ft., 6 in. sections.

The dimensions of the test slab are shown in Fig. 3.3. An 8-in. slab thickness and a 2 ft, 6 in. slab overhang were selected because they are representative of a typical Texas SDHPT bridge deck. The overhang projects from a more massive base section of concrete which is anchored to the test floor with 12 A193 B7 steel rods, 1 in. in diameter. The rods are arranged in groups of four and are post-

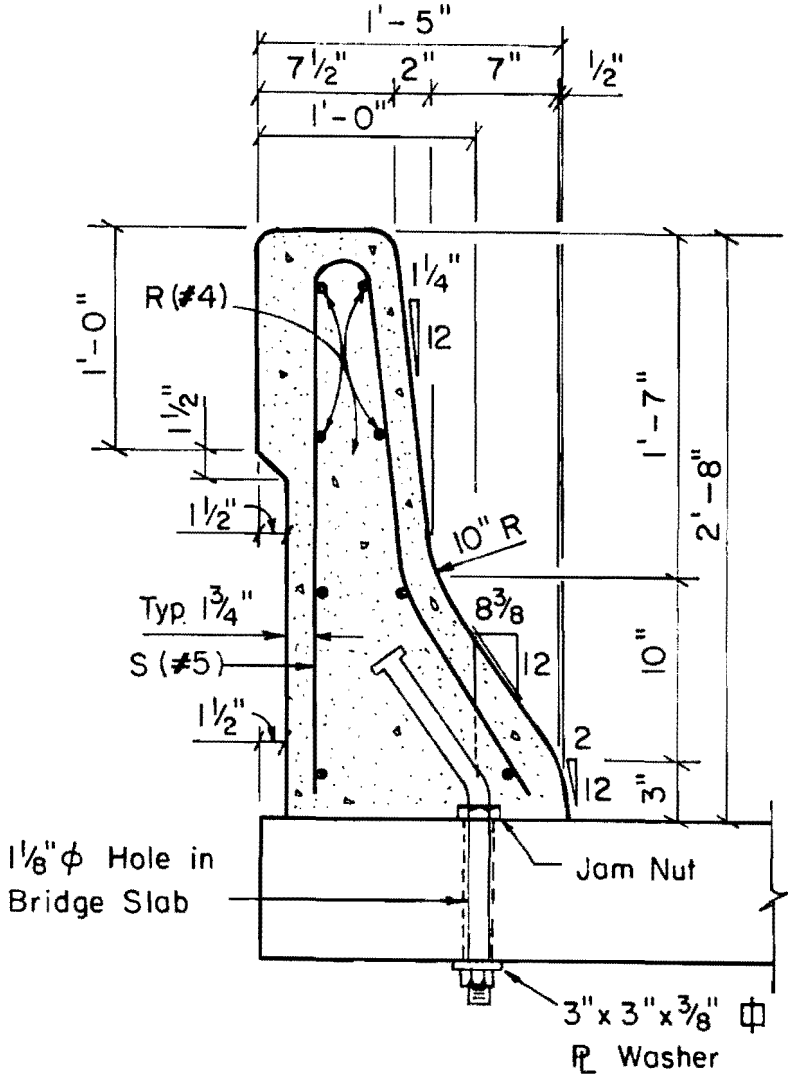

Fig. 3.1 Texas SDHPT cast-in-place T5 traffic barrier

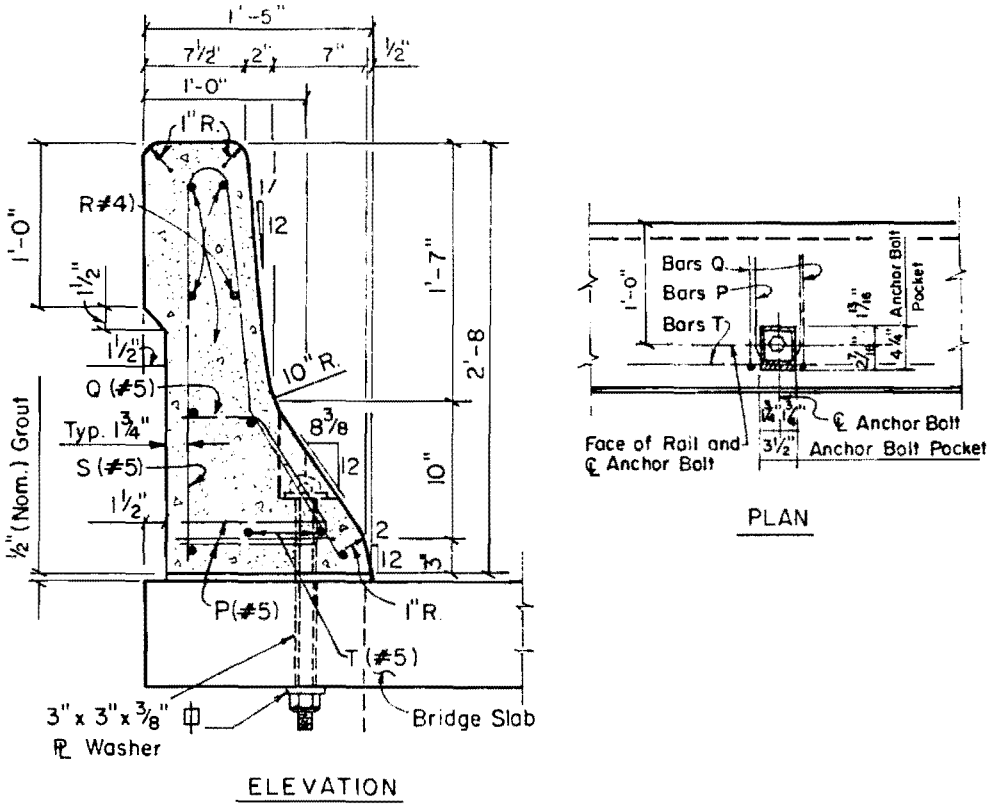

Fig. 3.2 Texas SDHPT precast T5 traffic barrier

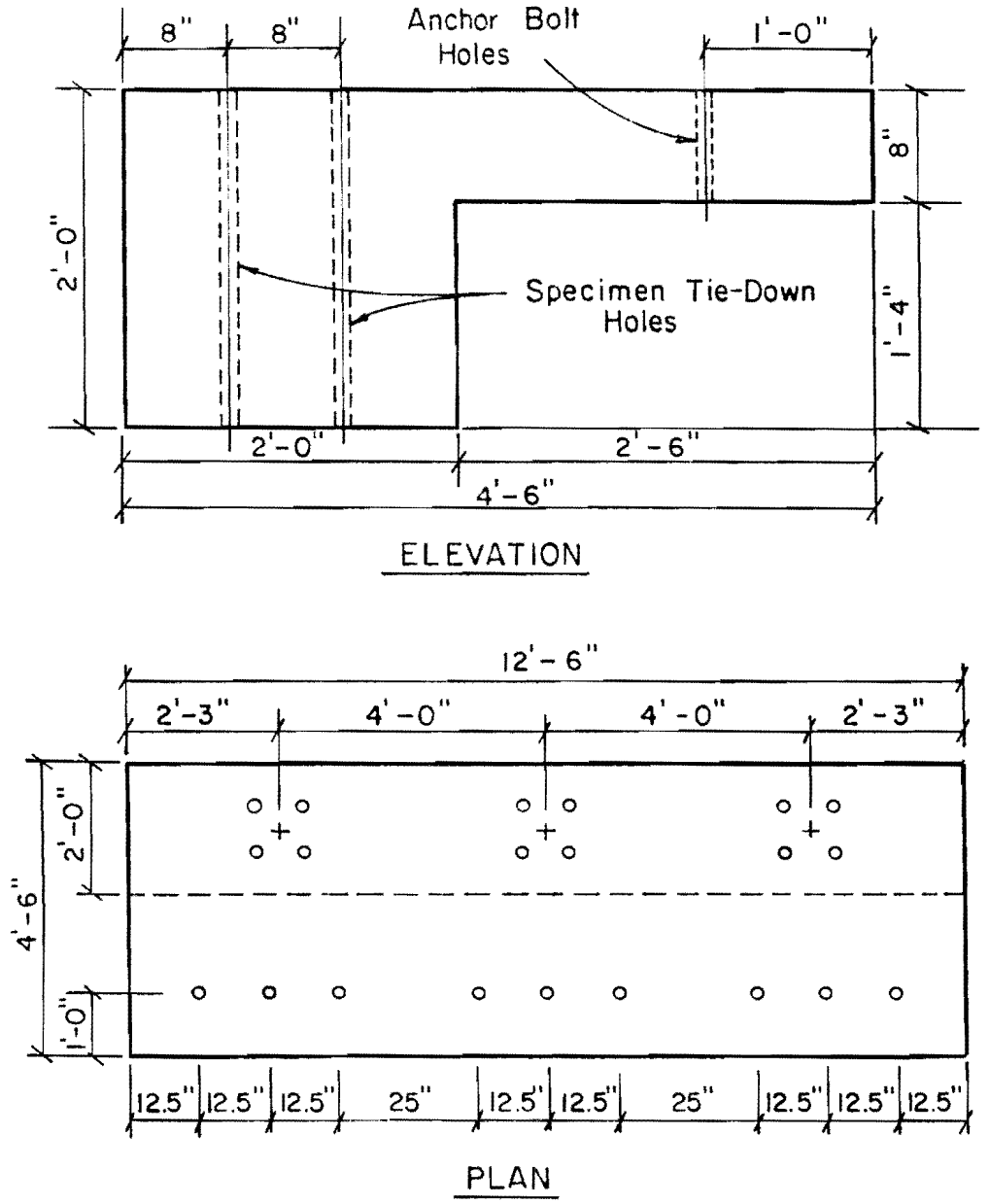

Fig. 3.3 Test slab

tensioned to 25 kips each in order to firmly secure the specimen to the test floor.

3.1.3 Reinforcement. Reinforcing details for the cast-in-place and precast barriers are illustrated in Figs. 3.1 and 3.2, respectively. The dimensions of Bars S, P, and Q used in the barriers are given in Fig. 3.4. All other reinforcing bars shown are straight, and run the entire length of the barrier.

The Texas SDHPT specifies a maximum spacing of 10 in. for the transverse bars (type "S") used in T5 barriers. However, in order to prevent a barrier failure during testing, the spacing of transverse bars was decreased in both test barriers. The modified spacings for the cast-in-place and precast barriers are shown in Figs. 3.5 and 3.6, respectively. A somewhat irregular spacing was required in the precast barrier in order to accommodate anchor bolt pockets and mounting holes for the loading beam. In both barriers, a group of four Bars S was concentrated at each end of the load beam to resist punching shear. In addition, an extra Bar R was placed in each barrier and an extra Bar T was placed in the precast barrier.

A standard Texas SDHPT slab overhang detail is shown in Fig. 3.7. This reinforcement layout was used in the test slab (Fig. 3.8) in order to reproduce field conditions. The Bars A used in the test slab were anchored in the specimen base to simulate the continuity of reinforcement found in an actual bridge deck. The spacing of Bars A was also slightly altered to facilitate the placement of anchor bolt holes (see Fig. 3.2 1). Eight longitudinal #5 bars were placed in the specimen base to provide greater ease of construction and flexural strength required during lifting of the specimen.

3.1.4 Materials. The materials were selected in accordance with standard Texas SDHPT specifications.

Concrete

The barriers and the slab were cast with standard Texas SDHPT Class C concrete mix, which had a design strength of 4000 psi. Compression and split cylinder tests were performed on cylinders made during each casting. Concrete strengths were determined by averaging the results of three cylinders for each type of test. Compressive and tensile concrete strengths are listed in Table 3.1.

Anchor Bolts, Nuts, Washers

Two grades of straight and bent anchor bolts were considered: A193, Grade B7 bolts, specified by the Texas SDHPT; and proposed A36 bolts, proposed in this research. All bolts were 1-in. diameter,

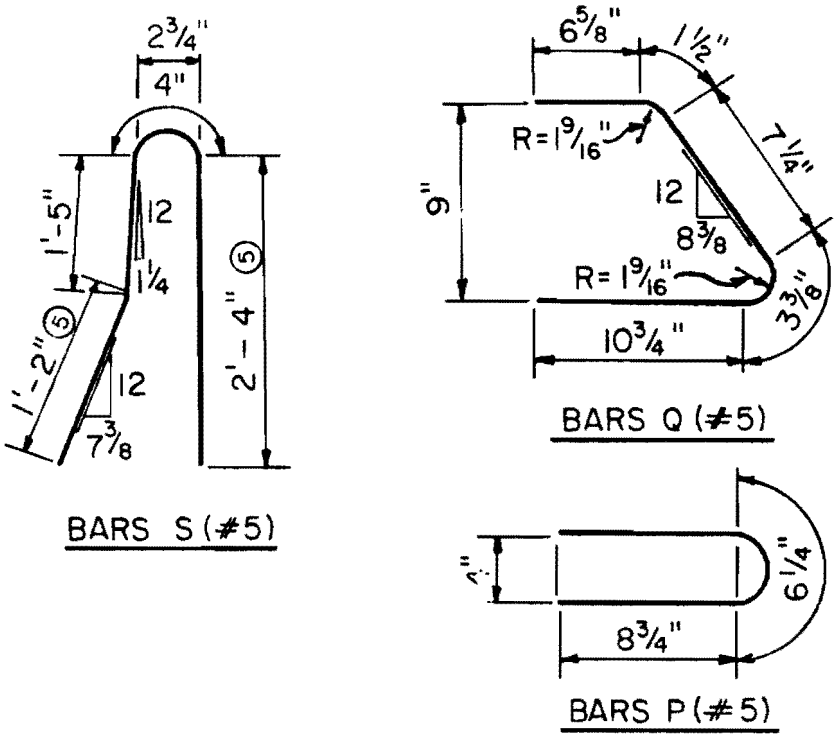

Fig. 3.4 Barrier reinforcing bar dimensions

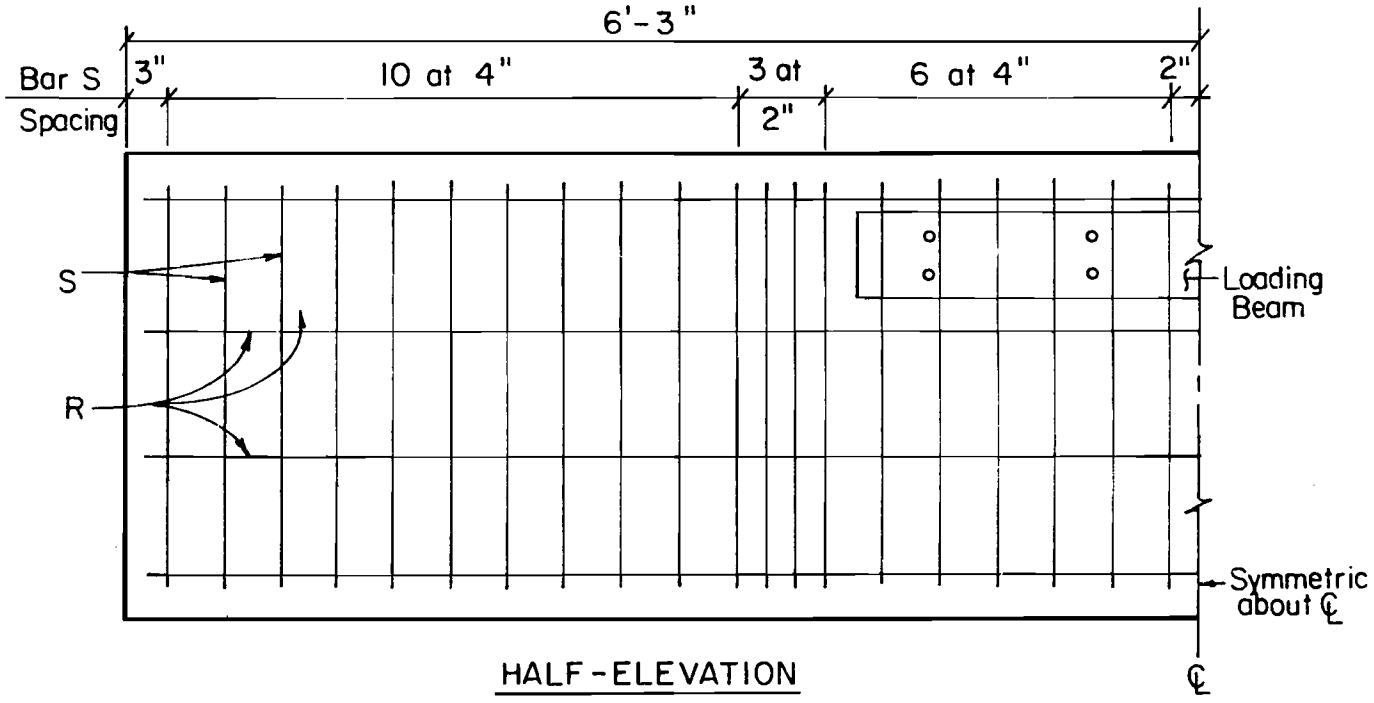

Fig. 3.5 Spacing of transverse reinforcement in cast-in-place barrier

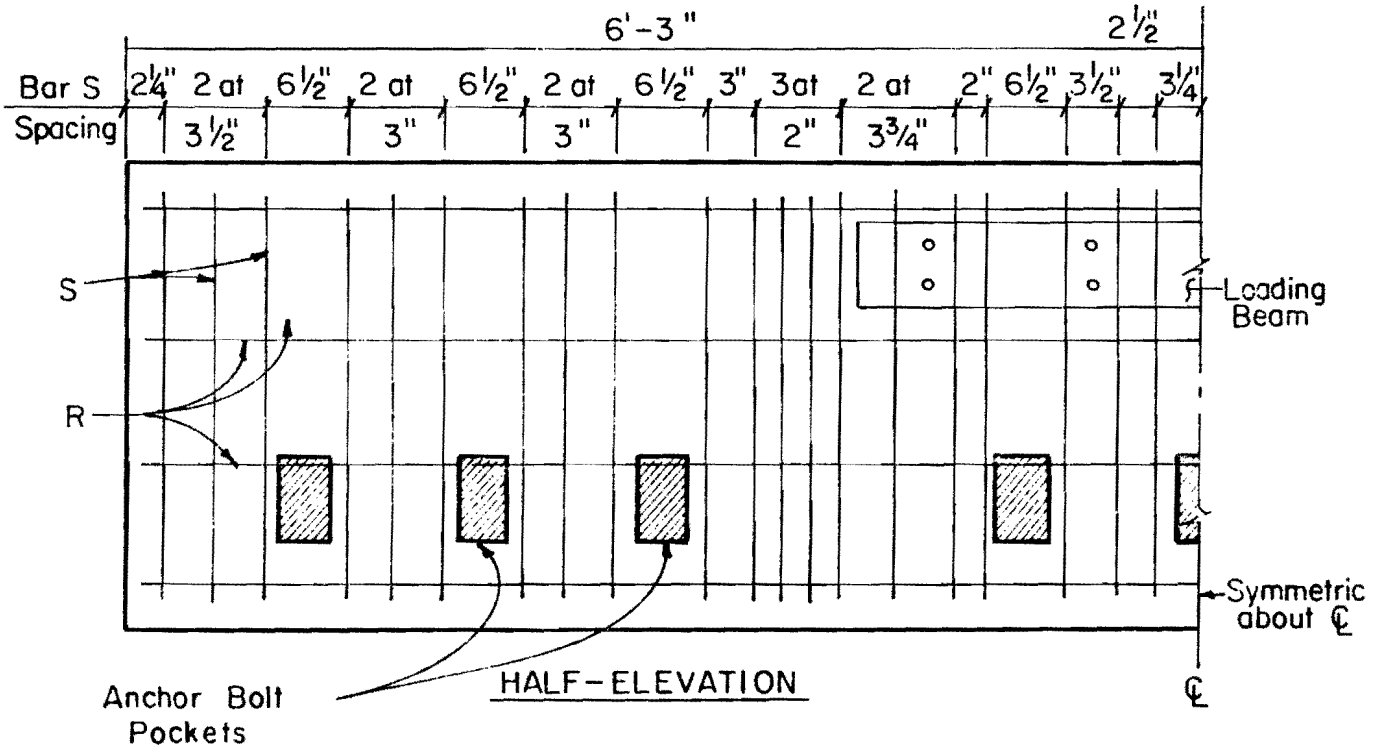

Fig. 3.6 Spacing of transverse reinforcement in precast barrier

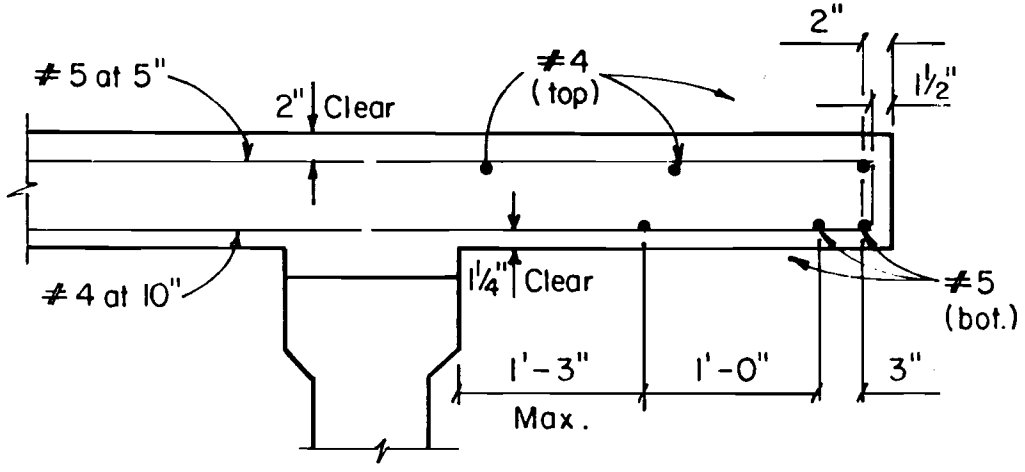

Fig. 3.7 Typical Texas SDHPT slab overhang detail

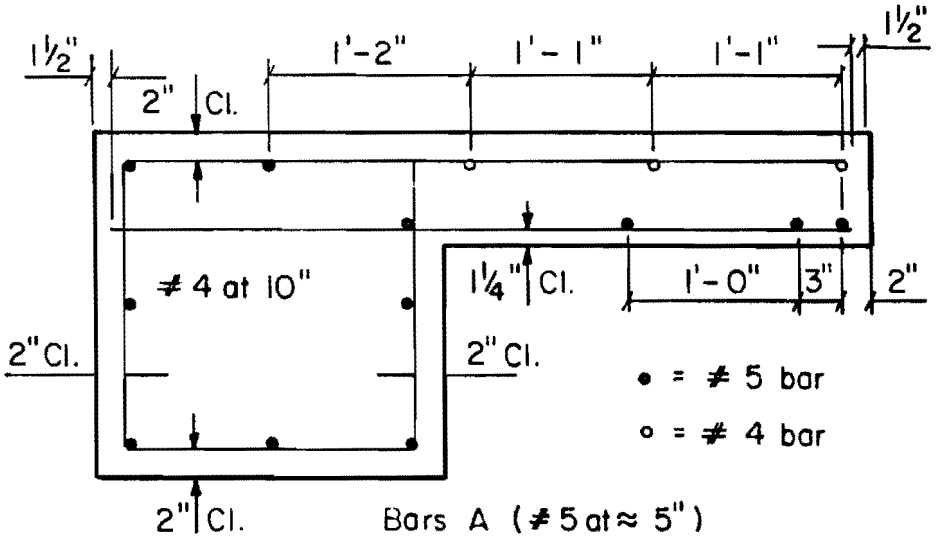

ELEVATION

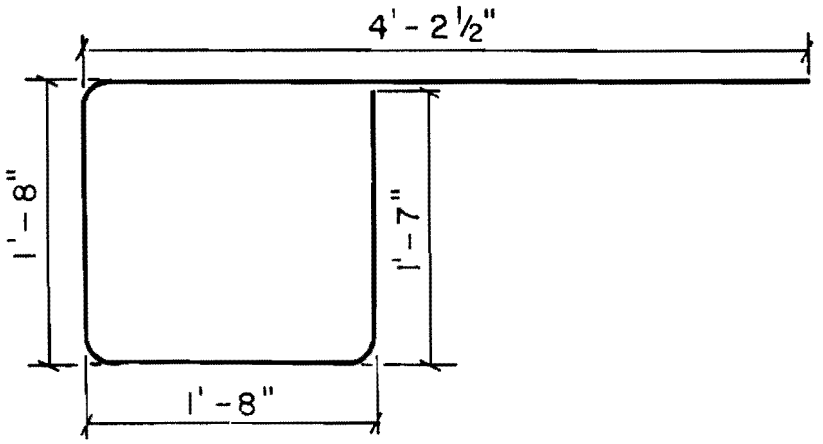

BARS A

Fig. 3.8 Test slab reinforcing details

TABLE 3.1 CONCRETE STRENGTHS

Test	Test Date	Test Slab				Cast-in-Place Barrier				Precast Barrier			
		Age (days)	f_c' (psi)	$*f_t$ (psi)	$**f_t$ (psi)	Age (days)	f_c' (psi)	$*f_t$ (psi)	$**f_t$ (psi)	Age (days)	f_c' (psi)	$*f_t$ (psi)	$**f_t$ (psi)
C STAT 1	10-22-85	133	5650	564	475	84	5100	536	479	—	—	—	—
C STAT 2	10-29-85	140	5780	570	—	—	—	—	—	81	6260	593	510
CSTAT 3	10-29-85	140	5780	570	—	—	—	—	—	81	6260	593	510
MPACT 1	11-6-85	—	—	—	—	—	—	—	—	89	6590	609	—

* Based on $f_t = 7.5\sqrt{f_c'}$

** Based on split cylinder test :

$$f_t = \frac{2P}{\pi ld}$$

matched with 1-in. heavy hex nuts of the same grade. All plate washers were A36 steel. According to Texas SDHPT specifications, all bolts, nuts, and washers were galvanized. Class 2A and 2B fit tolerances were specified for the bolts and nuts, and the nuts were tapped after galvanizing.

Tensile tests were performed on each type of bolt. Bolt strengths are listed in Table 3.2. Each value represents the average of three or more test results. As expected, the 4193-B7 bolts were much stronger than the A36 bolts, and were less ductile (smaller strain at failure). However, even the bent A193-B7 bolts failed in the threads rather than near the bent region, indicating sufficient ductility.

Reinforcing Steel

All reinforcing bars used in the barriers and the test slab were either #4 or #5, Grade 60 bars conforming to ASTM A615. Tensile tests were performed on each type of bar, and tensile strengths were determined by averaging the results of three tests. The tensile strengths for each type of reinforcing bar are shown in Table 3.3.

3.1.5 Fabrication. Although cast-in-place barriers are normally cast directly on the bridge slab, the cast-in-place barrier used in this study was precast in order to simplify construction and project scheduling. Standard metal T5 barrier forms, available in 10-ft sections, were obtained and a wooden base was constructed. Holes were drilled in the base at the desired bolt locations. Since two sections of metal forms were required to form the 12 ft, 6 in. barriers, the forms and the wooden base were each 20 ft long. Wooden end pieces were constructed and placed to obtain the desired barrier length. After the base and end pieces were coated with lacquer, the front face barrier form was lowered into place and bolted to the base using predrilled holes in the base. The bent anchor bolts were then inserted through the wooden base and secured with jam nuts, as shown in Fig. 3.9. After the forms were caulked and coated with form oil, the reinforcing cage was lowered into position over the anchor bolts (Fig. 3.10). The back face barrier form was then oiled, positioned, and bolted to the base, as shown in Fig. 3.11. The metal forms were bolted together across the top to prevent separation during casting operations. Concrete was cast using a concrete bucket and overhead crane, and was consolidated with mechanical vibrators. The top surface was then trowelled smooth and covered with polyethylene sheets to aid curing.

The precast barrier was fabricated in a similar manner. The bolt holes in the base were patched and the forms were cleaned, relacquered and reoiled. The reinforcing cage was then positioned on

TABLE 3.2 BOLT STRENGTHS

Bolt	P_y (kips)	σ_y (ksi)	ϵ_y	P_{ult} (kips)	σ_{ult} (ksi)	ϵ_{ult}	Comments
A193,B7 Straight	—	—	—	93.3	154	4.27×10^{-2}	bolt fractured in threads
A36 Straight	28.3	46.7	5.88×10^{-3}	44.5	73.5	9.8×10^{-2}	" " " "
A193,B7 Bent	—	—	—	76.6	126	—	bolt straightened completely and fractured in threads
A36 Bent	26.4	43.6	—	42.5	70.1	—	" " " " " "

TABLE 3.3 REINFORCING BAR STRENGTHS

Rebar Type	σ_y (ksi)	ϵ_y	σ_{ult} (ksi)	ϵ_{ult}
Test Slab, # 4	56.4	2.7×10^{-3}	92.4	1.36×10^{-1}
Test Slab, # 5	53	2.1×10^{-3}	83.6	1.43×10^{-1}
Barriers, # 4	57.3	2.23×10^{-3}	93.5	1.05×10^{-1}
Barriers, # 5	64.8	2.48×10^{-3}	96.6	1.09×10^{-1}

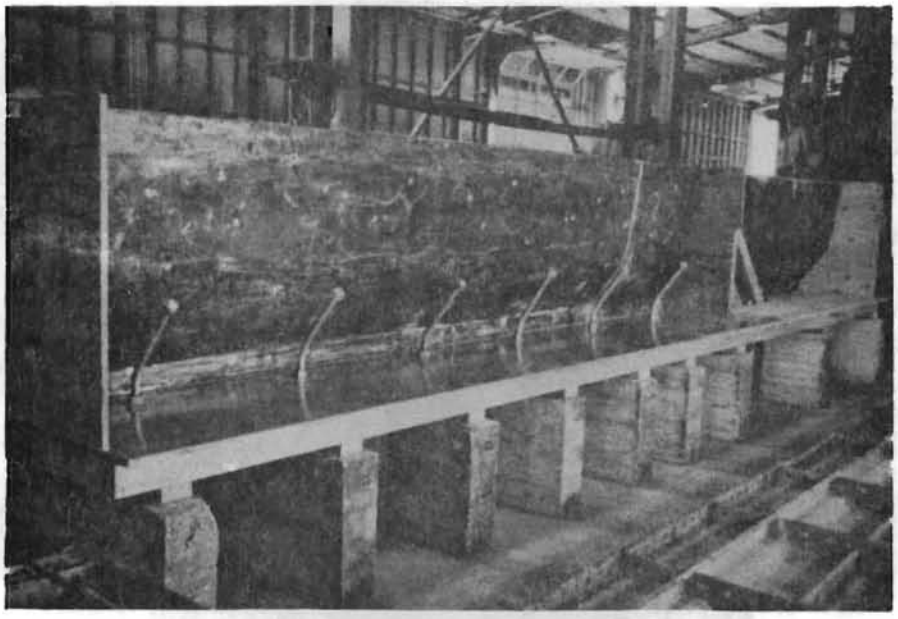

Fig. 3.9 Cast-in place barrier forms prior to placement of reinforcing cage

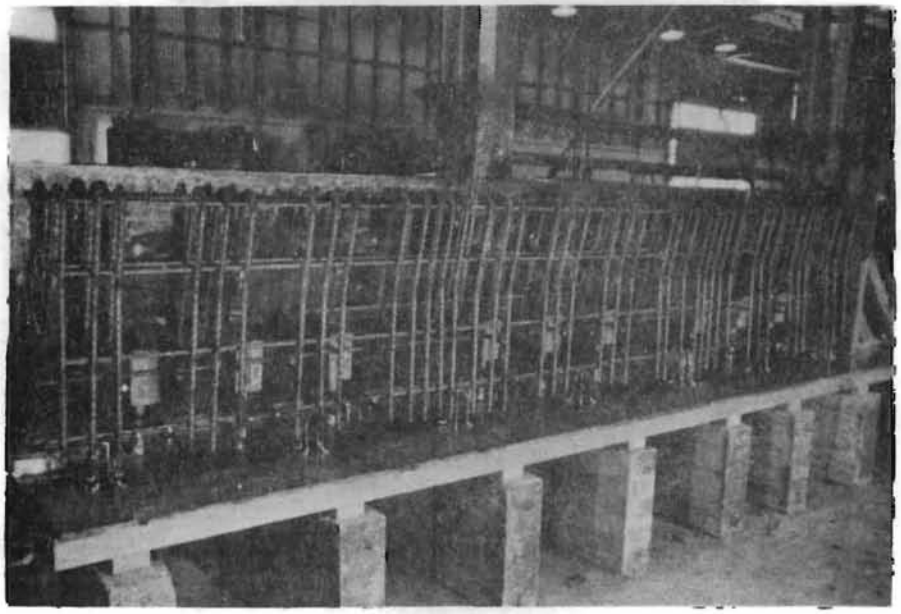

Fig. 3.10 Cast-in place barrier forms after placement of reinforcing cage

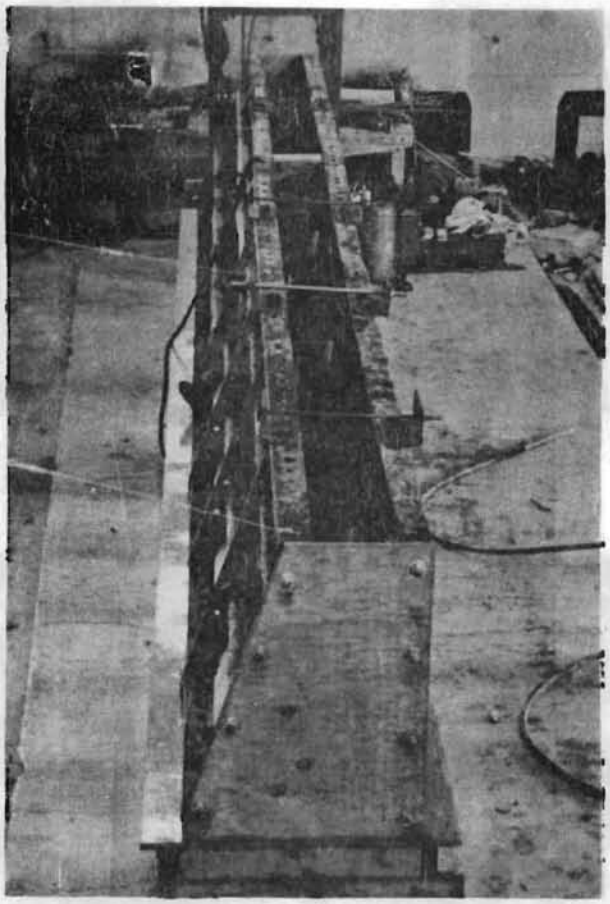

Fig. 3.11 Cast-in place barrier forms prior to concrete placement

the base, as shown in Fig. 3.12. The front face barrier form was lowered into place and secured (Fig. 3.13). Anchor bolt pockets were formed with wooden blocks bolted to the metal forms. The anchor bolt holes were formed with pieces of 1-in. PVC pipe held in place by holes in the wooden blocks and dowels in the base. A typical anchor bolt loction is shown in Fig. 3.14. The back face barrier form was then positioned, and casting operations proceeded as with the cast-in-place barrier.

After construction of the test slab formwork, the forms were lacquered, caulked, and oiled. The reinforcing cage was then lowered into the forms, as shown in Fig. 3.15. Specimen tie-down holes and anchor bolt holes were formed with pieces of 1-1/2 in. and 1 in. PVC pipe, respectively. The sections of PVC were held in place by dowels on the forms and on 2x4's which were positioned across the top of the forms, as shown in Fig. 3.16. Concrete placement was accomplished using an overhead crane and bucket and mechanical vibrators. After the test slab was anchored to the test floor, each barrier was, in turn, anchored to the slab on a 1/2-in. grout pad. The grout contained a sand to portland cement ratio of 2-to-1, by volume.

During casting of both barriers and the test slab, standard 6 in. x 12 in. cylinders were cast. After four or five days, the specimen formwork was stripped and the cylinders were removed from the molds. All specimens and cylinders were cured under the same conditions.

3.2 Existing vs. Proposed Anchorage Design.

Current Texas SDHPT T5 Barrier specifications designate a maximum spacing of 50 in. for the 1-in. diameter A193, Grade B7 anchor bolts. In the case of a 12 ft, 6 in. barrier section, such as the ones used in this study, this spacing results in a three-bolt anchorage. The proposed anchorage design specifies the use of 1 in. diameter A36 anchor bolts, spaced at 25 in. This results in a six-bolt anchorage for a 12 ft, 6 in. barrier section.

Barrier capacities for both existing and proposed anchorage designs are computed in Appendix A and listed in Table 3.4. Values were computed for each major failure mode using equations 2.4 through 2.7. In addition, capacities were calculated using both nominal and actual material strengths. Anchor bolt yielding loads were also computed by substituting f_y for f_{ult} in Eq. 2.4.

Calculated bolt yielding loads were lower than concrete pullout loads for both anchorage designs. This suggests theoretically that both designs possess the desired degree of ductility. However,

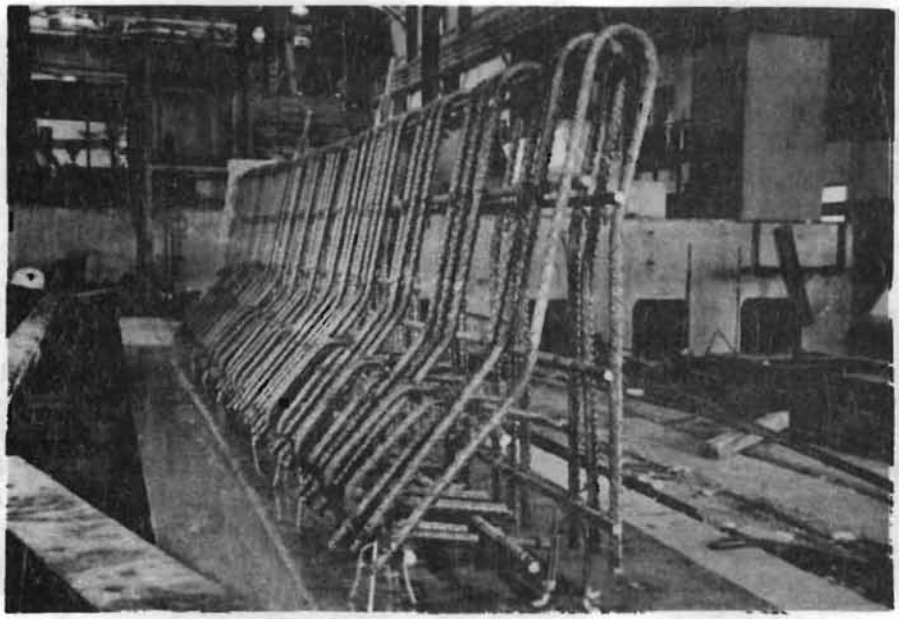

Fig. 3.12 Precast barrier reinforcing cage

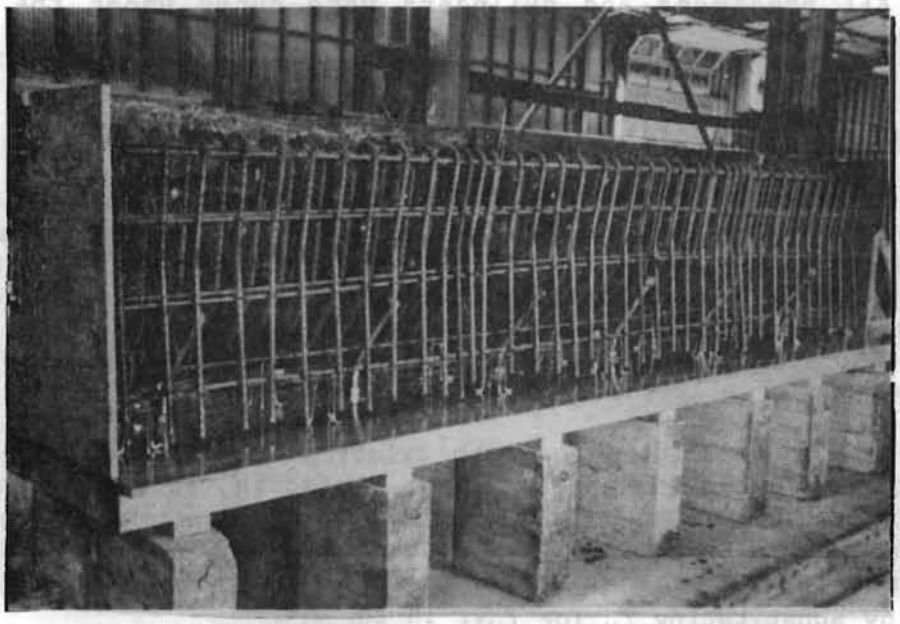

Fig. 3.13 Precast barrier formwork prior to placement of back face barrier form

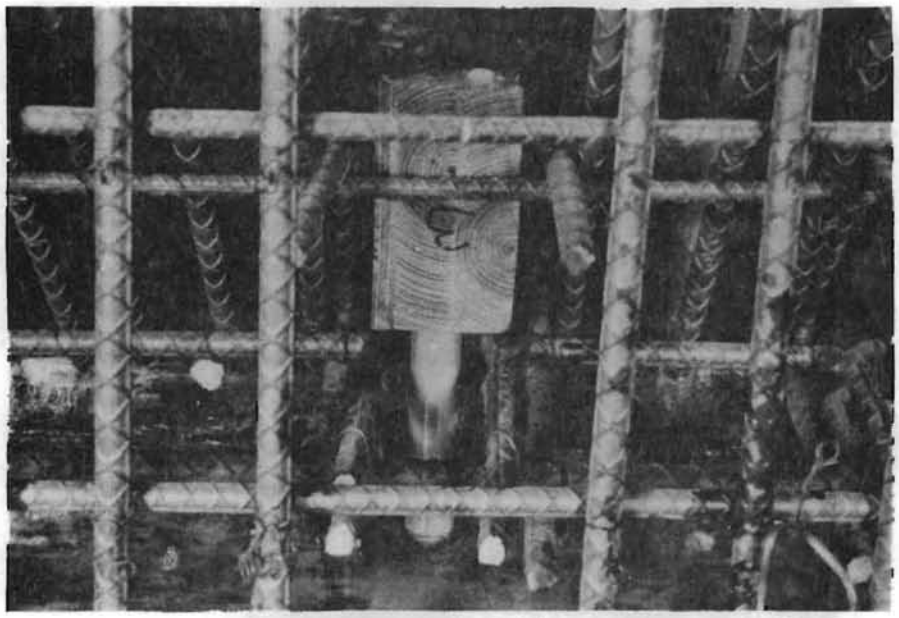

Fig. 3.14 Precast barrier anchor bolt location prior to concrete placement

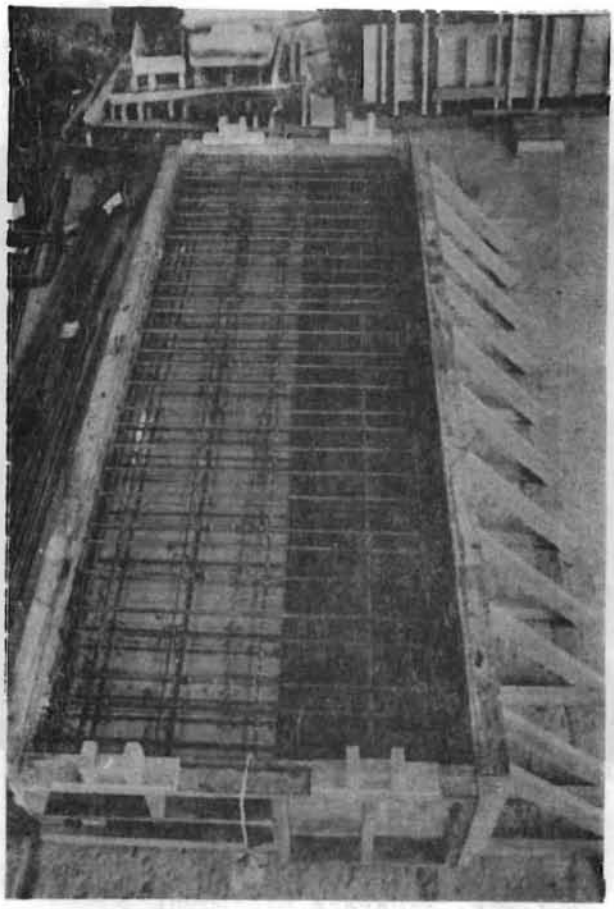

Fig. 3.15 Test slab forms and reinforcing cage

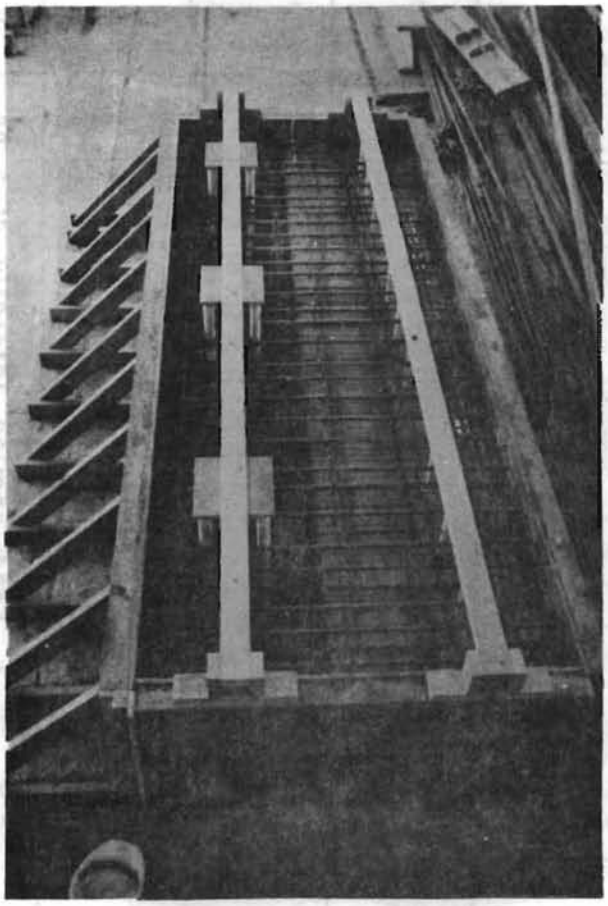

Fig. 3.16 Test slab forms with PVC pipes

TABLE 3.4 BARRIER CAPACITIES FOR EXISTING AND PROPOSED DESIGNS

		* Barrier Capacity (kips)				
		Bolt Yielding	Bolt Fracture	Concrete Pullout	Shearing of Slab	Flex. Failure of Slab
Existing Design	nominal	75.7	89.8	105	0.39 ksi < 0.8 ksi acceptable	110
	actual	76.1	111	126	0.5 ksi < 0.8 ksi acceptable	101
Proposed Design	nominal	52.2	98.9	105	0.42 ksi < 0.8 ksi acceptable	110
	actual	67.8	106	126	0.48 ksi 0.8 ksi acceptable	101

* Load applied laterally at a height of 26 inches above the slab

the proposed A36 anchor bolts, though having a lower ultimate strength, possess a much longer yield plateau than that of the A193, Grade B7 bolts. In addition, the nominal bolt yielding load of the proposed design is considerably lower than that of the existing design (both designs have the same concrete pullout load). Therefore, due to greater anchor bolt ductility and a lower bolt yielding load, the proposed anchorage design provides increased energy absorption capabilities and protection against excessive slab damage. The proposed design also provides a greater ultimate barrier strength than the existing design (98.9 kips as compared to 89.8 kips, both based on bolt fracture) because of decreased bolt spacing.

3.3 Testing Apparatus.

All tests were performed on the testing floor of the Ferguson Structural Engineering Laboratory at the Balcones Research Center of The University of Texas at Austin. The testing floor is specially equipped with tie-down holes arranged in groups of four. The holes in each group are on 8-in. centers, and the groups are arranged in a square pattern on 4-ft centers.

3.3.1 Loading System. The loading system is shown in Figs. 3.17 and 3.18. Loads were applied with a 100-kip capacity hydraulic ram, bolted to a steel reaction frame constructed of double channel sections. Like the test specimen, the reaction frame was anchored to the testing floor with twelve steel tie-down rods, each of which was post-tensioned to 25 kips. Loads were transferred to the barriers with a four foot long loading beam. The loading beam, a heavily stiffened W6 x 20 section, was bolted to the ram and to the barriers using predrilled holes in the barriers.

The hydraulic loading system is shown schematically in Fig. 3.19. Hydraulic fluid was supplied to the ram by a high pressure hydraulic pump. It was passed through two "line tamers" and two servo valves acting in parallel. The line tamers were used to dampen unwanted surges in pressure. The servo valves, which regulate the flow of hydraulic fluid to the ram, were controlled with a Shore-Western SC3000A Series Servo Controller. The servo controller was operated manually during all static tests. During the dynamic test, the servo controller was governed by an Exact Model 336 Function Generator. The function generator produced a ramp waveform, resulting in an impact load with a triangular variation over time.

3.3.2 Instrumentation and Data Acquisition. Loads applied to the barriers were measured using a Lebow 100 kip capacity strain-gage load cell. The load cell was positioned between the hydraulic ram and the loading beam, as shown in Fig. 3.17.

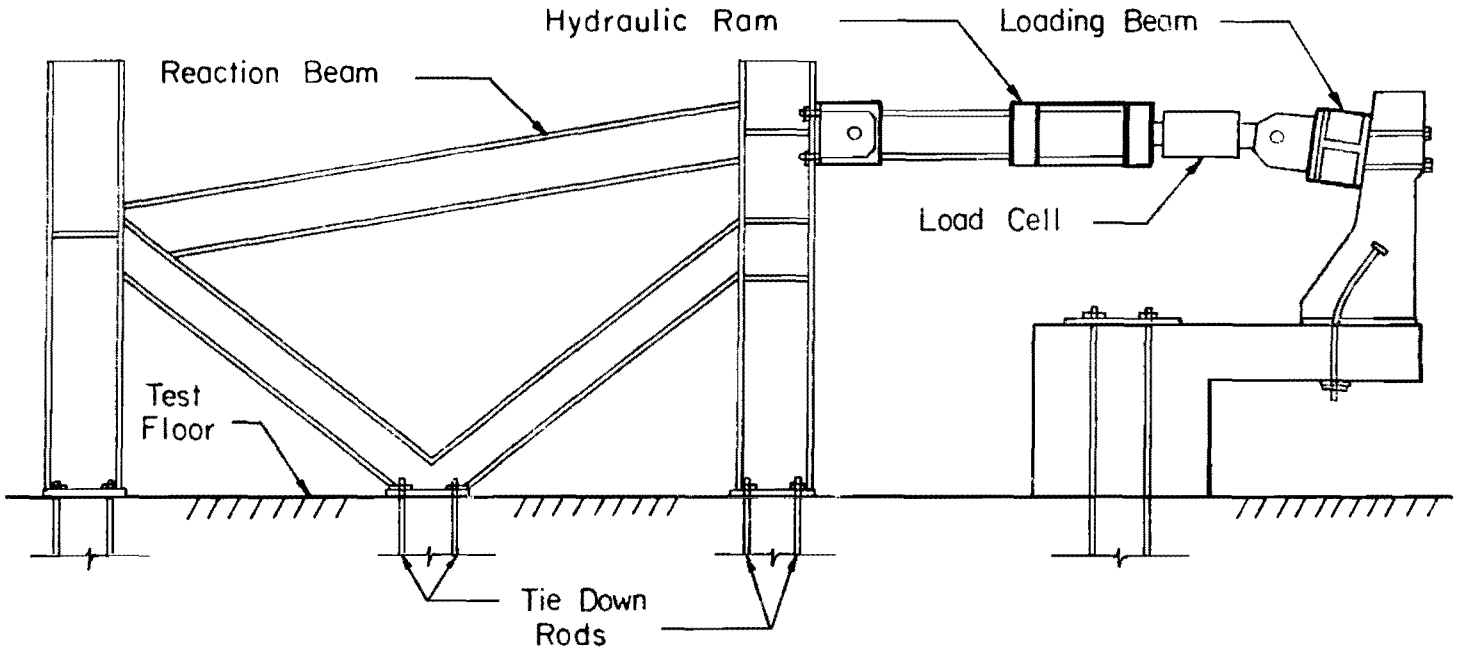

Fig. 3.17 Loading system

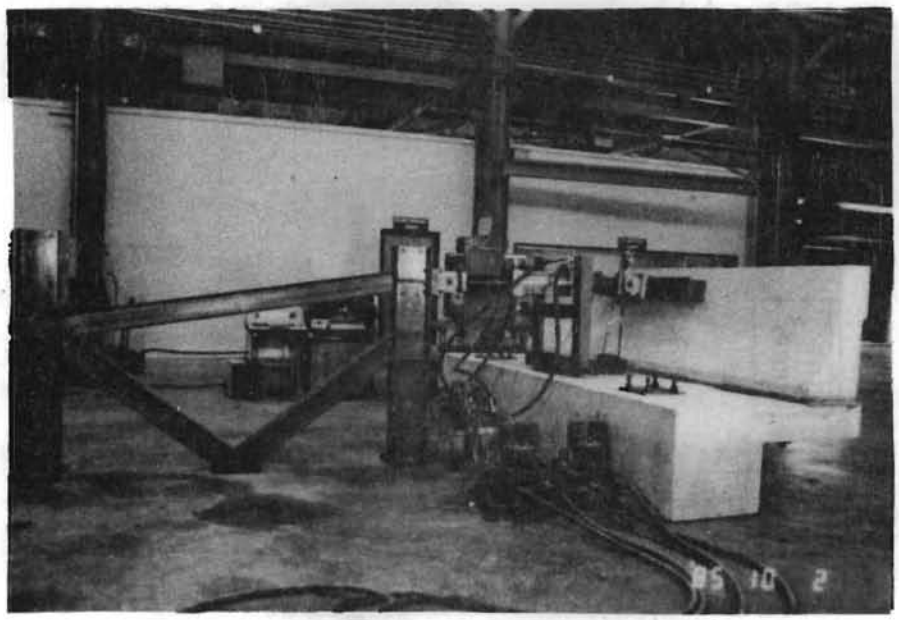

Fig. 3.18 Test set-up and loading system

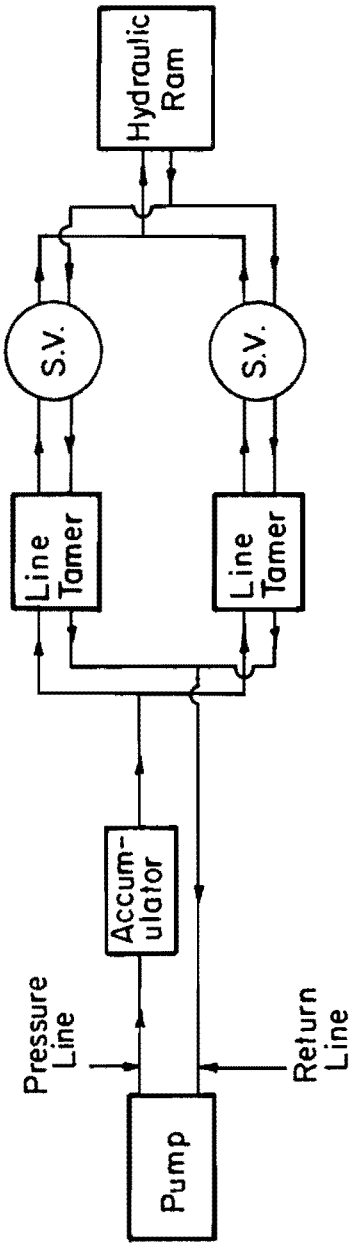

Fig. 3.19 Hydraulic system

Tensile forces acting on the anchor bolts were measured with full bridge, compressive load cells. The load cells were constructed specifically for this project and were individually calibrated prior to their use in the barrier tests. As shown in Fig. 3.20, the load cells were constructed of hollow steel tubes, which fit around each anchor bolt underneath the slab.

Electrical resistance strain gages with a gage length of 0.32 in. were used to measure reinforcing bar strains in the test slab. The gages were attached to specially prepared surfaces on the bars with an epoxy adhesive. After lead wires were attached to the gages, the gages were waterproofed and covered with a protective rubber pad. The gages were placed on top transverse reinforcing bars (Bars A) near anchor bolt locations. Strain gage locations in the test slab are shown in Fig. 3.21.

Lateral barrier deflections at the point of loading were measured with a 12-in. linear potentiometer. The potentiometer was mounted on the side of the hydraulic ram and its plunger was attached to the shaft of the ram.

Leads from the load cells, strain gages and the potentiometer were connected to a data acquisition system, which recorded the data on computer diskettes. Data for the static tests was recorded using a Hewlett-Packard microcomputer. Dynamic test data was recorded using two Data 6000 high-speed data acquisition units.

3.4 Testing Sequence

The first test, designated CSTAT1, was a static test performed on the cast-in-place barrier using the proposed anchorage design (six 1 in. diameter A36 bolts, spaced at 25 in.). Upon completion of CSTATI, the barrier was disconnected and lifted from the slab. The grout pad was then removed from the surface of the slab.

After the slab surface was cleaned, a new grout pad applied and the precast barrier was lowered into position. The precast barrier was fabricated with nine anchor bolt holes which matched the hole locations in the test slab (see Fig. 3.3), providing a variety of possible anchor bolt spacings.

After the new grout pad was allowed to cure, a static test, designated CSTAT2, was performed on the precast barrier using three A36 anchor bolts spaced at 50 in. A final static test, designated CSTAT3, was then performed on the precast barrier using two A36 anchor

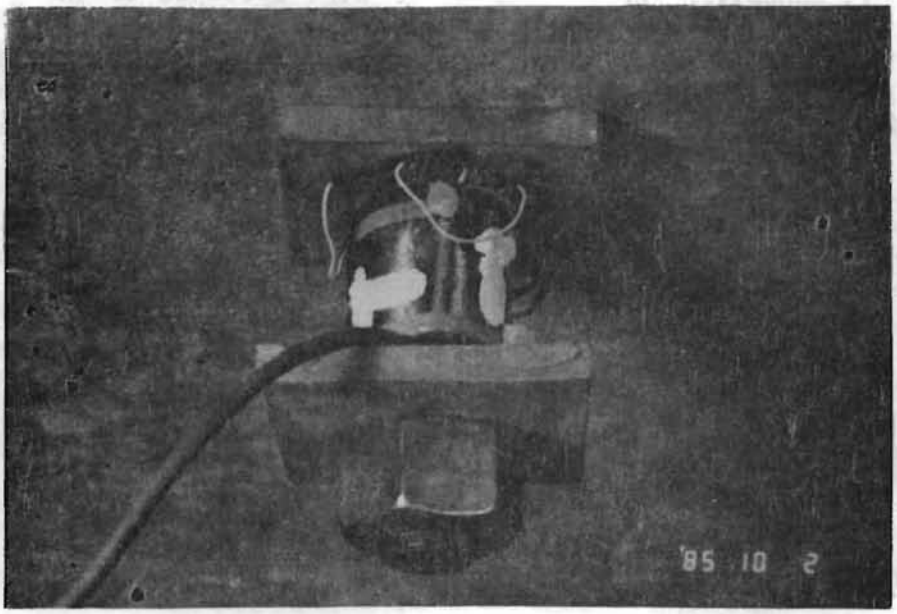

Fig. 3.20 Bolt load cell in position

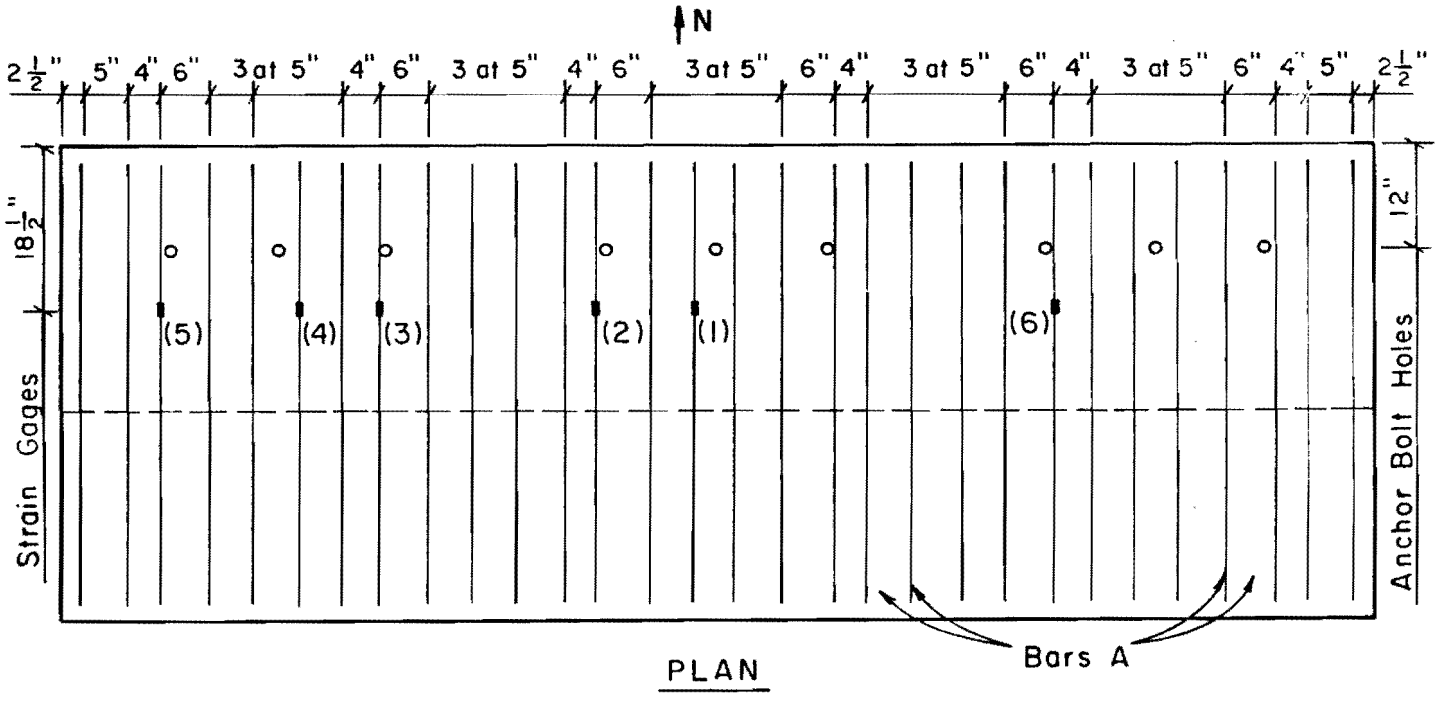

Fig. 3.21 Strain gage locations in test slab

bolts spaced at 75 in. All three static tests were discontinued prior to bolt failure due to excessive slab cracking.

A dynamic test, designated MPACT1, was then performed on the precast barrier using three A36 anchor bolts spaced at 50 in. The bolts were sawed in half in order to reduce the total effective tensile stress area of the bolts by about 50 percent. Repeated impact loads were applied to the barrier as the magnitude of the load and the pulse length were gradually increased. Loading continued until fracture of the anchor bolts occurred.

CHAPTER 4

TEST RESULTS

4.1 Introduction

Some of the results in this section are presented graphically. Where reinforcing bar stresses are presented, bars are identified by a strain gage number. The number and corresponding location of each strain gage are shown in Fig. 3.21. In most instances, only stresses for bars near anchor bolts are presented for each test.

Where bolt loads are presented, bolts are identified by a bolt number. For each test, the anchor bolts were numbered from east to west. The numbers and corresponding locations of anchor bolts for all four tests are shown in Fig. 4.1.

All displacements presented represent the lateral movement of the barrier at the point of loading, approximately 26 in. above the slab.

4.2 Static Test Results

Graphs of load vs displacement, load vs bolt loads and load vs reinforcing bar stresses for the three static tests are presented in the following sections.

4.2.1 CSTAT1 Results. CSTAT1 was a static test performed on the cast-in-place barrier using six 1-in. diameter A36, anchor bolts, spaced at 25 in. (Fig. 4.1). The load was applied in increments of approximately 5 kips. At a load of 15 kips, a curved flexural crack developed in the center of the slab (Fig. 4.2), surrounding the central anchor bolts 3 and 4. Straight flexural slab cracks later developed at loads of 28.8, 35, and 43.4 kips. These cracks are shown in Fig. 4.3.

At a load of 35 kips, inclined cracks developed at the edge of the slab, as shown in Fig. 4.4. The cracks propagated from the top surface of the slab at points approximately 1 ft apart, centered around the location of anchor bolt #3. Additional inclined cracks developed at loads of 40 and 43.4 kips, as shown in Fig. 4.5. The 43.4 kip load also produced flexural cracks in the barrier, as shown

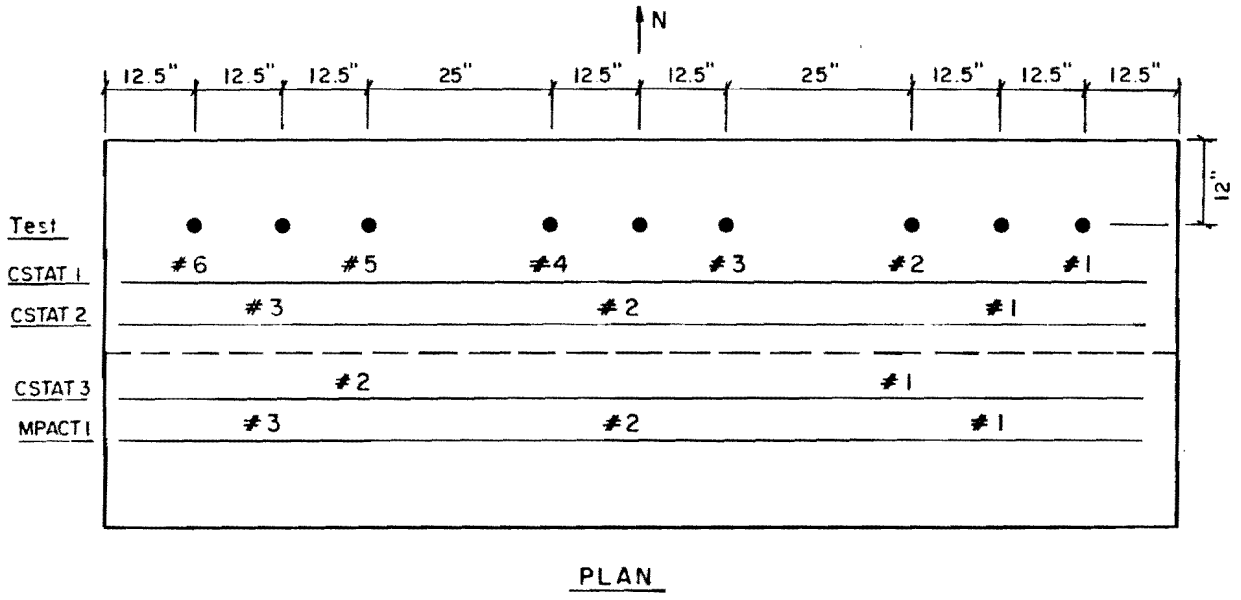

Fig. 4.1 Anchor bolt locations for testing sequence

Fig. 4.2 Initial slab cracking: CSTAT1

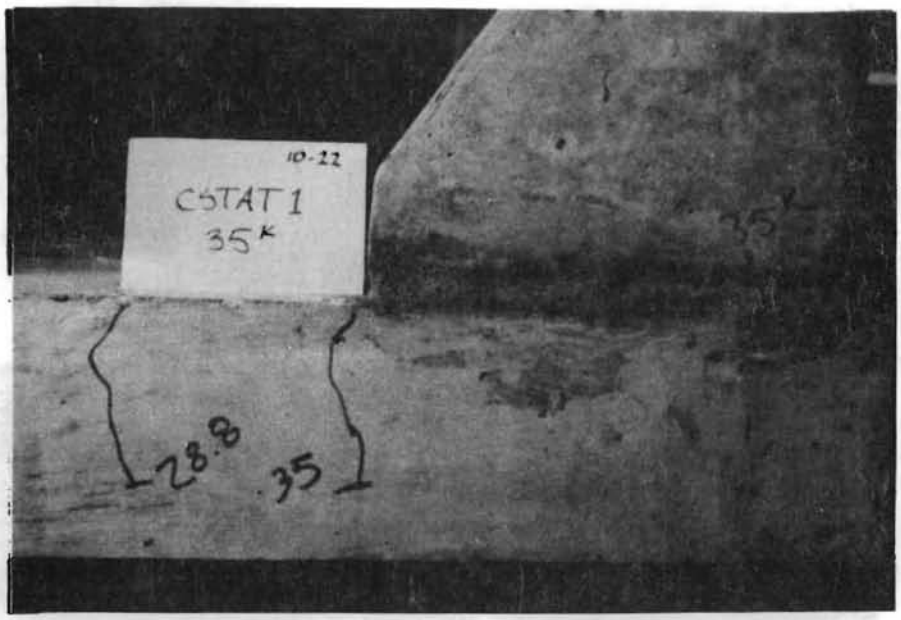

(a) East edge of slab

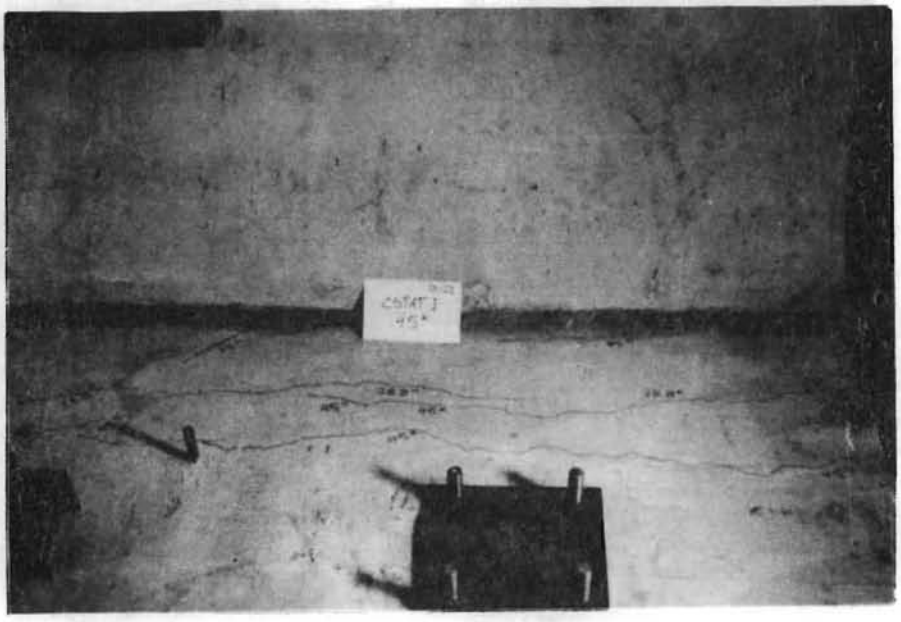

(b) Surface of slab

Fig. 4.3 Slab cracking: CSTAT1

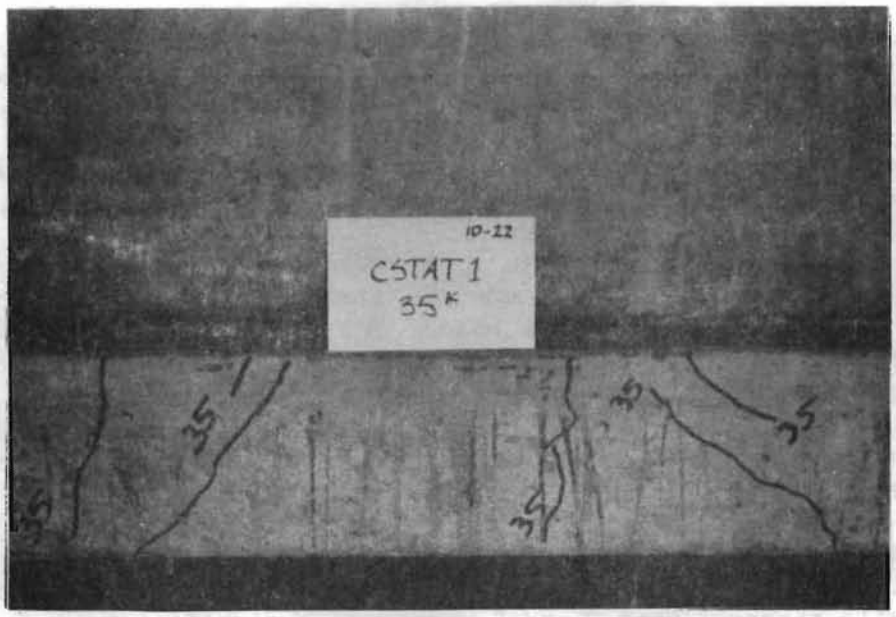

Fig. 4.4 Initial inclined slab cracking: CSTAT1

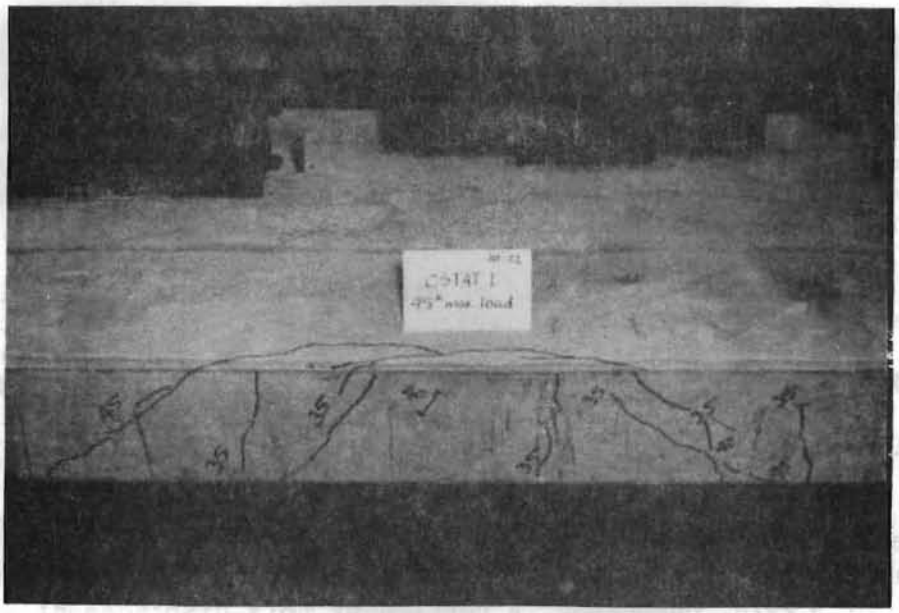

Fig. 4.5 Inclined slab cracking (after removal of cast-in-place barrier): CSTAT1

in Fig. 4.6. Loading was discontinued after the 43.4-kip load, due to excessive widening of the inclined slab cracks. The load was decreased to zero in 10-kip increments.

The maximum horizontal displacement of the barrier was approximately 1.03 in., as shown in Fig. 4.7. Upon unloading, a permanent set of 0.25 in. was observed.

Figures 4.8 and 4.9 illustrate the distribution of bolt loads, as related to the applied load. Bolts 1, 2, and 3 carried higher tensile loads than the remaining three bolts. In addition, loads among the eastern three bolts (1, 2 and 3) were distributed in such a way that bolts nearer the loading point carried higher loads. This trend was not evident among bolts 4, 5, and 6. None of the six anchor bolts yielded.

The distribution of stresses among slab reinforcing bars is shown in Fig. 4.10. The bar nearest the loading point carried the highest tensile stress. Bars 2 and 5 underwent a significant increase in stress at loads of approximately 26 and 29 kips, respectively, possibly due to slab cracking at those load levels. None of the bars yielded.

4.2.2 CSTAT2 Results. CSTAT2 was a static test perofrmed on the precast barrier using three 1-in. A36 anchor bolts, spaced at 50 inches. the load was initially applied in 5-kip increments. At higher loads, the increments were considerably smaller. Loading was discontinued after a maximum load of 37.5 kips, due to excessive widening of the existing inclined slab cracks. The load was returned to zero in 10-kip increments.

No new flexural slab cracks or excessive widening of existing ones was observed during CSTAT2. However, new inclined cracks at the edge of the slab were observed at loads 27 kips and greater, as shown in Fig. 4.11. The new cracks developed west of the existing ones. Figure 4.11 also shows flexural cracking of the back face of the barrier. Minor cracking of the front face of the barrier is shown in Fig. 4.12.

The load-displacement behavior observed during CSTAT2 was very similar to that of CSTAT1. As shown in Fig. 4.13, a maximum displacement of 1.2 in. occurred. A portion of this displacement was due to rigid-body rotation of the barrier, as shown in Fig. 4.14. Note the separation at the front (tension) side of the barrier.

Figure 4.15 illustrates the distribution of bolt loads. The outer two bolts (1 and 3) assumed a considerably greater load than the center bolt (2), and approached the yielding load (28.3 kips). Note

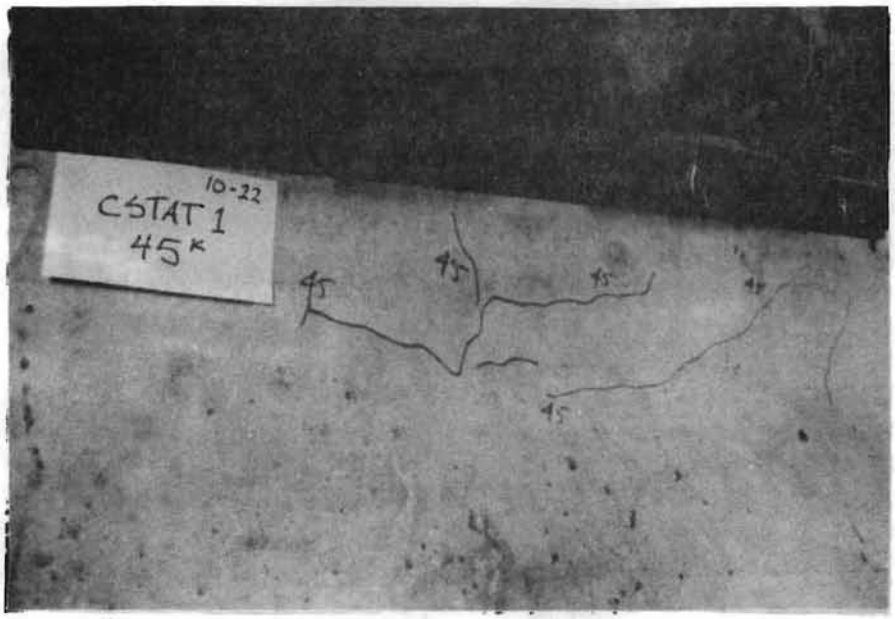

(a) Front face of barrier

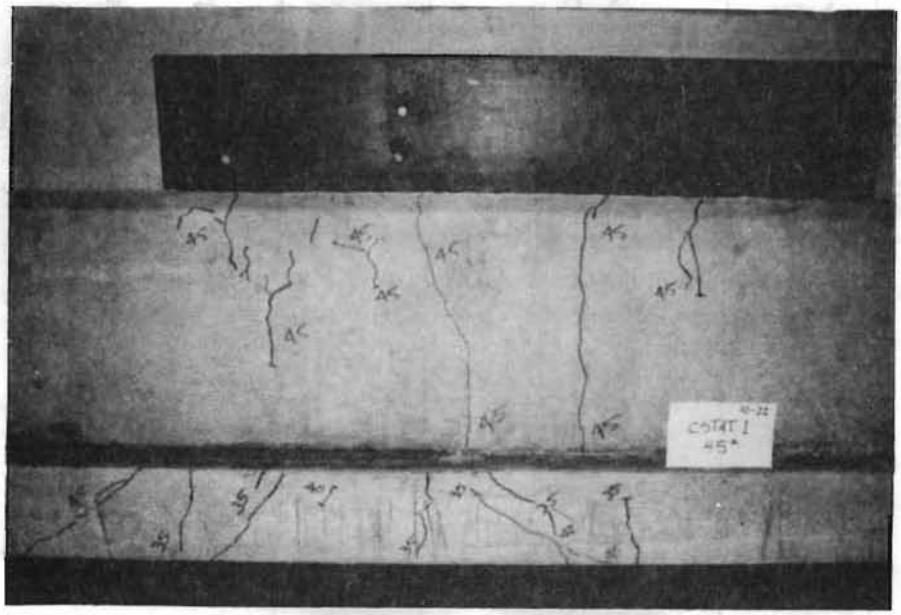

(b) Back face of barrier

Fig. 4.6 Cracking of cast-in-place barrier: CSTAT1

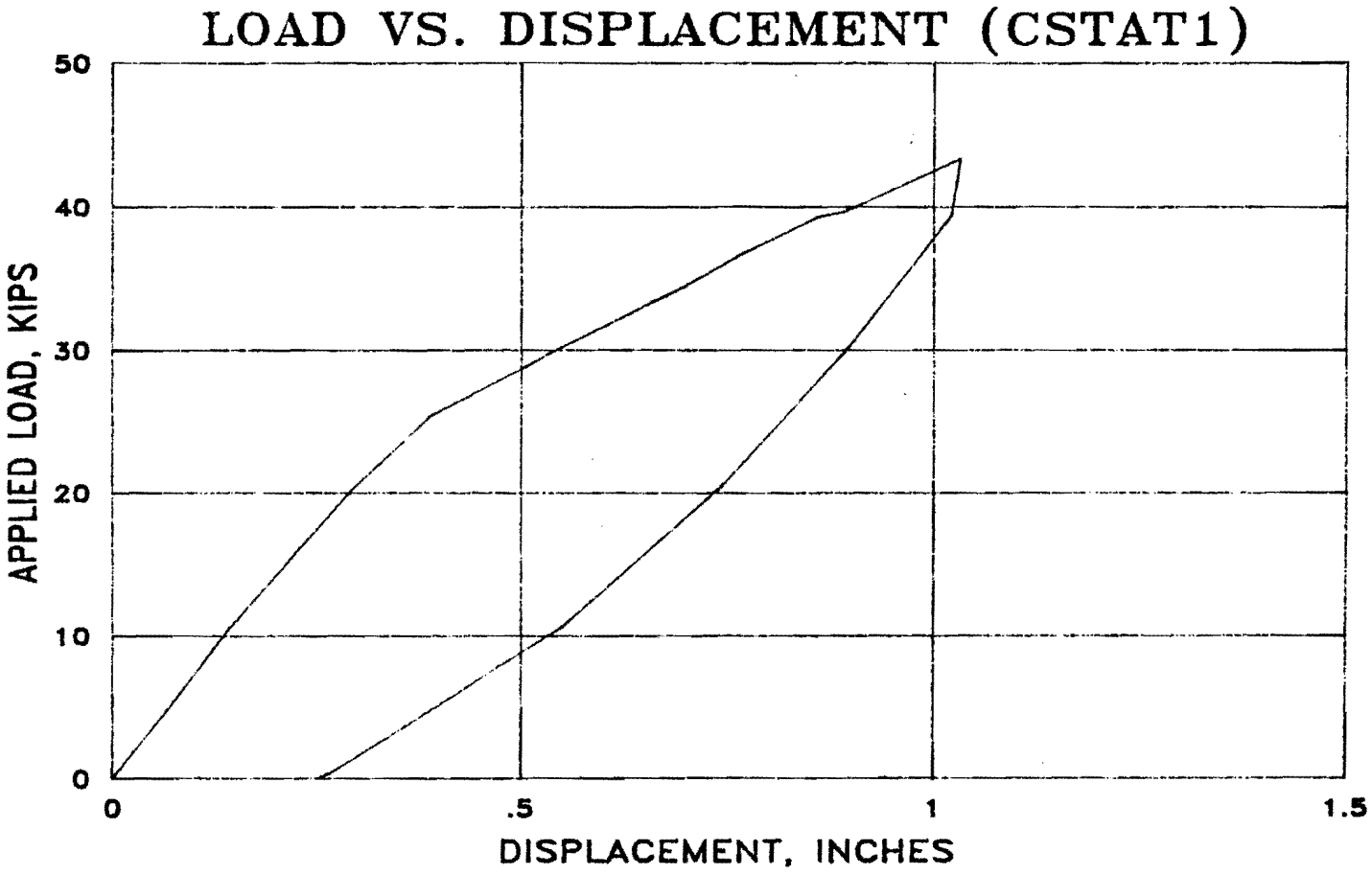

Fig. 4.7 Load vs. displacement: CSTAT1

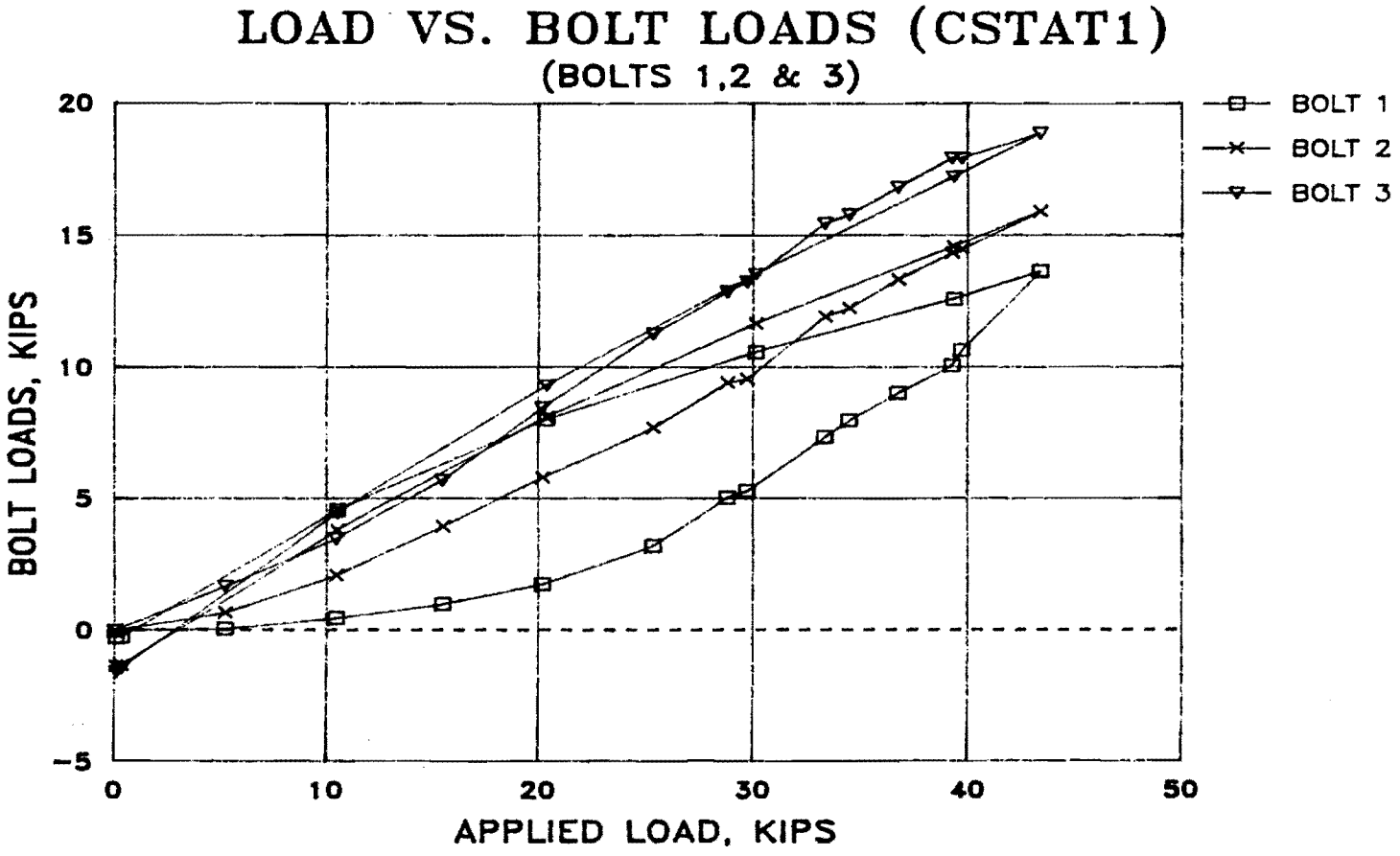

Fig. 4.8 Load vs. bolt loads - bolts 1,2 & 3: CSTAT1
(refer to Fig. 4.1 for anchor bolt locations)

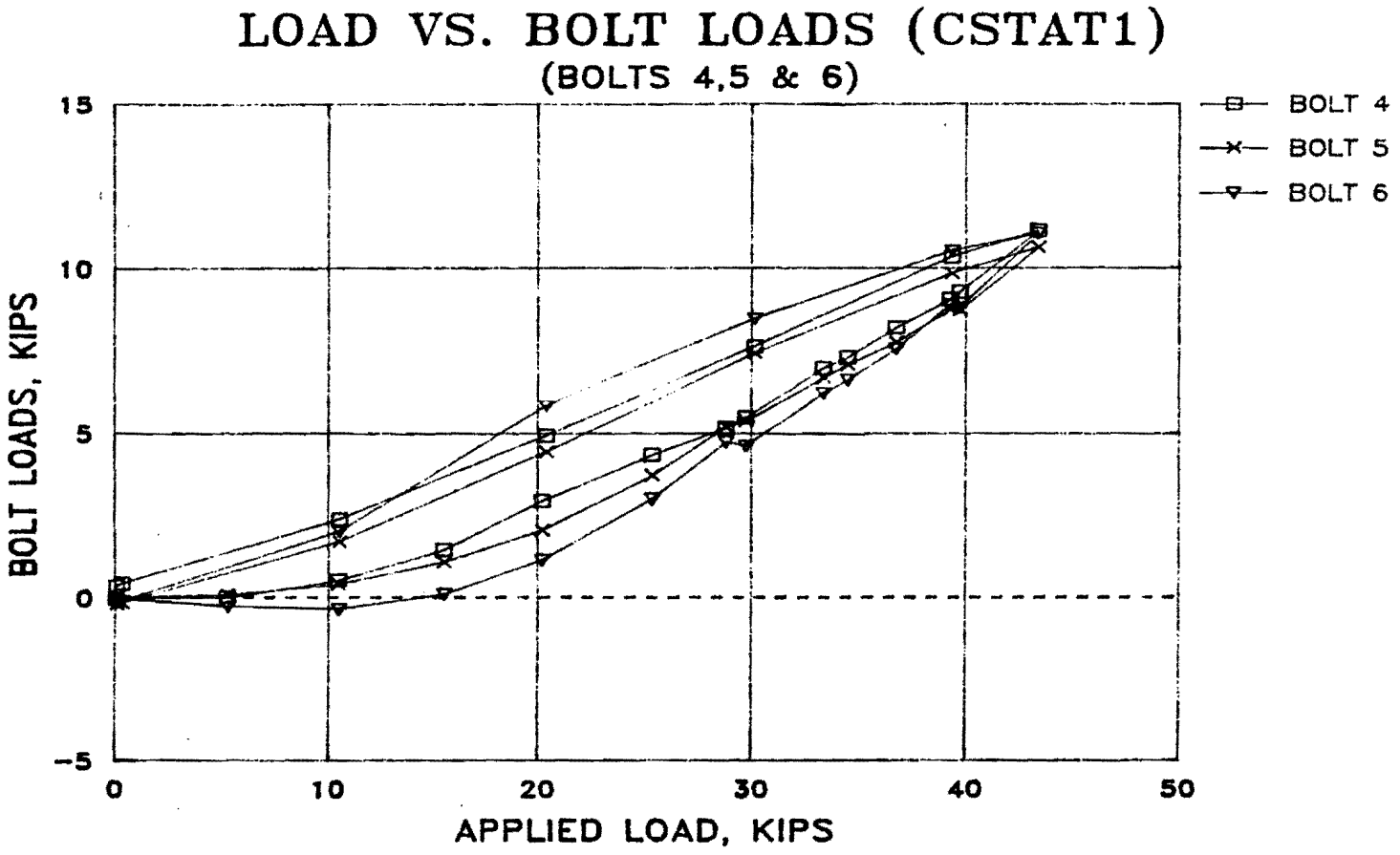

Fig. 4.9 Load vs. bolt loads - bolts 4,5 & 6: CSTAT1
(refer to Fig. 4.1 for anchor bolt locations)

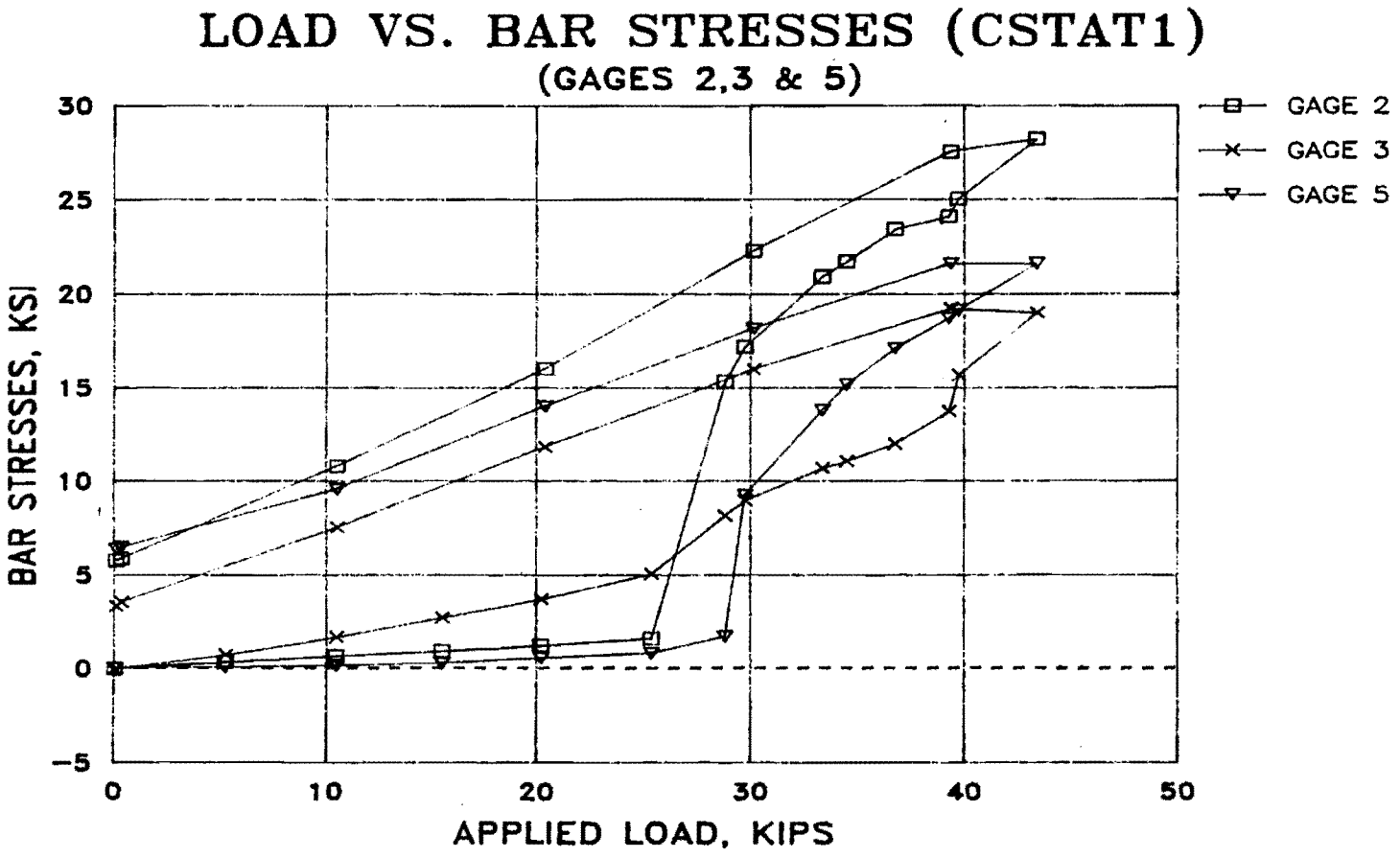

Fig. 4.10 Load vs. bar stresses - gages 2,3 & 5: CSTAT1
(refer to Fig. 3.21 for strain gage locations)

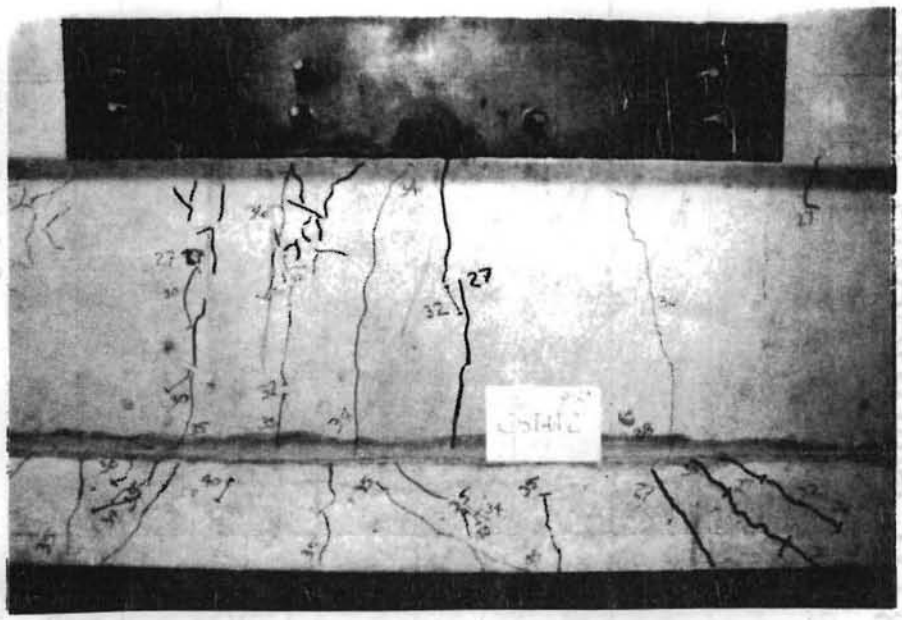

Fig. 4.11 Inclined slab cracking and cracking of precast barrier: CSTAT2

(a) West end of barrier

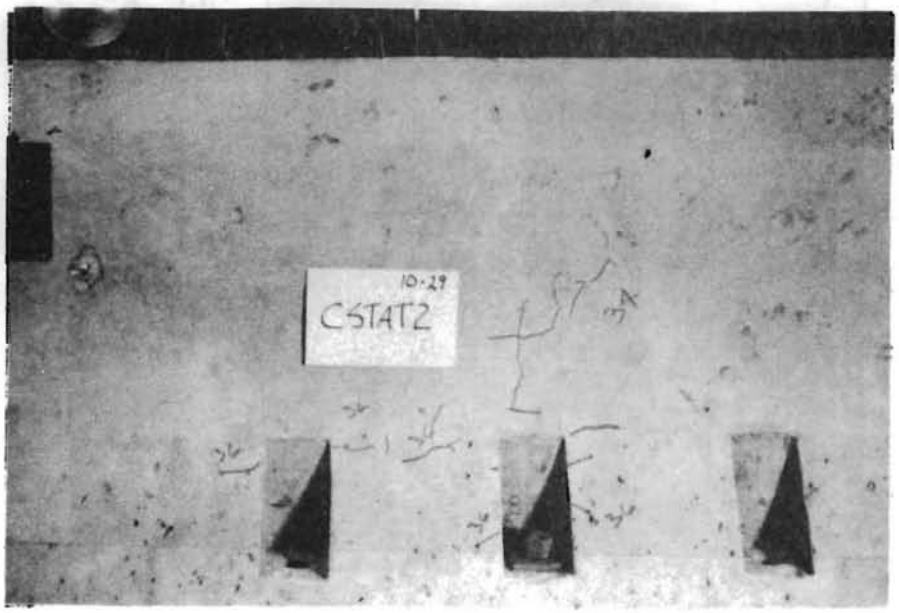

(b) East end of barrier

Fig. 4.12 Cracking of precast barrier: CSTAT2

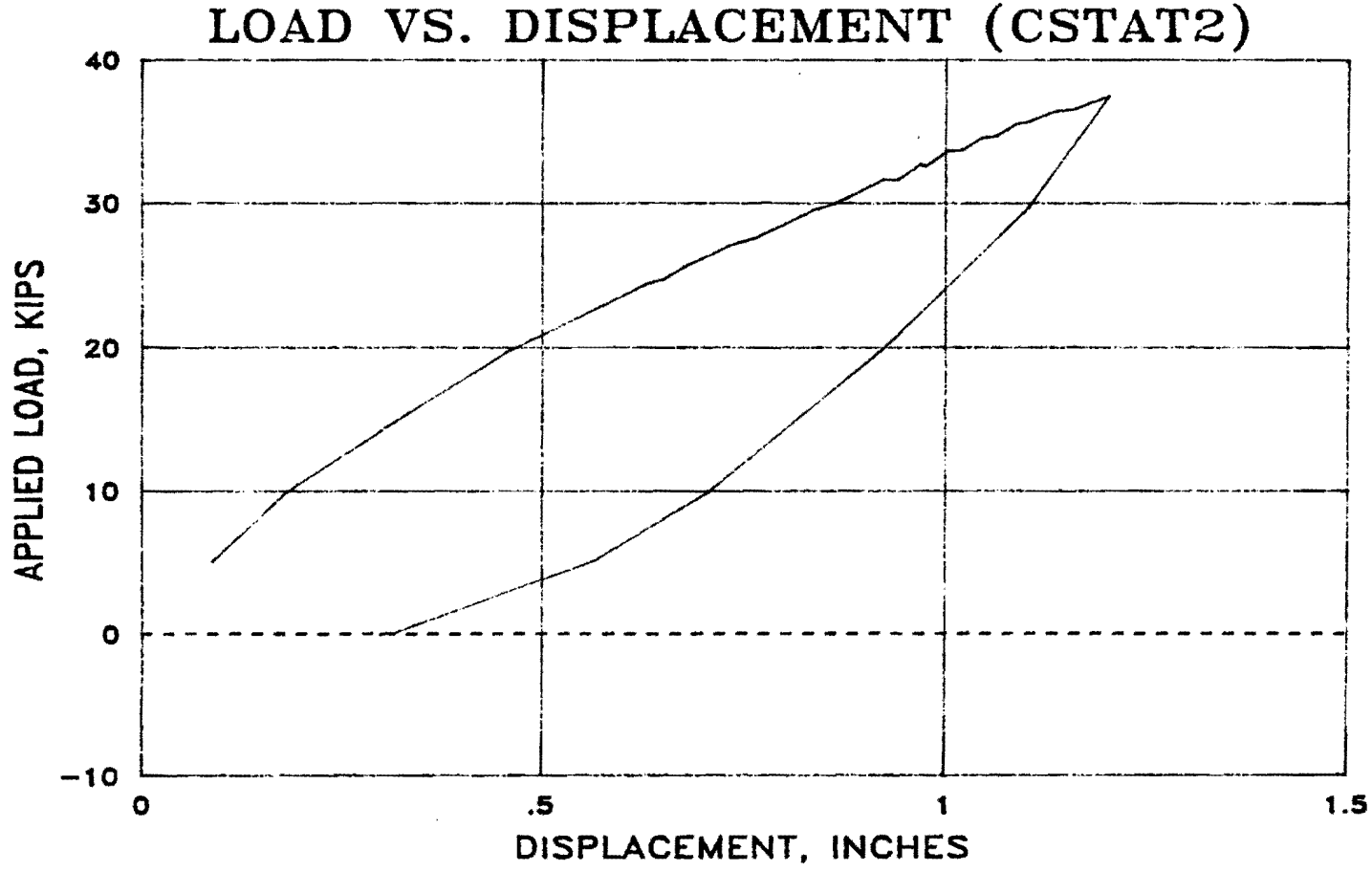

Fig. 4.13 Load vs. displacement: CSTAT2

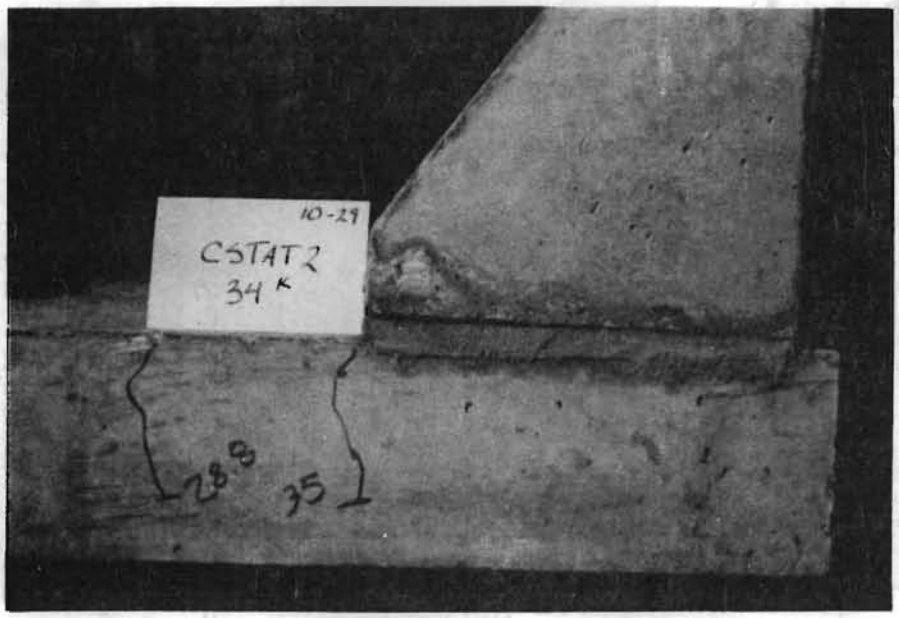

Fig. 4.14 Rotation of precast barrier: CSTAT2

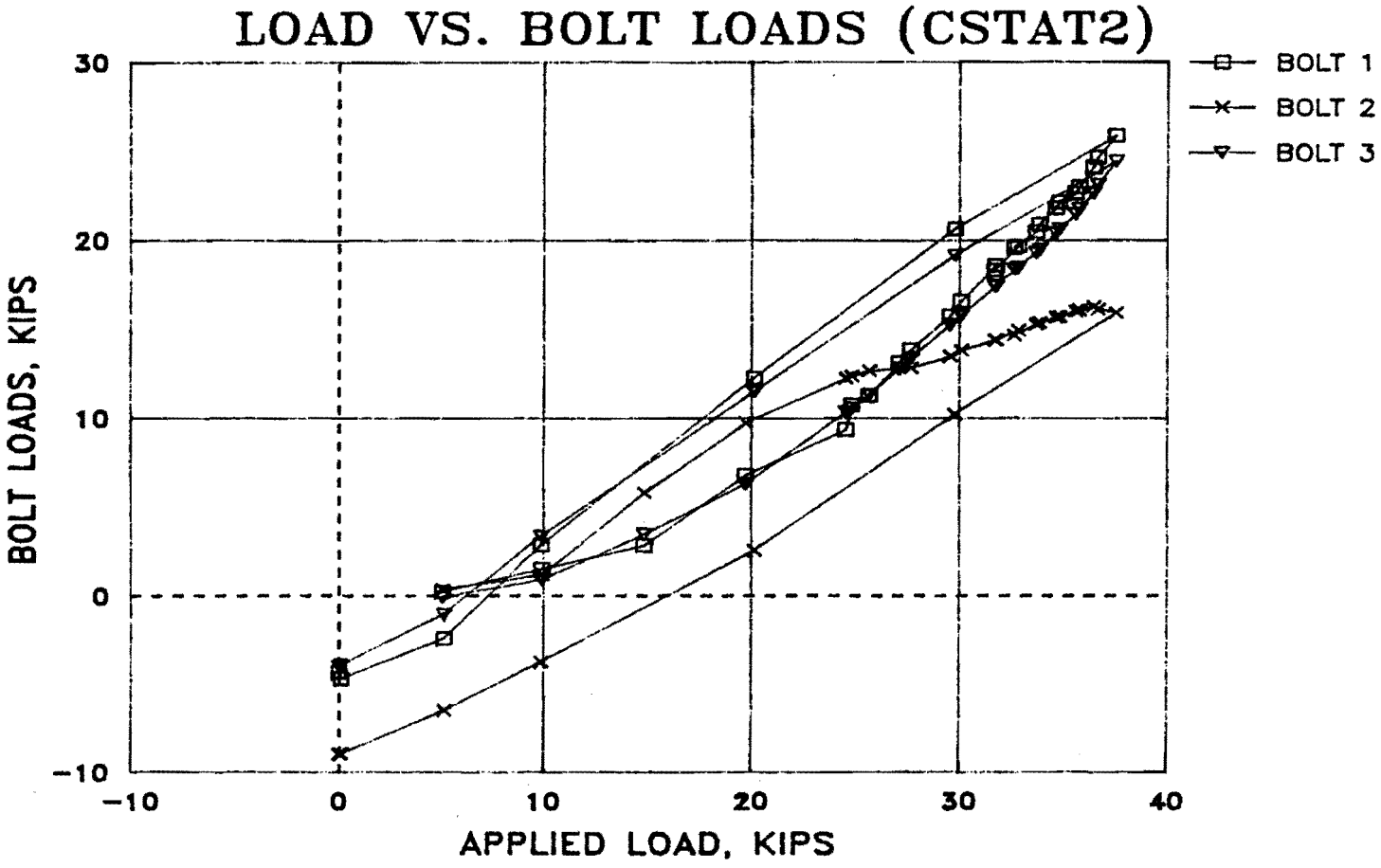

Fig. 4.15 Load vs. bolt loads: CSTAT2
(refer to Fig. 4.1 for anchor bolt locations)

the basically linear relationship between the bolt loads and the applied load.

Bar stresses vs applied load are shown in Fig. 4.16. A fairly linear relationship between the applied load and the bar stresses was observed. The bar nearest the center bolt (Gage 1) assumed a considerably larger stress than the bar near an outside bolt (Gage 4). However, neither bar approached yielding.

4.2.3 CSTAT3 Results. The final static test, CSTAT3, was perofrmed on the precast barrier using two 1-in. A36 anchor bolts, spaced at 75 in. Load was initially applied in 5-kip incrments, with the increments decreasing at higher loads. Loading was discontinued after a maximum load of 29.4 kips, due to excessive widening of existing inclined slab cracks. Maximum crack widths of 0.2 in. were observed. The load was decreased to zero in 5-kip increments.

No new cracks developed in the slab during CSTAT3. Only minor additional cracks were observed in the barrier. A maximum barrier displacement of 0.9 in. was observed, as shown in Fig. 4.17. The load-displacement behavior of the barrier was basically linear.

Both loads are shown in Fig. 4.18. Both anchor bolts exhibited a linear load history with respect to the applied load. The bolts, which were positioned symmetrically about the central loading point, carried essentially equal tensile loads during the entire test. Maximum loads for bolts 1 and 2 were 26.6 and 27.8 kips, respectively, both of which were slightly less than the bolt yielding load.

Bar stresses are shown in Fig. 4.19. The bar near anchor bolt #2 (Gage 3) experienced a higher tensile stress than did the bar positioned between the two anchor bolts (Gage 1). Both maximum bar stresses were relatively small (around 15 ksi).

4.3 Dynamic Test Results

4.3.1 Introduction. The dynamic test, designated MPACT1, was performed on the precast barrier using three 1-in. A36 anchor bolts, spaced at 50 in. All previous barrier tests in this investigation had exhibited brittle failures. To achieve a ductile failure in this impact test, it was decided to reduce even further the cross-sectional area of the anchor bolts. Prior to testing, each anchor bolt was sawed approximately in half in the threads in order to obtain bolt fracture during loading.

Impact loads were applied to the barrier at nine loading levels, designated 1 through 9. Three pulses, designated A through C,

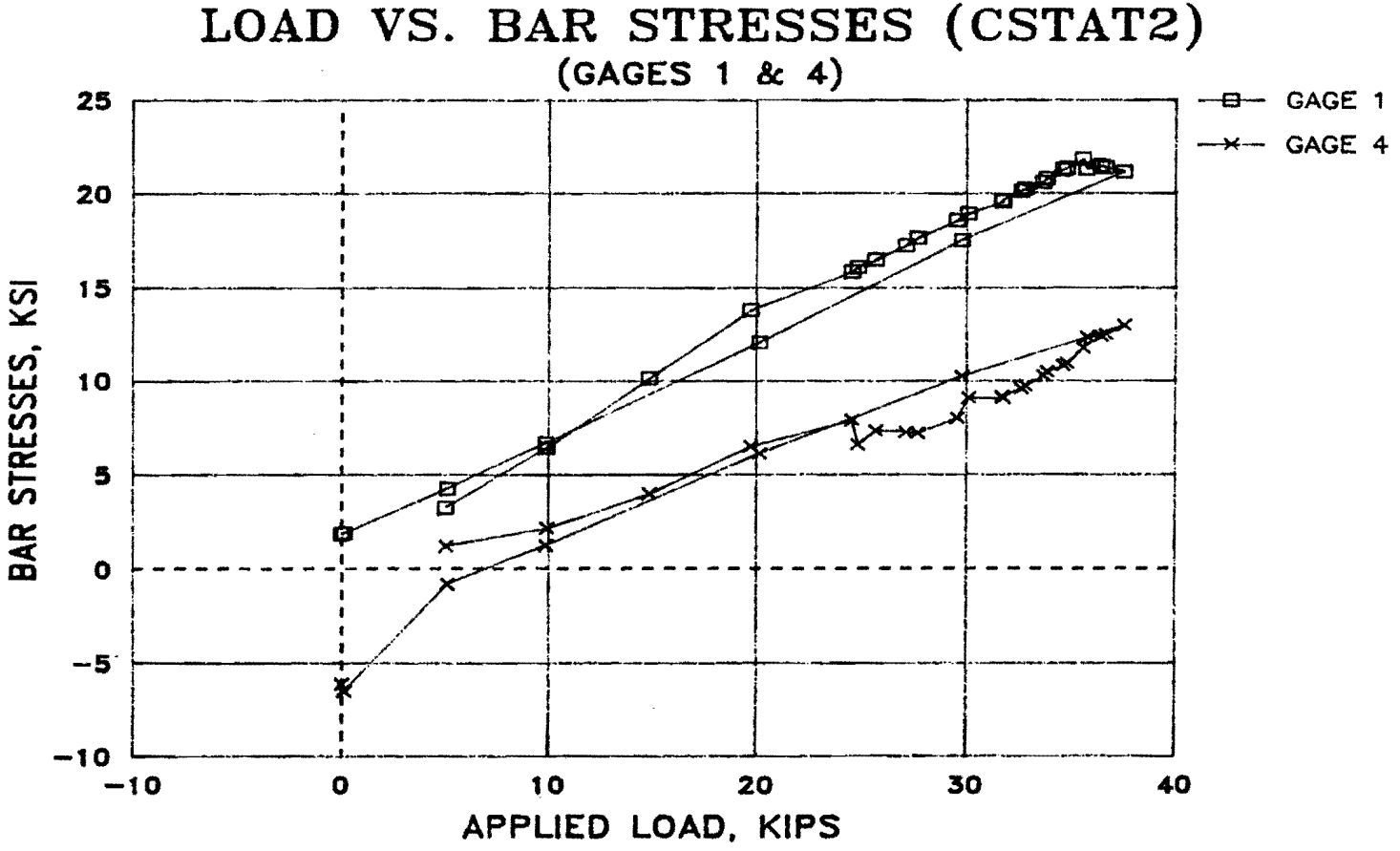

Fig. 4.16 Load vs. bar stresses - gages 1 & 4: CSTAT2
(refer to Fig. 3.21 for strain gage locations)

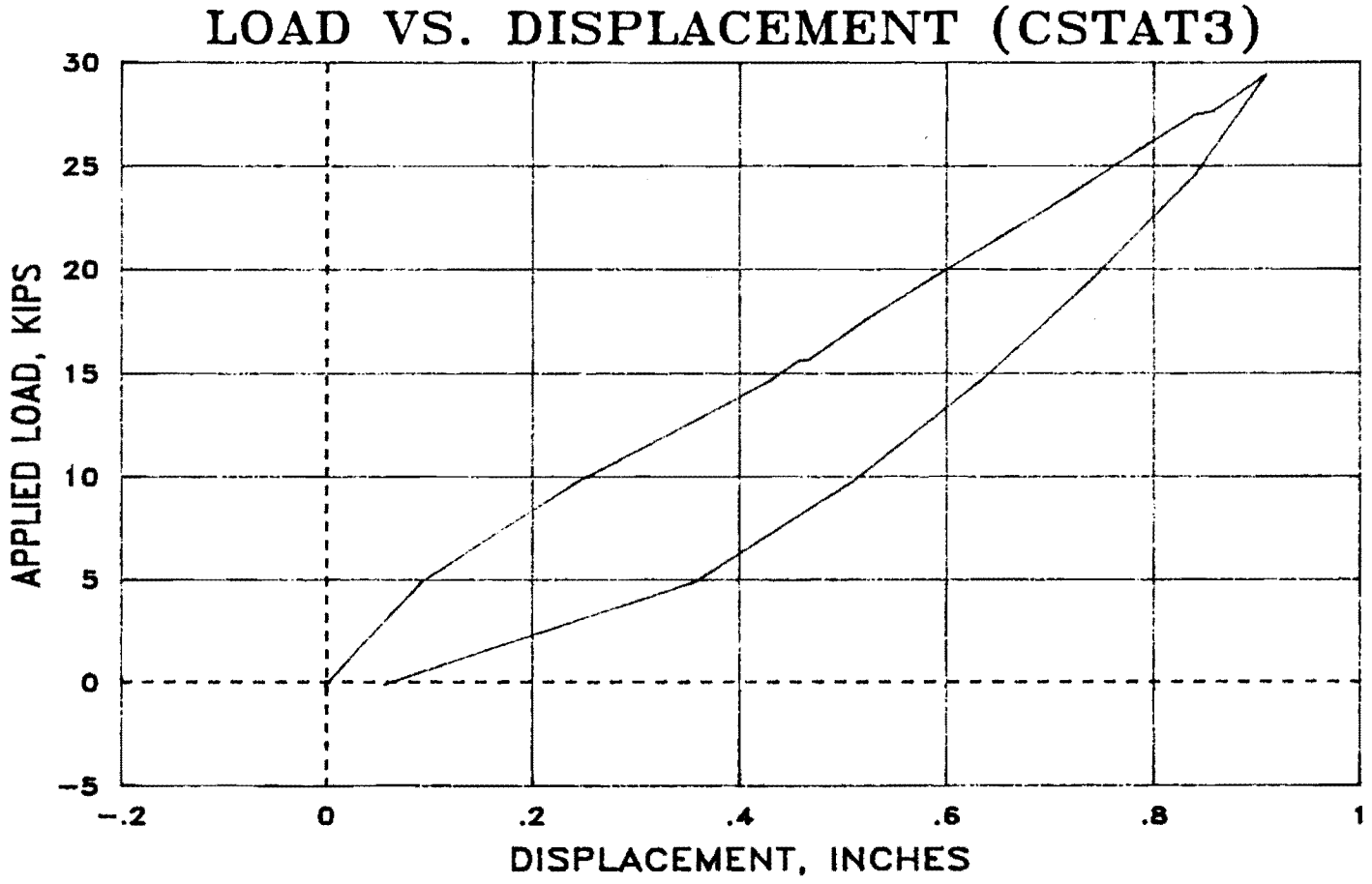

Fig. 4.17 Load vs. displacement: CSTAT3

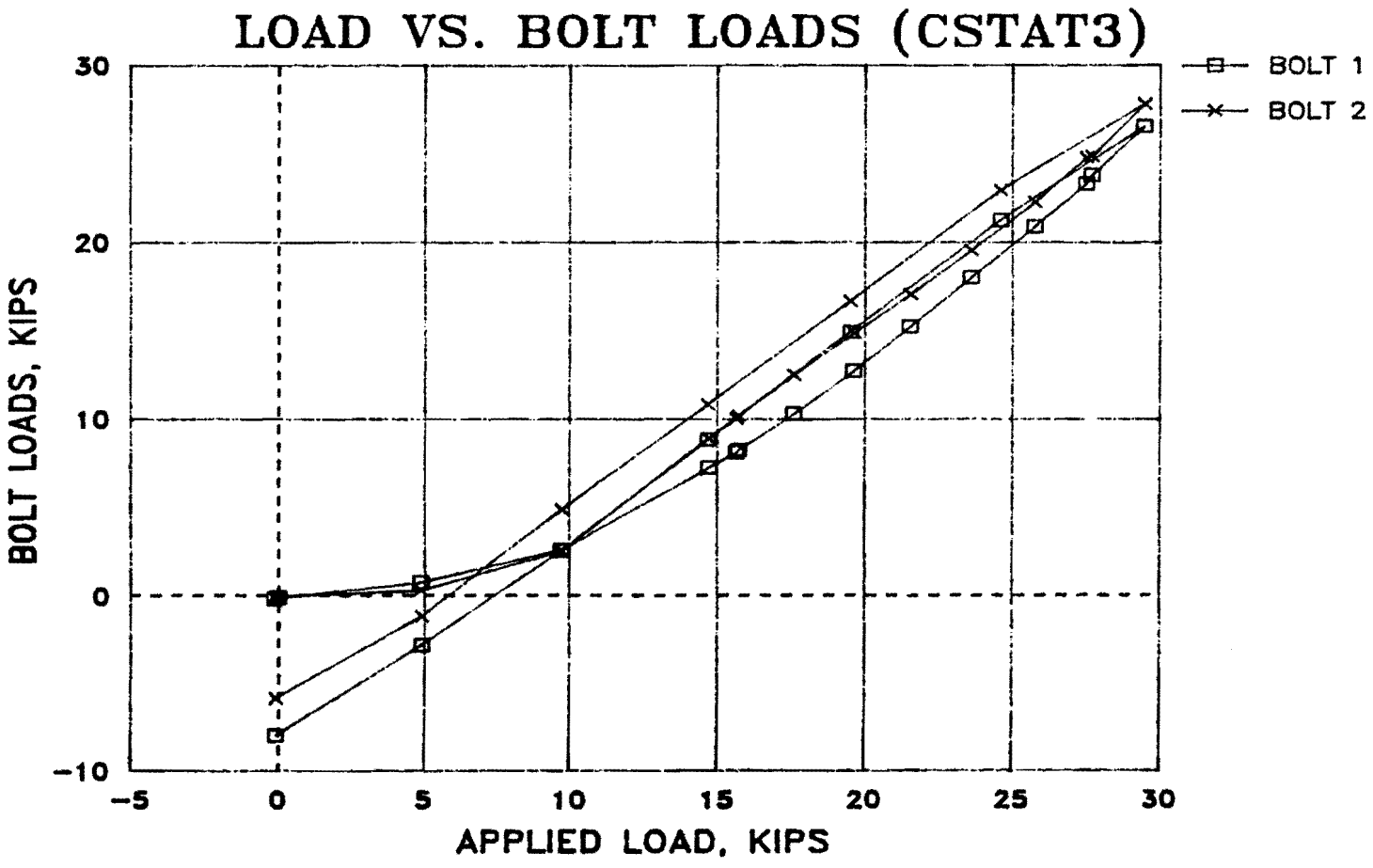

Fig. 4.18 Load vs. bolt loads: CSTAT3
(refer to Fig. 4.1 for anchor bolt locations)

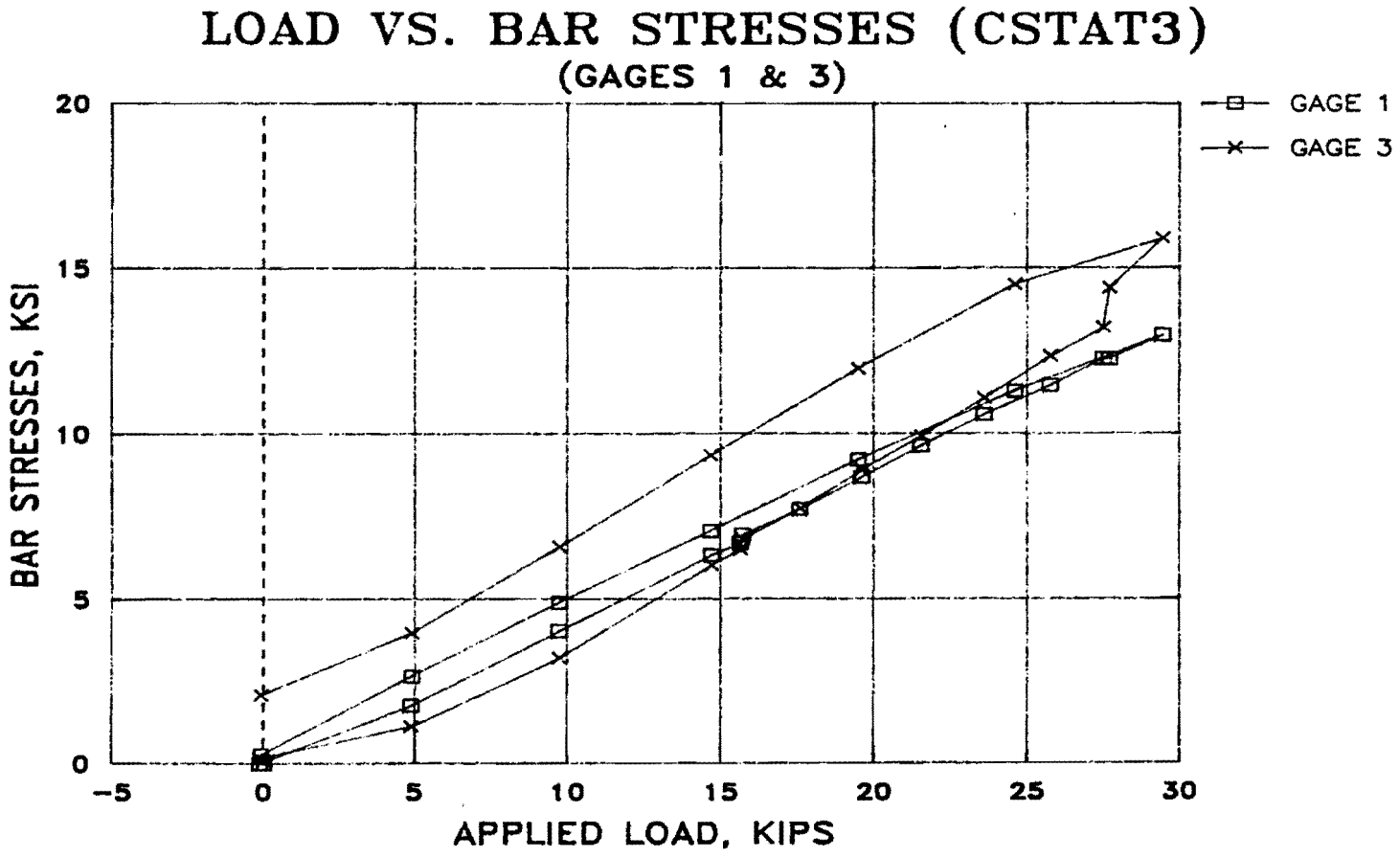

Fig. 4.19 Load vs. bar stresses - gages 1 & 3: CSTAT3
(refer to Fig. 3.21 for strain gage locations)

were applied at each load level. Failure occurred at load level 9A (that is, at the first pulse at load level 9).

A total of 25 tests were therefore conducted during MPACT1, and each test involved data from 8 channels. Little difference was observed among tests to similar peak load levels, and the strain gage data were hard to interpret because of the pre-existing damage from the static tests. To present as much meaningful data as necessary and at the same time keep the number of figures to a reasonable level, data are reported here only for
load levels 2, 4, 6, and 8.

Maximum loads for those load levels are shown in Table 4.1. Due to a malfunction of the data recording system, data for test 9A were not recorded. Based on the sewocontroller settings, the previously observed behavior at lower peak loads, and the calculated failure load as governed by fracture of the sawed bolts, the failure load is estimated at betwen 22 and 26 kips, and was probably closer to 22 kips. Graphs of load, displacement and bolt loads versus time for the first load at load levels 2, 4, 6, and 8 are presented in Appendix B. Graphs of load versus displacement for the first and third loads at each load level are also presented.

4.3.2 MPACT1 Results. At load level 2A, a maximum load of 5.76 kips was applied, and a maximum displacement of 0.16 in. was observed (Figs. B.1 and B.2). The pulse length was approximately 0.2 seconds. As shown in Figs. B.3 and B.4, both bolts exhibited very small tensile loads, with the easternmost bolt (1) assuming a slightly greater load than the central bolt (2).

Load level 4A corresponded to a maximum load of 10.4 kips and a maximum displacement of 0.39 in., as shown in Figs. B.7 and B.8. The pulse length was 0.2 seconds. The central bolt (2) began to assume a greater load than the eastern bolt (1), as shown in Figs. B.9 and B.10. However, both bolt loads were still small, in the 4 to 5-kip range.

Load level 6A corresponded to a maximum load of 11.7 kips and a maximum barrier displacement of 0.49 in. (Figs. B.13 and B.14). The pulse length was approximately 0.2 seconds. Bolts 1 and 2 registered tensile loads of 5.44 and 8.02 kips, respectively, as shown in Figs. B.15 and B.16.

At Load Level 7, corresponding to a maximum load of approximately 15 kips, a horizontal shearing crack developed at the edge of the slab at the location of the initial inclined cracks formed during CSTAT1. The crack is shown in Fig. 4.20. During all

TABLE 4.1 LOADING LEVELS FOR MPACT1

Load Level	Maximum Load , Kips
2	5.76
4	10.4
6	11.7
8	17.4
9	22 (estimated)

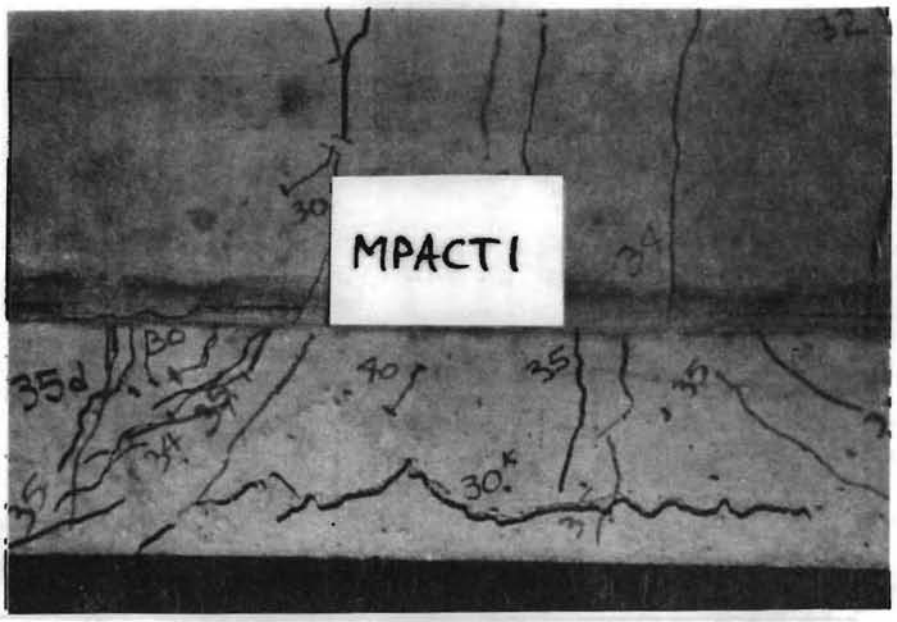

Fig. 4.20 Initial slab shearing crack: MPACT1

Fig. 4.21 Slab shearing failure: MPACT1

subsequent loads, the concrete above the crack began to shear downward.

At Load Level 8A, a maximum load of 17.4 kips and a maximum displacement of 0.8 in. were recorded, as shown in Figs. B.19 and B.20. The pulse length was approximately equal to 0.40 seconds. Bolts 1 and 2 registered loads of 10.3 and 15.9 kips respectively, as shown in Figs. B.21 and B.22. The predicted bolt yield and bolt fracture loads for the altered bolts were 14.2 and 22.3 kips, respectively.

Failure occurred at Load 1Lvel 9A. Although data were unavailable for this load level, it is estimated that the maximum load was in the range of 22 to 26 kips. Failure was marked by the fracture of all three anchor bolts. Fracture of the bolts was accompanied by a slab shearing failure (Fig. 4.21) at the location of the shearing crack found at Load Level 7.

Figures B.5, B.6, B.11, B.12, B.17, B.18, B.23 and B.24 show barrier load-displacement behavior for the first and third loadings at Load Levels 2, 4, 6, and 8, respectively. At each load level, the load-displacement behavior for the first (A) and third (C) loadings are practically identical. This indicates no appreciable degradation of barrier response within each load level.

4.4 General

All anchor bolts used in CSTAT1, CSTAT2, CSTAT3, and MPACT1 were examined after each test. It should be noted that no evidence of shear distress was observed in any of the bolts.

CHAPTER 5

DISCUSSION OF RESULTS

5.1 General

This chapter contains interpretation of data from the static and dynamic barrier tests, as well as, an evaluation of cast-in-place and precast barrier performance. The remainder of the chapter is devoted to a discussion of the failure mechanisms observed.

5.2 Discussion of Data

This section contains a discussion of load-displacement behavior, bolt loads and reinforcing bar stresses for the static and dynamic tests. The discussion is based on graphical data for the static and dynamic tests, which are presented in Chapter 4 and Appendix B, respectively.

5.2.1 Load-Displacement Behavior. The load-displacement behavior observed during the three static tests was fairly consistent. (See Figs. 4.7, 4.13, and 4.17). Displacment increased at an increasing rate during loading and failed to return to zero upon unloading, indicating permanent deformation. The loss of lateral stiffness shown in those figures is due to slab cracking, crushing of the grout pad in the compression zone, and seating of the anchor bolts. Evidence of slab cracking can be seen in Fig. 4.7. The loading portion of the load-displacement curve for CSTAT1 is bilinear, with a change in slope occurring at a load of 25 kips. This bilinearity is not present in the two subsequent static tests (Figs. 4.13 and 4.17).

The performance of the anchorage systems had the greatest effect on barrier system stiffness. The stiffest anchorage (six A36 bolts, used in CSTAT1), produced an average loading stiffness of approximately 42 kips per inch. Average stiffnesses of 31 and 33 kips per in. were obtained for CSTAT2 and CSTAT3, respectively. It is interesting to note that the stiffness obtained for CSTAT2, using three A36 bolts, was less than that obtained for CSTAT3, which involved the use of only two A36 bolts.

Load vs. displacement curves for the dynamic test, MPACT1, are presented in Appendix B. In comparing the curves for the first

pulse at Load Levels 2, 4, 6, and 8 (Figs. B.5, B.11, B.17, and B.23, respectively), it can be seen that the average barrier system stiffness decreases with each increasing load level. Pulses 2A, 4A, 6A, and 8A correspond to stiffnesses of approximately 36, 27, 27, and 22 kips per in., respectively. This loss of stiffness is expected, due to the deterioration of the slab as loads are increased. However, no degradation was observed within each load level. When curves for pulses A and C within the same load level are compared (Figs. B.5 and B.6, for example), virtually no difference is discernible. Therefore, no apparent additional damage was sustained after the first pulse at each load level.

5.2.2 Bolt Loads. It was generally expected that anchor bolts nearer the point of loading would carry more load than outside bolts, due to the torsional flexibility of the barriers. Most of the test results confirmed this expectation. As shown in Fig. 4.8, the distribution of loads among the three easternmost bolts used in CSTAT1 followed the expected pattern. However, the three westernmost bolts carried almost identical maximum loads (Fig. 4.9), although the distribution of loads during loading followed the pattern. During CSTAT2 (Fig. 4.15), the central bolt (2) carried less load than the two outside bolts. This is possibly due to an outward redistribution of vertical compressive stress acting on the slab, caused by the inclined slab cracks sustained during CSTAT1. The distribution of bolt loads for CSTAT3 (Fig. 4.18) was as expected: the bolts, which were positioned symmetrically about the loading point, each carried approximately the same load.

The ratio of individual bolt loads to applied load increased as fewer anchor bolts were used, as expected. This can be seen by comparing the average bolt loads for a given applied load in Figs. 4.8, 4.9, 4.15, and 4.18. In CSTAT3, where only two anchor bolts were used, maximum bolt loads approached the test yielding load.

During the dynamic test (MPACT1), in which three anchor bolts were used, the central bolt (2) carried a greater load than the easternmost bolt (1) at every reported load level except Level 2 (Figs. B.3, B.4, B.9, B.10, B.15, B.16, B.21, and B.22). Again, this was the expected pattern of bolt load distribution.

It should be noted that some inaccuracy is inherent in the bolt load data due to preloading of bolts and differences in the amount of preload among bolts in a particular anchorage. The data for MPACT1 may be further affected by an eccentric loading of the bolt load cells, caused by the cuts which were made in the bolts in order to reduce their area and produce a ductile failure.

5.2.3 Reinforcing Bar Stresses. As in the case of the anchor bolts, it was expected that bars closer to the loaded point on the barrier would experience higher tensile stresses. This was generally confirmed by the static tests. As shown in Fig. 4.10, the bar (Gage 2) located near a central anchor bolt (4) in CSTAT1 experienced a higher stres than the outer bars. Note that Gages 2 and 5, located near Bolts 4 and 6, respectively, underwent a sudden increase in stress at a load near 25 kips. This increase was caused by flexural cracking of the slab, which was previously deduced from the abrupt change in slope of the load-displacement curve for CSTAT1 (Fig. 4.7), at that same load.

The distribution of bar stresses in CSTAT2 (Fig. 4.16) followed the above pattern. However, as shown in Fig. 4.19, the bar stresses monitored in CSTAT3 did not reflect that same behavior. The bar positioned in the center of the slab, between the two anchor bolts (Gage 1 of Fig. 3.21), experienced a lower maximum tensile stres than the bar positioned near Anchor Bolt 2 (Gage 3). This was partly due to the fact that moment transfer from the barrier to the slab was concentrated at anchor bolt locations. In addition, the central portion of the slab had lost some load-carrying capacity because of inclined cracking. Due to probable damage to the gages during the prior static tests, strain gages were not monitored during dynamic testing.

5.3 Barrier Performance

The observed performances of the cast-in-place and the precast barriers were virtually identical. Because both barriers were heavily reinforced in order to force a failure in the anchorage zone itself, only minor cracking was sustained by each barrier. The cracks were initiated at relatively high loads and had no noticable effect on the performance of either barrier. Although both barriers were flexurally very stiff, each exhibited some torsional flexibility, as might be expected. This flexibility was evidenced by the tendency of anchor bolts and reinforcing bars near the point of loading to sustain higher loads than the bolts and reinforcement located farther from the loading point. Slab damage was also limited to an area surrounding the loading point.

No difference was observed between the behavior of the bent anchor bolts (used in the cast-in-place barrier), and the straight bolts (used in the precast barrier). Because the bends in the bent bolts were completely confined by concrete, they were not expected to alter bolt behavior. The bolt tests described in Chapter 3 confirmed this assumption.

The tests performed in this study were intended to provide an understanding of barrier anchorage zone behavior at failure. It should be noted that local failure of the barrier itself, although intentionally prevented in this case, is a distinct possibility in the case of a normally reinforced barrier.

5.4 Description of Failure

Anchor bolt fracture occurred during pulse 9A of MPACT1, at an estimated load of 22 kips. The bolts fractured at the locations where cuts had been made. Fracture of the anchor bolts was accompanied by a local shearing failure of the top corner of the slab, near the free edge (Figs. 2.4 and 4.21). However, most of the cracking which led to the shearing failure had already occurred at Load Level 7, corresponding to a maximum load of approximately 15 kips (Fig. 4.20).

The local shearing failure surface had an approximate width of 18 inches. This unanticipated localized effect was caused by the torsional flexiblity of the barrier, which prevented the barrier from distributing compressive loads to the entire length of the slab. Consequently, localized zones of compression tended to be centered around the point of loading and around the anchor bolt locations.

Some of the failure surfaces of the shearing mechanism coincided with the inclined cracks sustained by the slab during CSTAT1 (Fig. 4.4). The inclined cracks were part of a flexural-torsional failure mechanism which had begun to develop during CSTAT1. This mechanism is shown schematically in Fig. 5.1. It was characterized by failure surfaces which projected downward and outward from the localized compression zone, forming a trapezoidal prism. The development of the mechanism in the test slab can be seen in Fig. 4.5. This type of failure mechanism had been anticipated and designed against in the steel post barrier tests of Ref. 7. However, it was not expected in the concrete barrier tests described here.

5.5 Ductility Associated with Observed Failure Mechanism

Although the concrete barriers tested in this study did exhibit bolt fracture at failure, it is obvious that the anchorage designs used in this series of tests lacked sufficient ductility. A flexural-torsional failure mechanism began to form at relatively low loads, and fracture of the anchor bolts was accompanbied by a brittle shearing failure of the top outside corner of the slab. The initial cracks leading to the development of the flexural-torsional mechanism formed during CSTAT1, in which six anchor bolts were used. It is

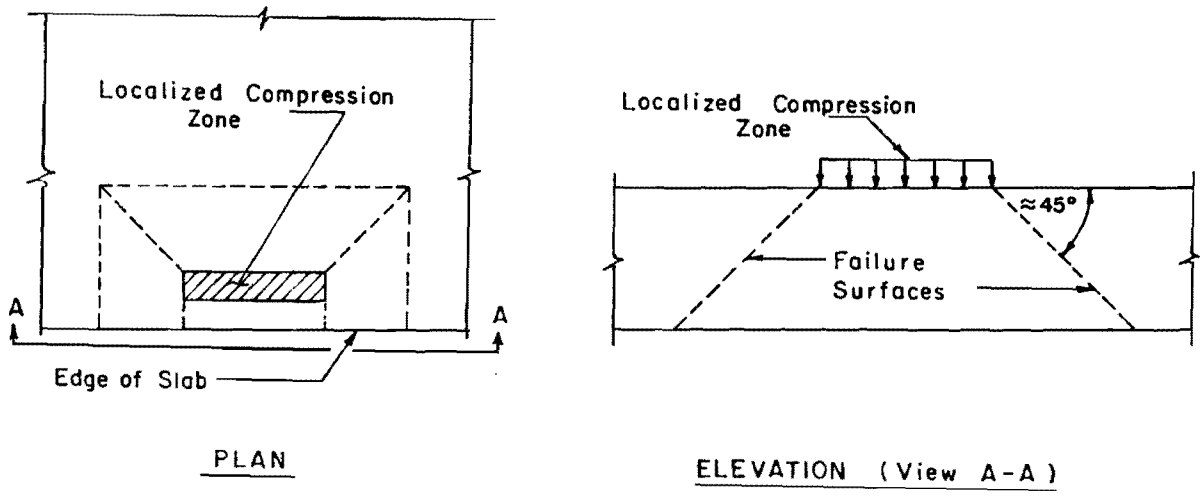

Fig. 5.1 Flexural-torsional failure mechanism

possible that a ductile failure may have been achieved, had not such a relatively strong anchorage system been used in the first test.

CHAPTER 6

SUMMARY, CONCLUSIONS, AND RECOMMENDATIONS

6.1 Summary

The purpose of this study was to investigate the behavior of proposed anchorage designs for two Texas SDHPT T5 concrete traffic barriers, subjected to static and dynamic loads. It was believed that the current design, which specifies the use of 1-in. diameter A193, Grade B7 anchor bolts, spaced at 50 in., lacked sufficient ductility. Therefore, an anchorage system consisting of 1-in. diameter, A36 bolts, spaced at 25 in., was proposed. Larger spacings of the proposed anchor bolts were also investigated.

Two barriers were constructed and tested: a cast-in-place barrier, with six 1-in. diameter A36 anchor bolts, spaced at 25 in.; and a precast barrier, capable of accommodating a variety of anchor bolt patterns. A 10-in. test slab, representing a typical Texas SDHPT slab overhang, was also constructed and used in all tests.

Four tests were conducted. The first, designated as CSTAT1, was a static test perofrmed on the cast-in-place barrier, anchored to the slab with the six-bolt configuration. The remaining two static tests, CSTAT2 and CSTAT3, were performed on the precast barrier. In CSTAT2, the barrier was anchored to the slab with three 1-in. diameter, A36 anchor bolts, spaced at 50 inches. Two 1-in. diameter, A36 anchor bolts, spaced at 75 inches, were used in CSTAT3. The final test, MPACT1, was a dynamic test performed on the precast barrier, anchored to the slab with three 1-in. diameter, A36 bolts, spaced at 50 inches. Each of the anchor bolts used in MPACT1 was sawed in half to encourage a ductile failure.

Brittle behavior was observed in the three static tests. Loading was discontinued furing these tests, due to the development of a localized flexural-torsional failure mechanism in the slab, located near the point of load application. Excessive slab cracking, which initiated the development of this mechanism, was sustained by the slab during the first static test (CSTAT1).

Somewhat greater ductility was observed in the dynamic test (MPACT1). Failure was achieved through fracture of the anchor bolts. However, anchor bolt failure was accompanied by a brittle shearing failure of the corner of the slab.

6.2 Conclusions

In general, the proposed anchorage design did not exhibit a ductile failure, even under static loads. It is therefore believed that the existing design, which specifies the use of anchor bolts with a similar total tensile capacity, would have behaved in a similarly brittle manner. Decreasing the number of bolts did promote more ductile failure modes, but at the cost of lower barrier strength.

The potential flexural-torsional failure mechanism was controlled by slab flexural reinforcement crossing the failure surfaces of the mechanism. However, the primary failure surface of the local shearing mechanism (which formed at fracture of the anchor bolts in MPACT1) was located outside the slab reinforcment. Because of the 2-in. top cover requirement specified by the Texas SDHPT, a barrier edge distance of approximately 3 inches would be reuqired in order for that shearing failure surface to be intercepted by transverse reinforcing bars.

In general, the tests indicated that the current and proposed concrete barrier anchorage designs have insufficient ductility. A possible solution is the use of smaller and/or lower strength anchor bolts. A smaller spacing of the bolts would then be required to avoid a loss of barrier system load capacity.

6.3 Recommendations

Further research to develop a more ductile anchorage system for the safety shape concrete traffic barrier is recommended. Because the current Texas SDHPT slab reinforcment scheme does not adequately resist the development of flexural-torsional and shearing failure mechanisms in the slab, anchor bolt strengths must be lowered. Therefore, any subsequent investigations should include the use of smaller and/or lower strength anchor bolts. A variety of anchor bolt spacings should also be investigated, in order to determine the effect of bolt spacing on overall barrier system capacity (assuming that a ductile failure mode can be obtained). It is believed that a decreased spacing of lower strength anchor bolts could prevent a loss of barrier capacity, while also providing the desired level of ductility.

APPENDIX A

APPENDIX A

EXISTING STRENGTH ANALYSIS

Using nominal material strength values:

Bolt Fracture:

$$P = \frac{A_b f_{ult}}{H}\left[Z - \frac{A_b f_{ult}}{1.7 f'_c b}\right] \qquad (Eq.\ 2.4)$$

$$= \frac{1.818(125)}{26}\left[10.5 - \frac{1.818(125)}{1.7(4)150}\right] = \underline{89.8 \text{ Kips}}$$

Substituting f_y for f_{ult} in the above equation, the load at bolt yielding can be determined:

$$P = \frac{1.818(105)}{26}\left[10.5 - \frac{1.818(105)}{1.7(4)150}\right] = \underline{75.7 \text{ Kips}}$$

Concrete Pullout:

$$P = \frac{4\sqrt{f'_c}A_c}{H}\left[Z - \frac{2.35\sqrt{f'_c}A_c}{f'_c b}\right] \qquad (Eq.\ 2.5)$$

$$= \frac{4\sqrt{4000}(1056)}{1000(26)}\left[10.5 - \frac{2.35\sqrt{4000}(1056)}{1000(4)150}\right] = \underline{105 \text{ Kips}}$$

Shearing Failure of Slab:

$$\frac{\mu N}{A_v} = \frac{T}{2b(D+B_1c)} = \frac{227.25}{2(150)(1.5+0.446)} = 0.39 \text{ ksi} < 0.8 \text{ ksi}$$

(acceptable) (Eq. 2.6)

Flexural Failure of Slab:

$$P = \frac{A_s f_y}{H}\left[d - \frac{A_s f_y}{1.7 f'_c b}\right] \qquad (Eq.\ 2.7)$$

$$= \frac{9.3(60)}{26}\left[5.69 - \frac{9.3(60)}{1.7(4)150}\right] = \underline{110 \text{ Kips}}$$

Using actural material strength values:

Bolt Fracture:

$$P = \frac{1.818(154)}{26}\left[10.5 - \frac{1.818(154)}{1.7(5.7)150}\right] = \underline{111 \text{ Kips}}$$

Bolt Yielding:

$$P = \frac{1.818(105)}{26}\left[10.5 - \frac{1.818(105)}{1.7(5.7)150}\right] = 76.1 \text{ Kips}$$

Concrete Pullout:

$$P = \frac{4\sqrt{5700}(1056)}{1000(26)}\left[10.5 - \frac{2.35\sqrt{5700}(1056)}{1000(5.7)150}\right] = 126 \text{ Kips}$$

Shearing Failure of Slab:

$$\frac{\mu N}{A_v} = \frac{279.97}{2(150)(1.5+0.385)} = 0.5 \text{ Ksi} < 0.8 \text{ Ksi}$$
(acceptable)

Flexural Failure of Slab:

$$P = \frac{9.3(53)}{26}\left[5.69 - \frac{9.3(53)}{1.7(5.7)150}\right] = 101 \text{ Kips}$$

PROPOSED DESIGN STRENGTH ANALYSIS

Using nominal material strength values:

Bolt Fracture:

$$P = \frac{3.636(69)}{26}\left[10.5 - \frac{3.636(69)}{1.7(4)150}\right] = 98.9 \text{ Kips}$$

Bolt Yielding:

$$P = \frac{3.636(36)}{26}\left[10.5 - \frac{3.636(36)}{1.7(4)150}\right] = 52.2 \text{ Kips}$$

Concrete Pullout:

as before, $P = 105$ Kips

Shearing Failure of Slab:

$$\frac{\mu N}{A_v} = \frac{250.88}{2(150)(1.5+0.492)} = 0.42 \text{ Ksi} < 0.8 \text{ Ksi}$$
(acceptable)

Flexural Failure of Slab:

as before, P = 110 kips

Using actual material strength values:

Bolt Fracture:

$$P = \frac{3.636(73.5)}{26}\left[10.5 - \frac{3.636(73.5)}{1.7(5.7)150}\right] = 106 \text{ Kips}$$

Bolt Yielding:

$$P = \frac{3.636(46.7)}{26}\left[10.5 - \frac{3.636(46.7)}{1.7(5.7)150}\right] = 67.8 \text{ Kips}$$

Concrete Pullout:

as before, $P = 126$ Kips

Shearing Failure of Slab:

$$\frac{\mu N}{A_v} = \frac{267.25}{2(150)(1.5+0.368)} = 0.48 \text{ Ksi} < 0.8 \text{ Ksi}$$ (acceptable)

Flexural Failure of Slab:

as before, P = 101 kips

Note - Since the bends in the bent bolts are restrained by concrete, the bends were assumed to have no effect on bolt behavior. Therefore, the actual strengths of the bent bolts were assumed to equal those of the straight bolts.

APPENDIX B

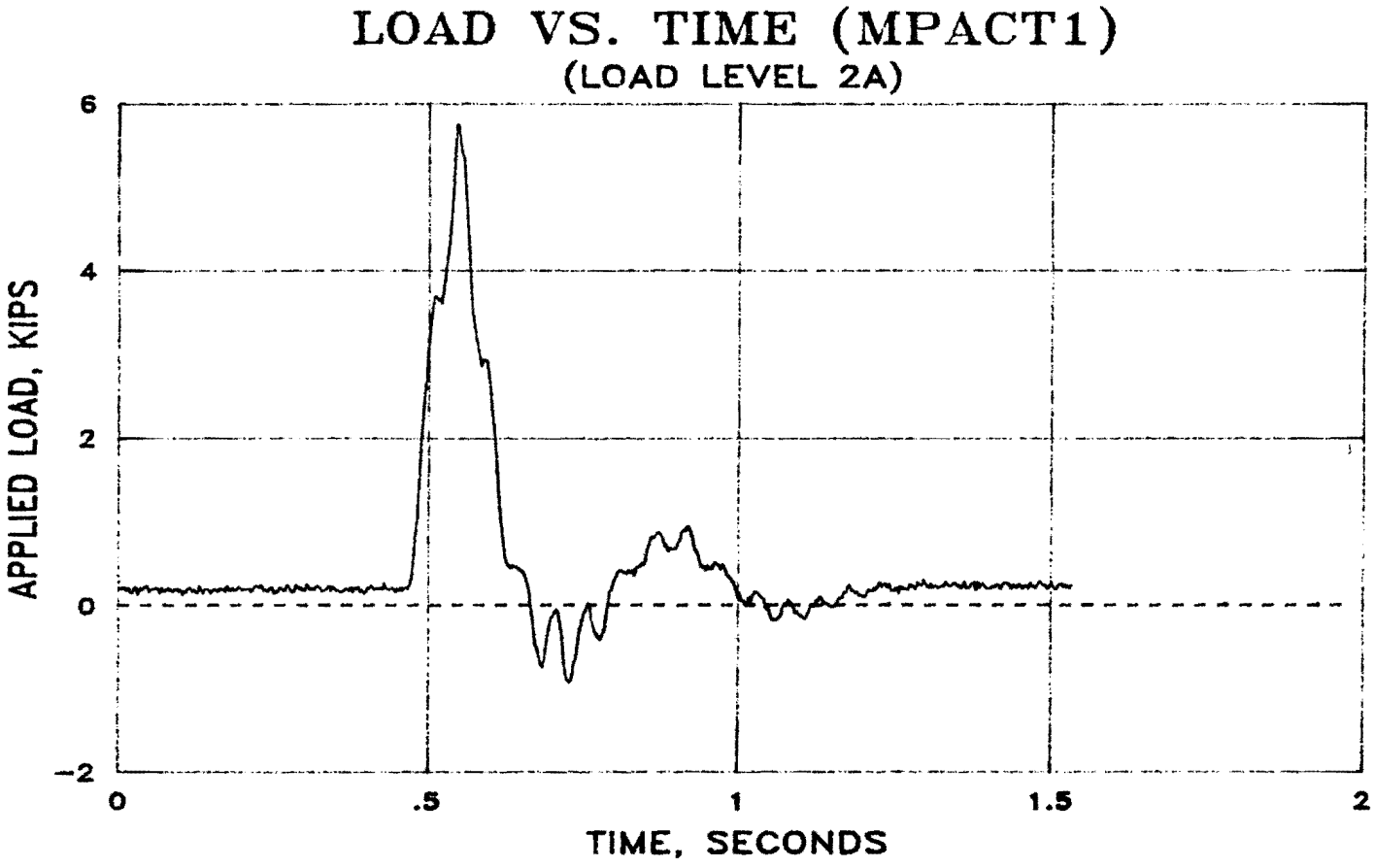

Fig. B.1 Load vs. time - load level 2A: MPACT1

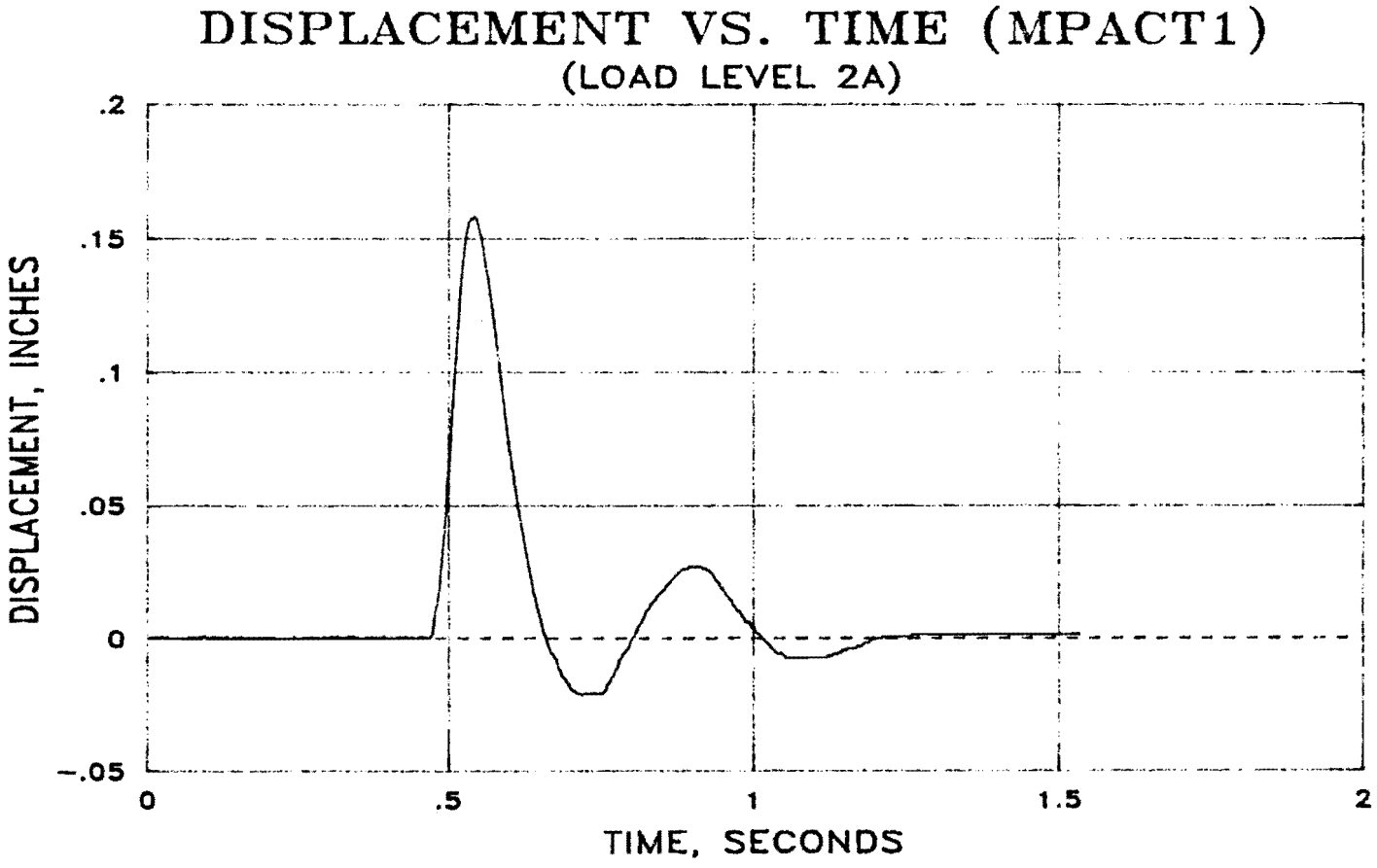

Fig. B.2 Displacement vs. time - load level 2A: MPACT1

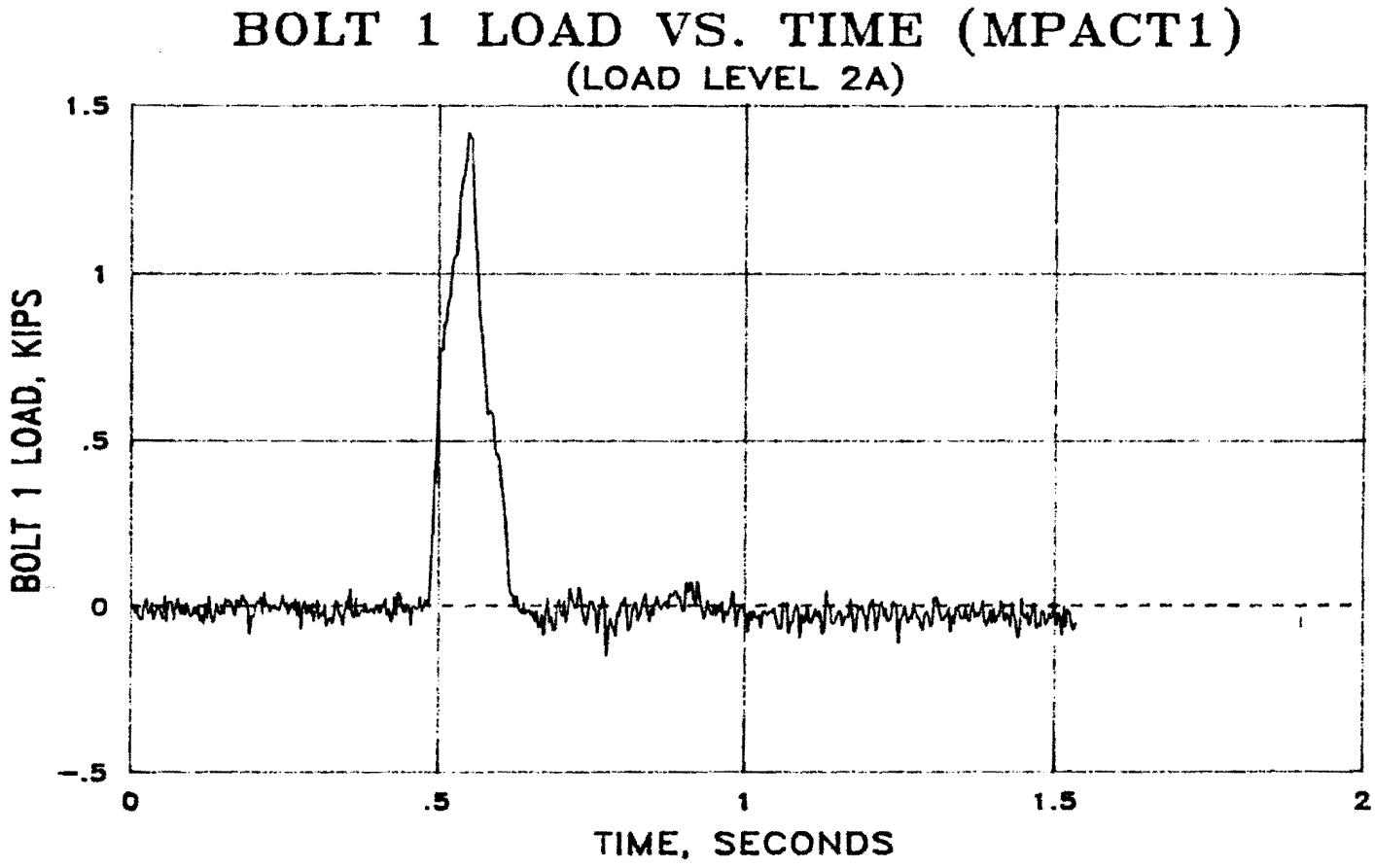

Fig. B.3 Bolt 1 load vs. time - load level 2A: MPACT1
(refer to Fig. 4.1 for anchor bolt locations)

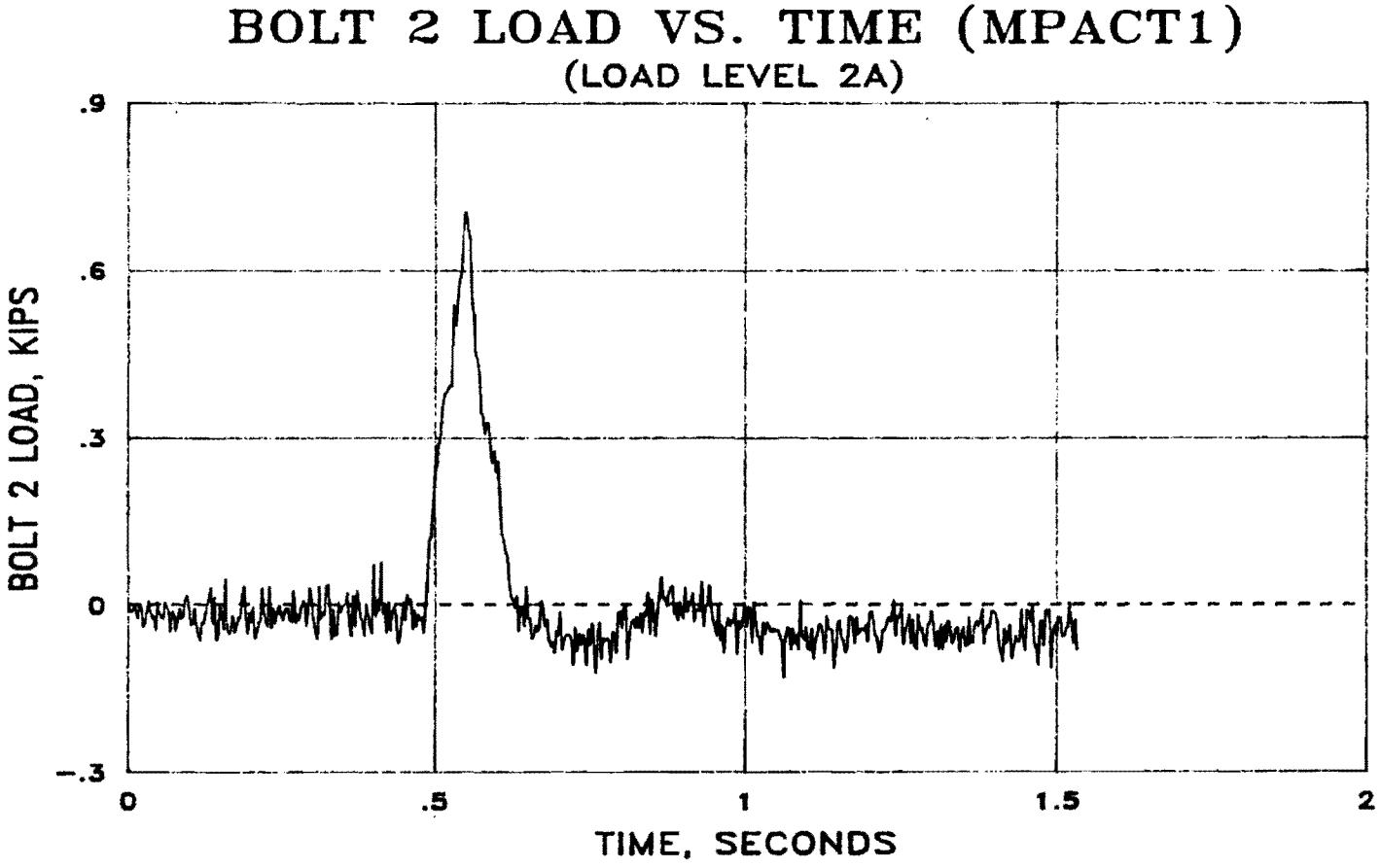

Fig. B.4 Bolt 2 load vs. time - load level 2A: MPACT1
(refer to Fig. 4.1 for anchor bolt locations)

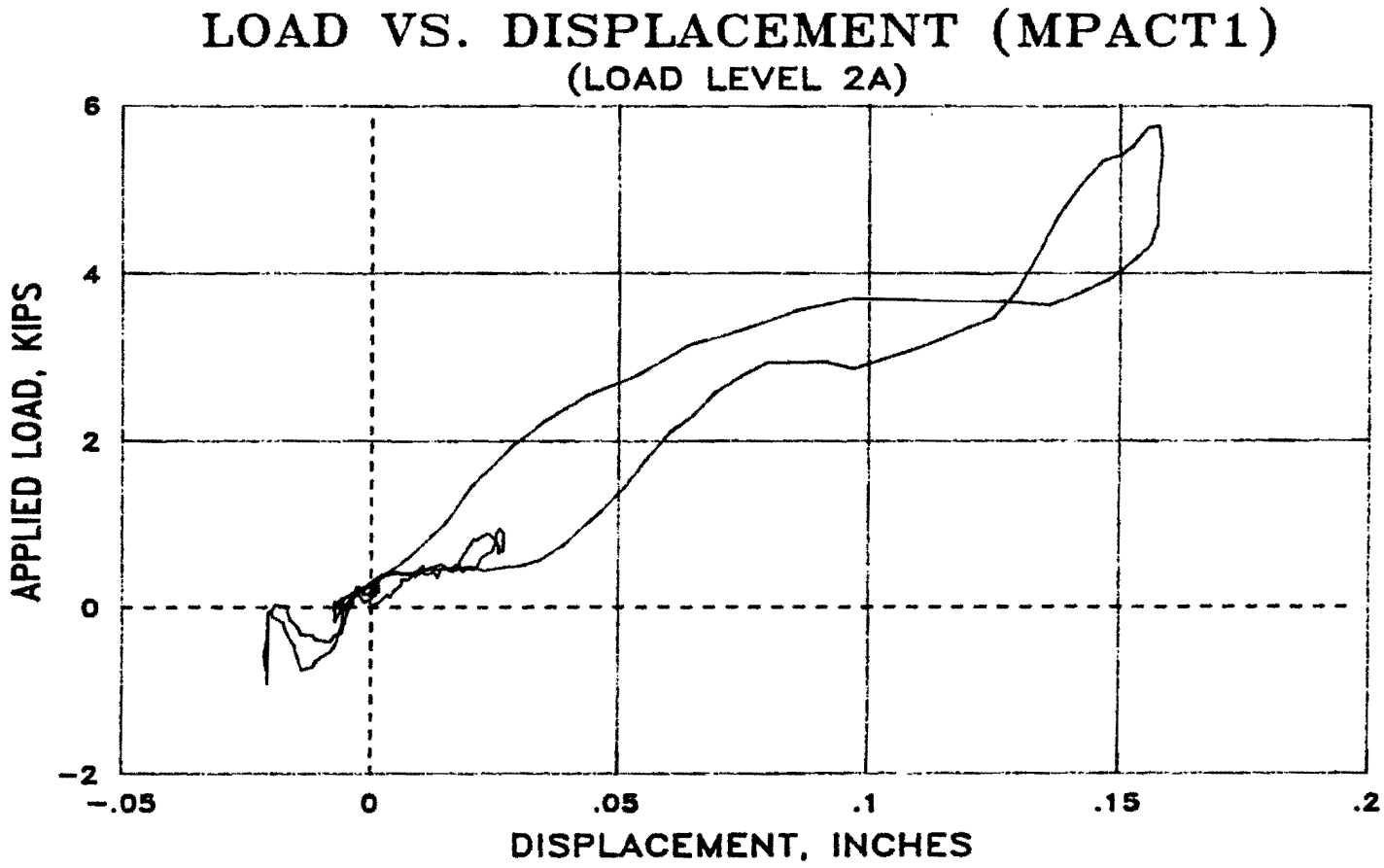

Fig. B.5 Load vs. displacement - load level 2A: MPACT1

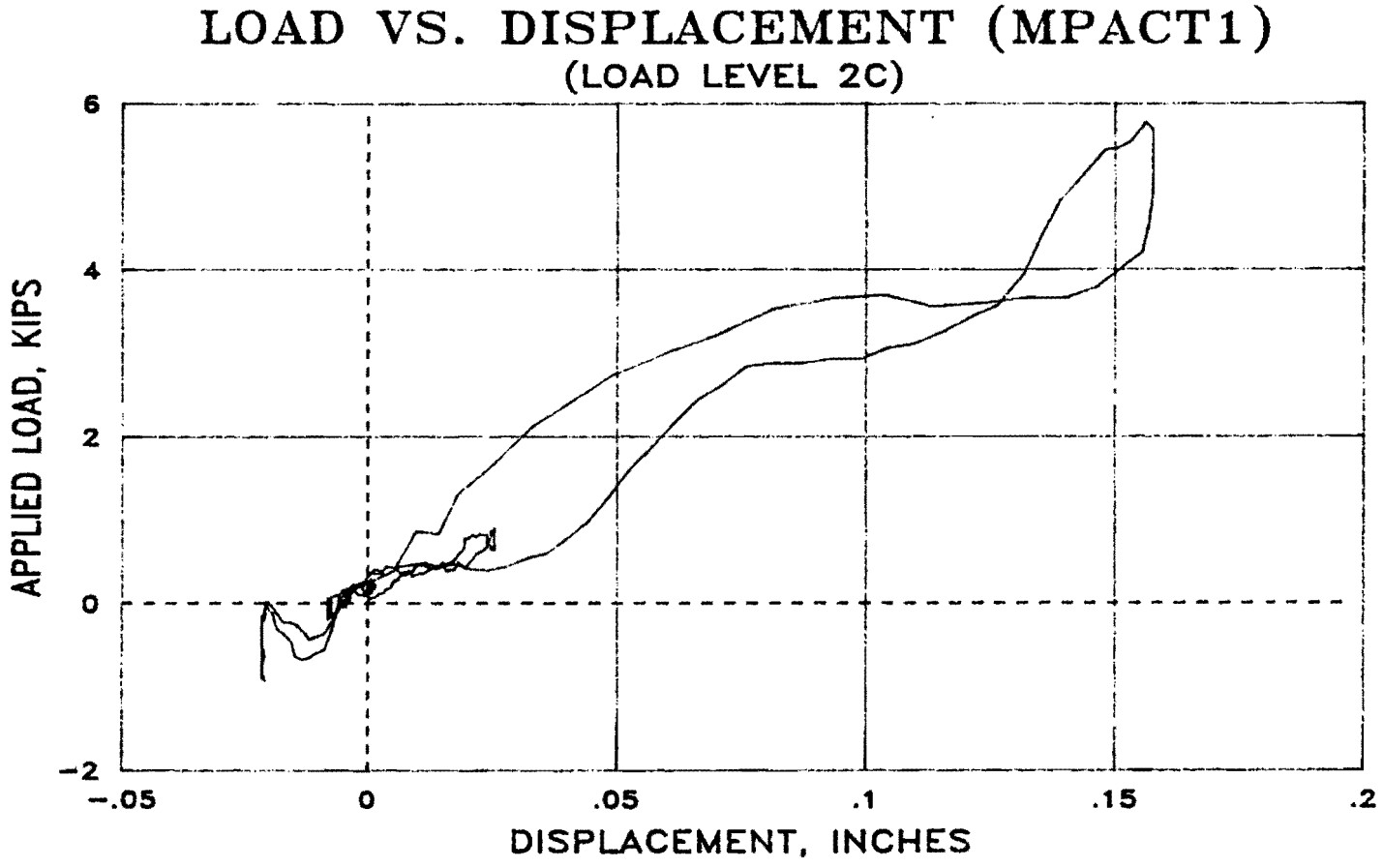

Fig. B.6 Load vs. displacement - load level 2C: MPACT1

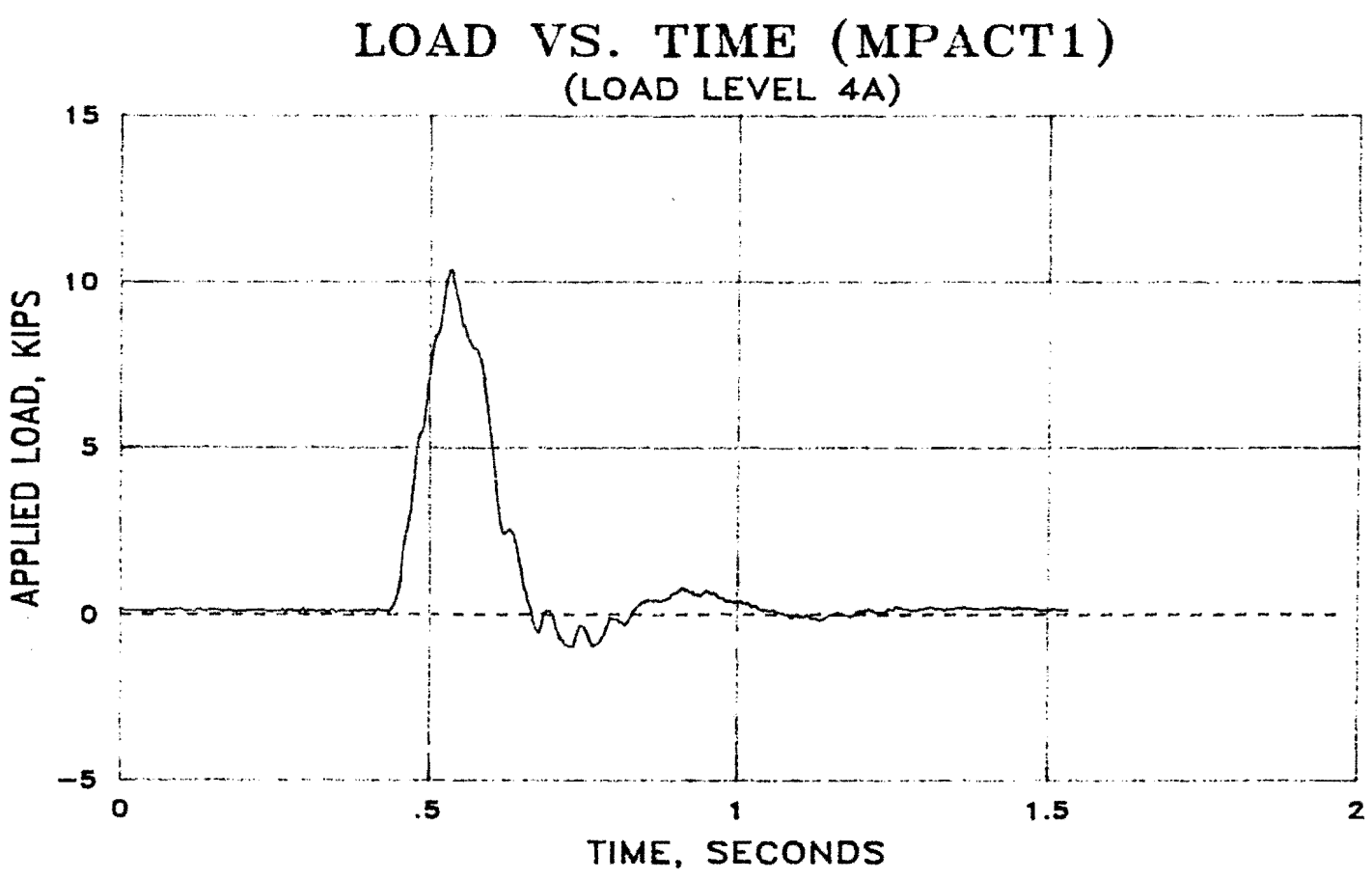

Fig. B.7 Load vs. time - load level 4A: MPACT1

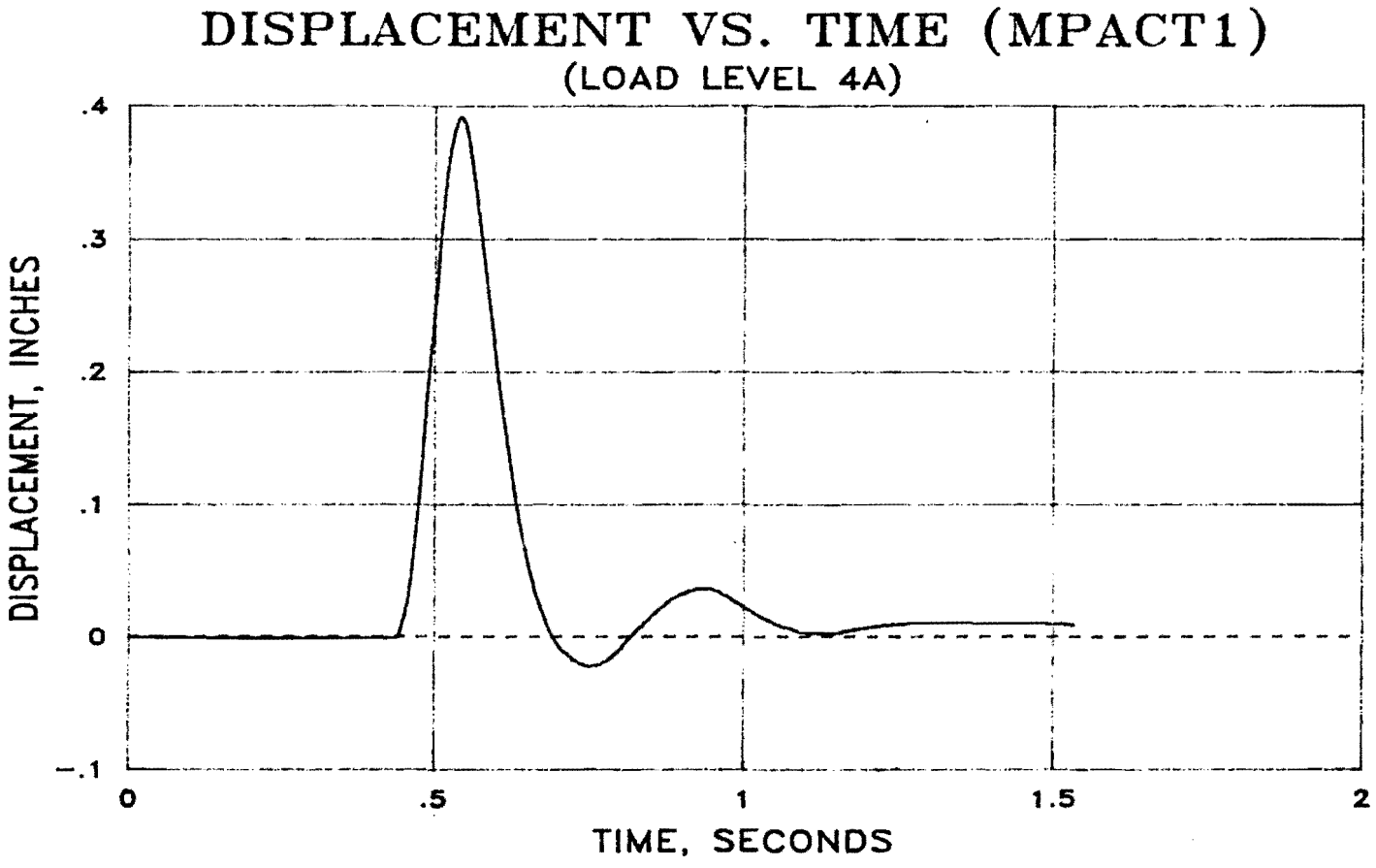

Fig. B.8 Displacement vs. time - load level 4A: MPACT1

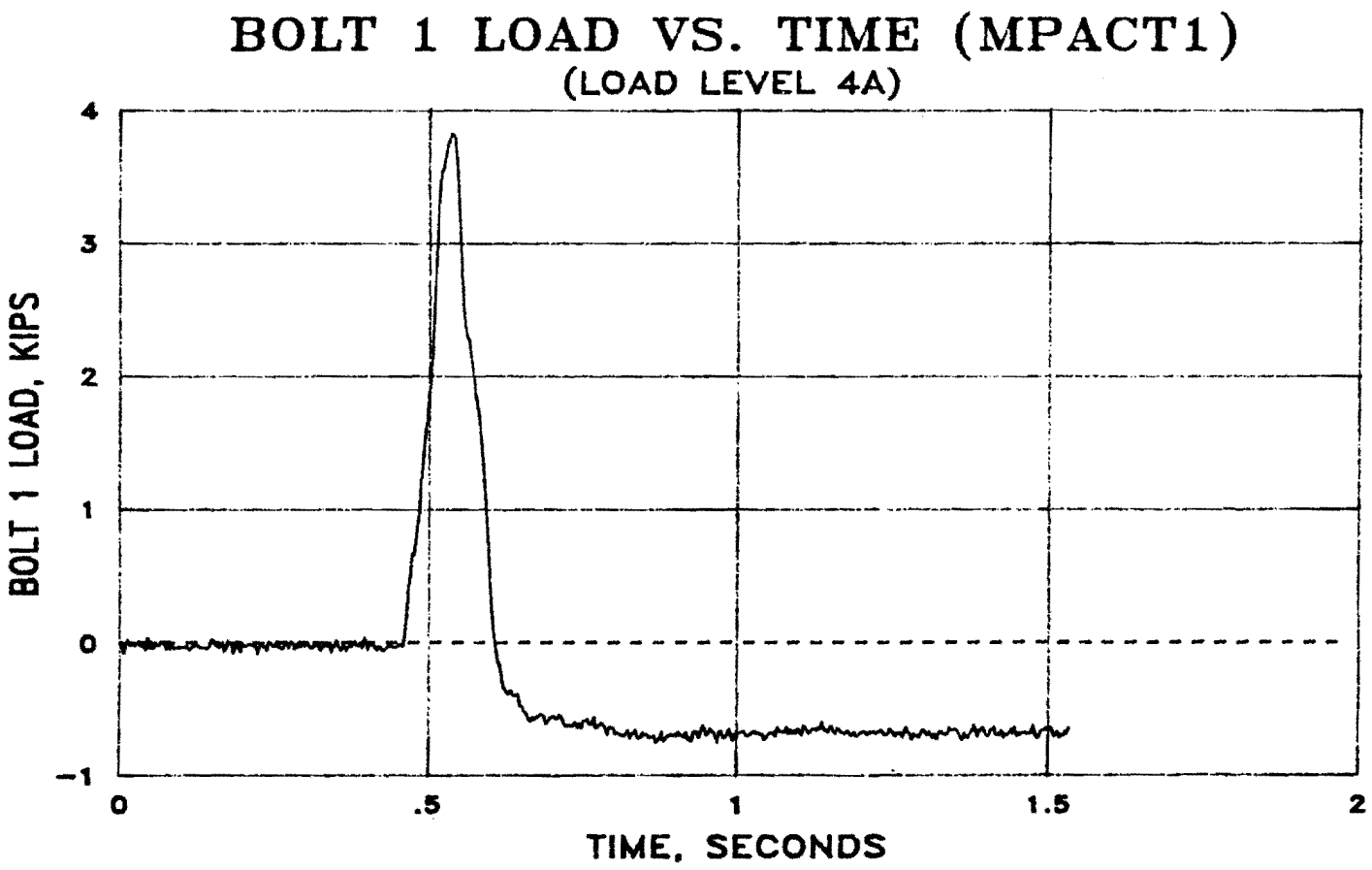

Fig. B.9 Bolt 1 load vs. time - load level 4A: MPACT1
(refer to Fig. 4.1 for anchor bolt locations)

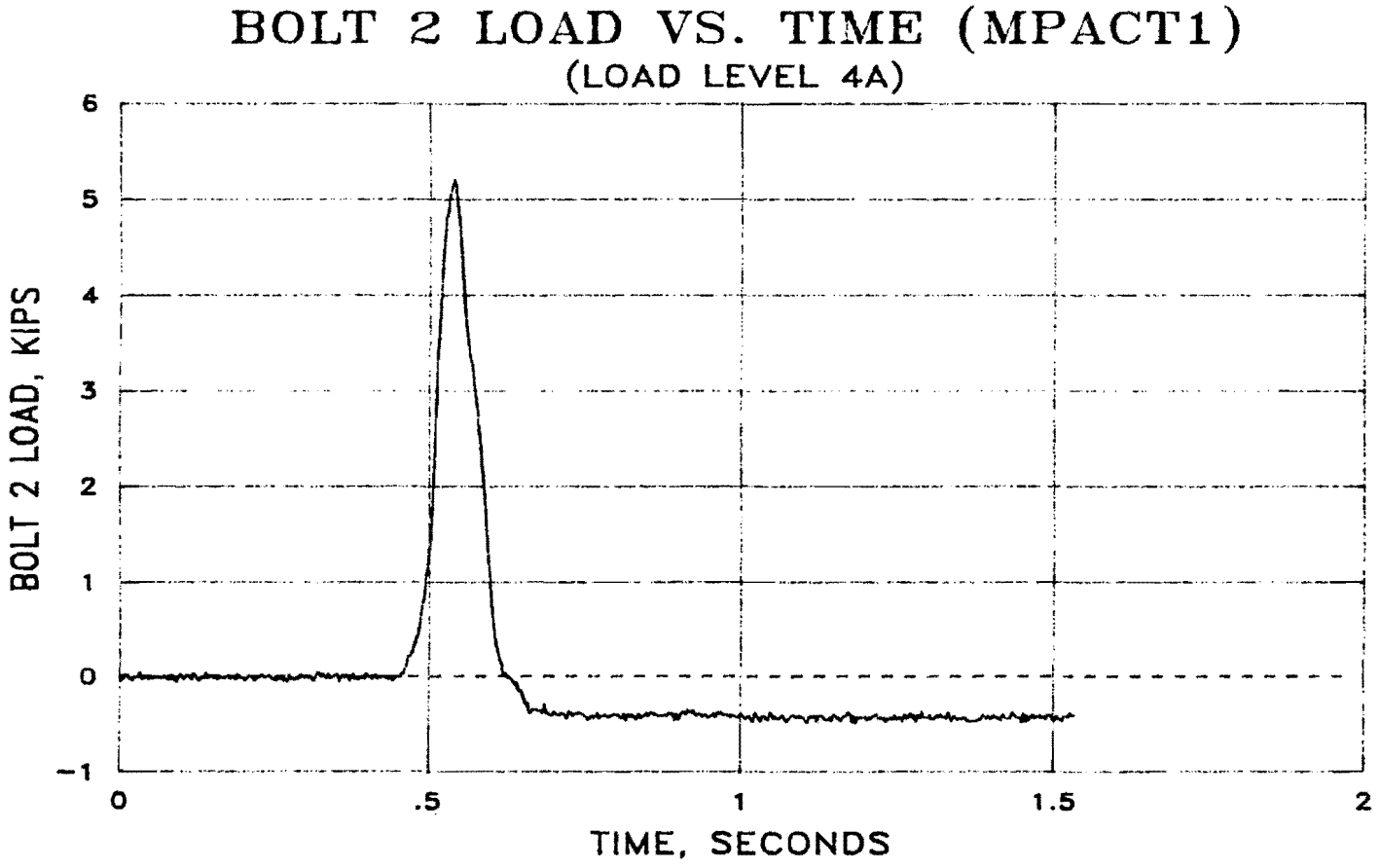

Fig. B.10 Bolt 2 load vs. time - load level 4A: MPACT1
(refer to Fig. 4.1 for anchor bolt locations)

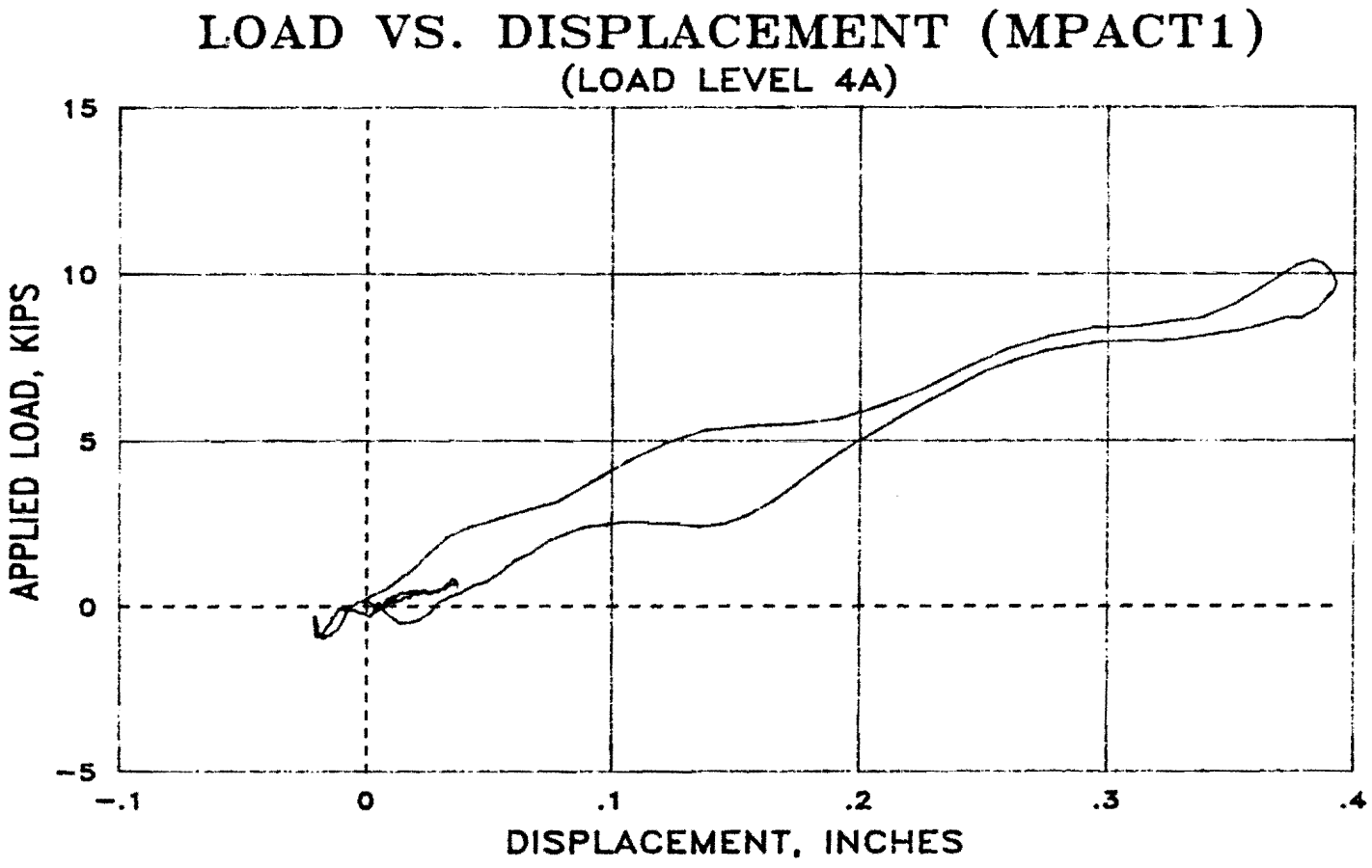

Fig. B.11 Load vs. displacement - load level 4A: MPACT1

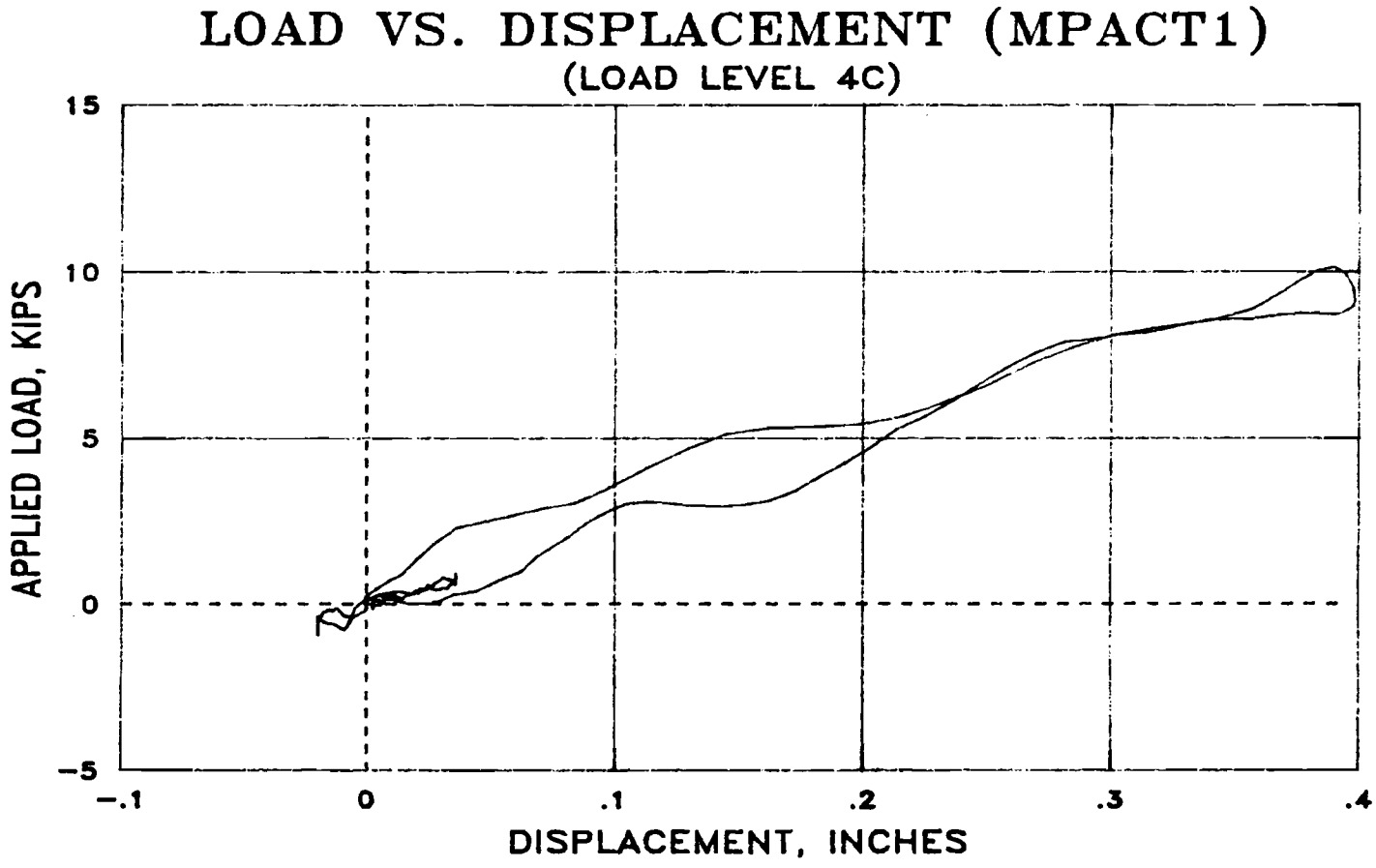

Fig. B.12 Load vs. displacement - load level 4C: MPACT1

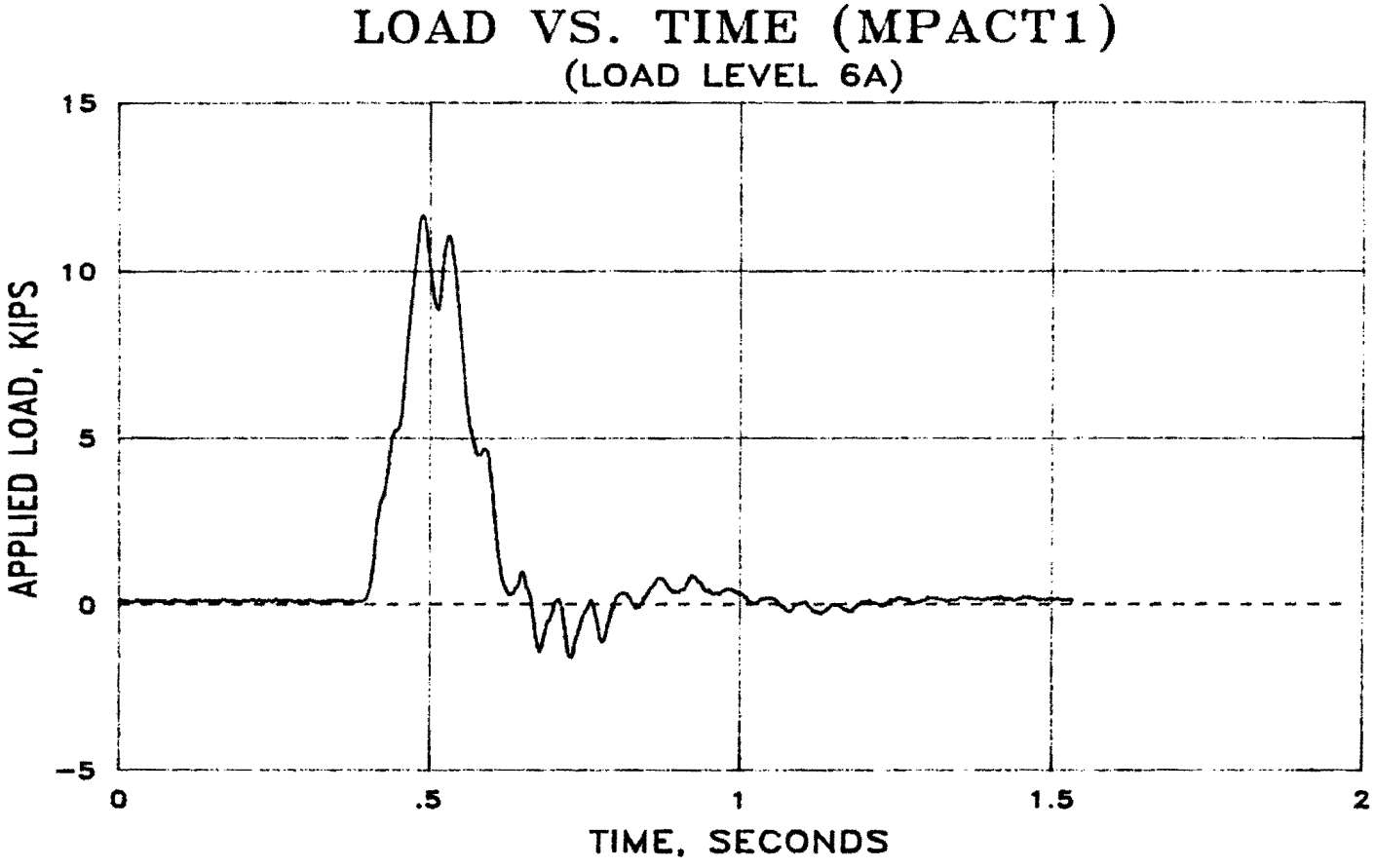

Fig. B.13 Load vs. time - load level 6A: MPACT1

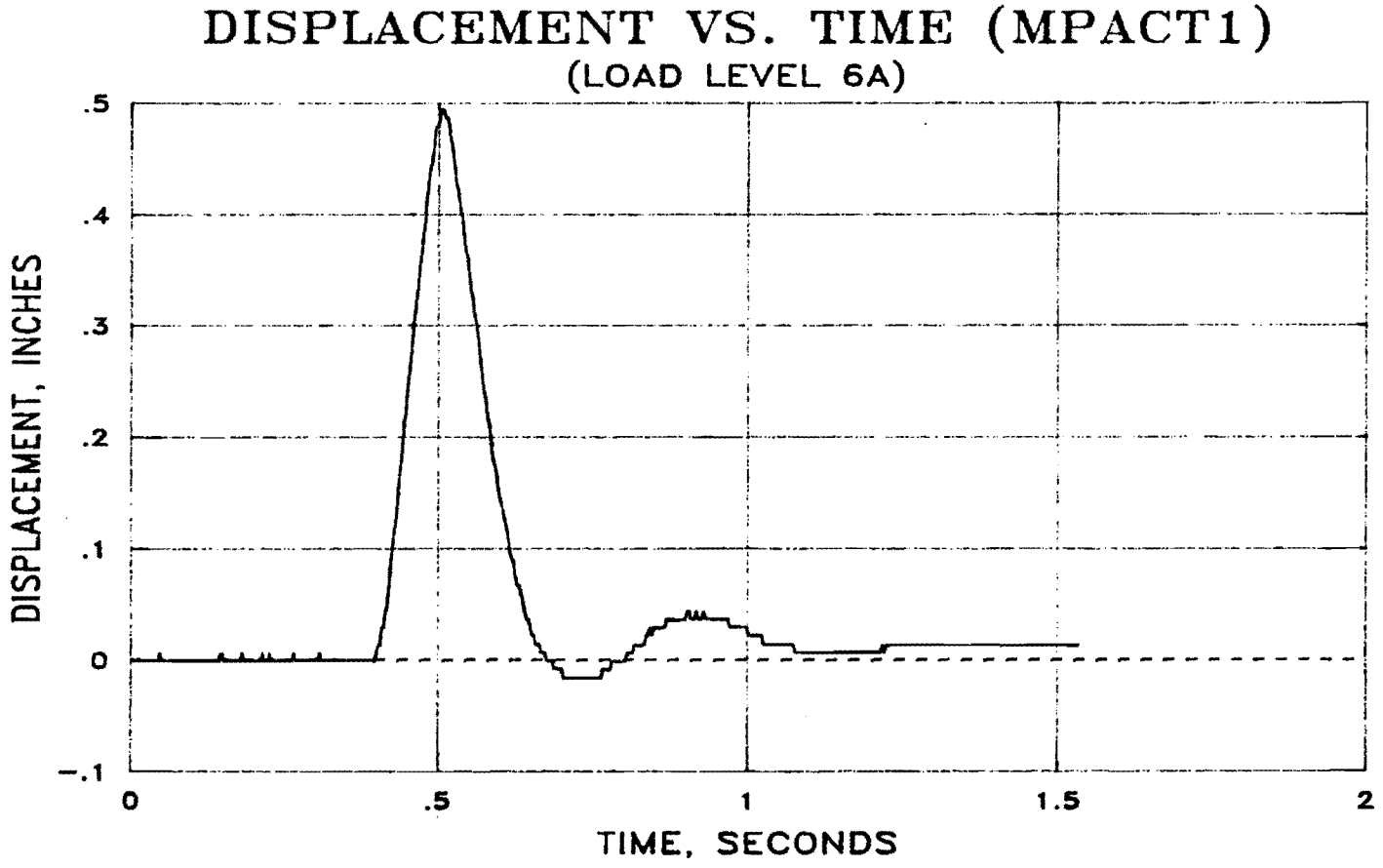

Fig. B.14 Displacement vs. time - load level 6A: MPACT1

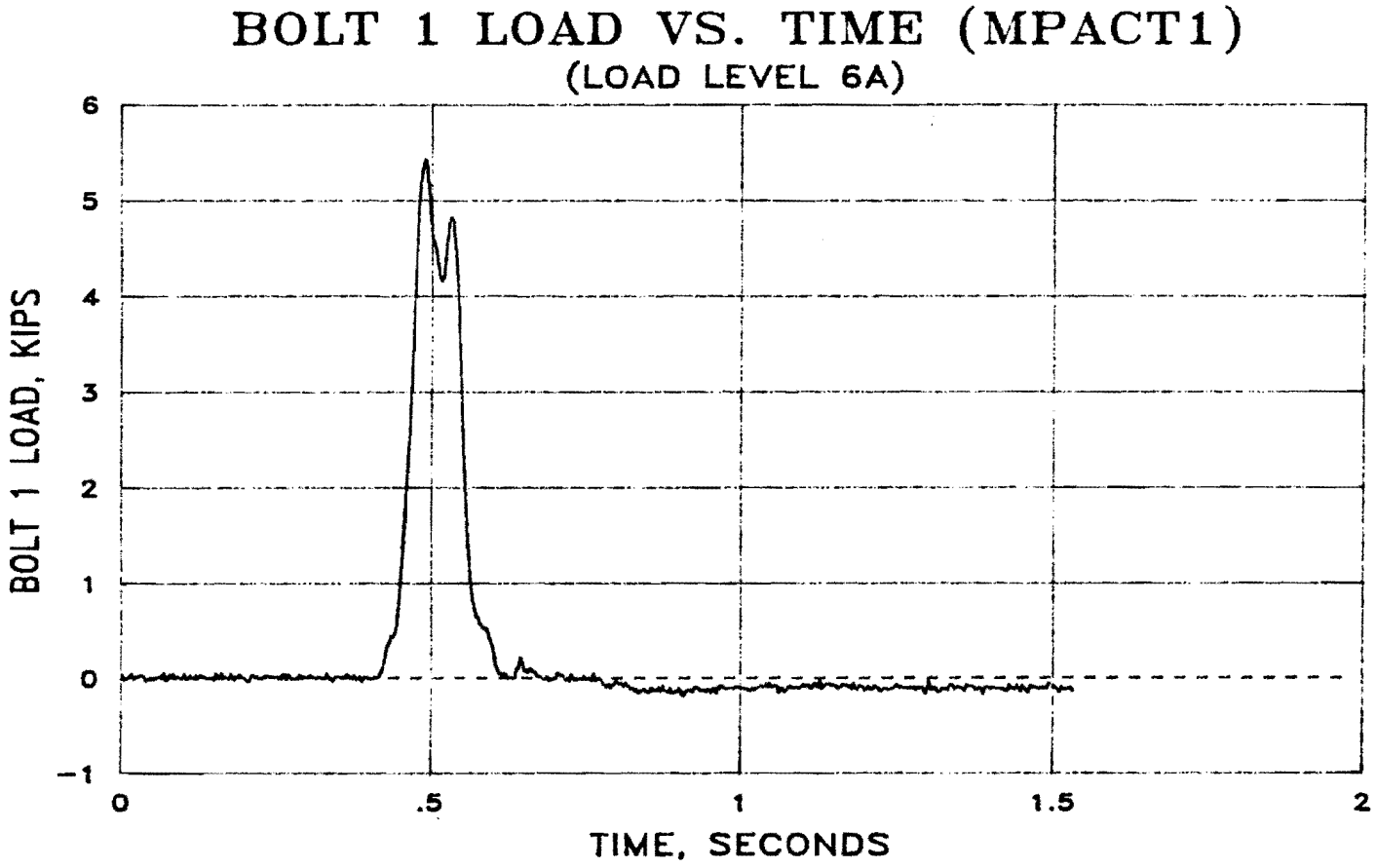

Fig. B.15 Bolt 1 load vs. time - load level 6A: MPACT1
(refer to Fig. 4.1 for anchor bolt locations)

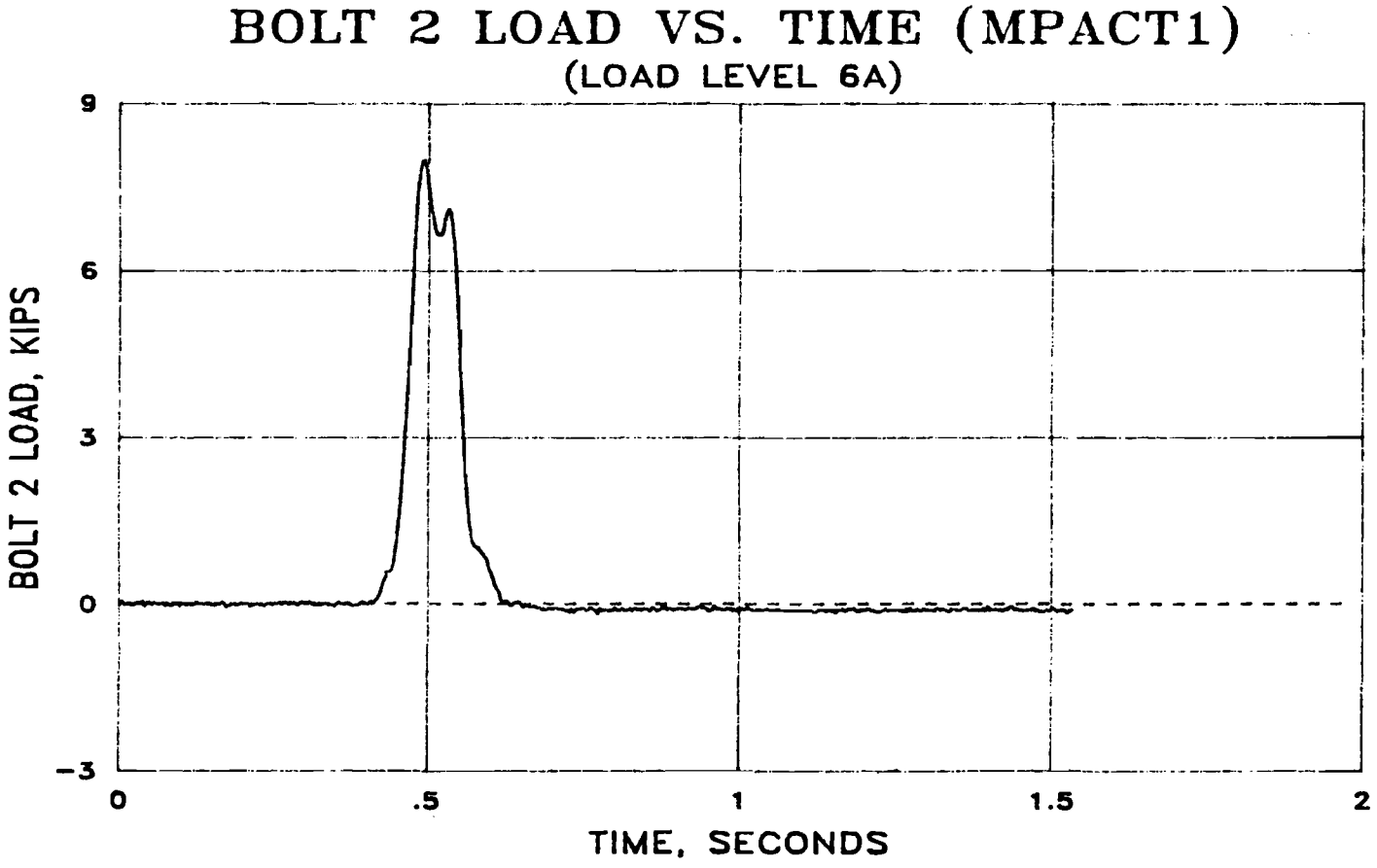

Fig. B.16 Bolt 2 load vs. time - load level 6A: MPACT1
(refer to Fig. 4.1 for anchor bolt locations)

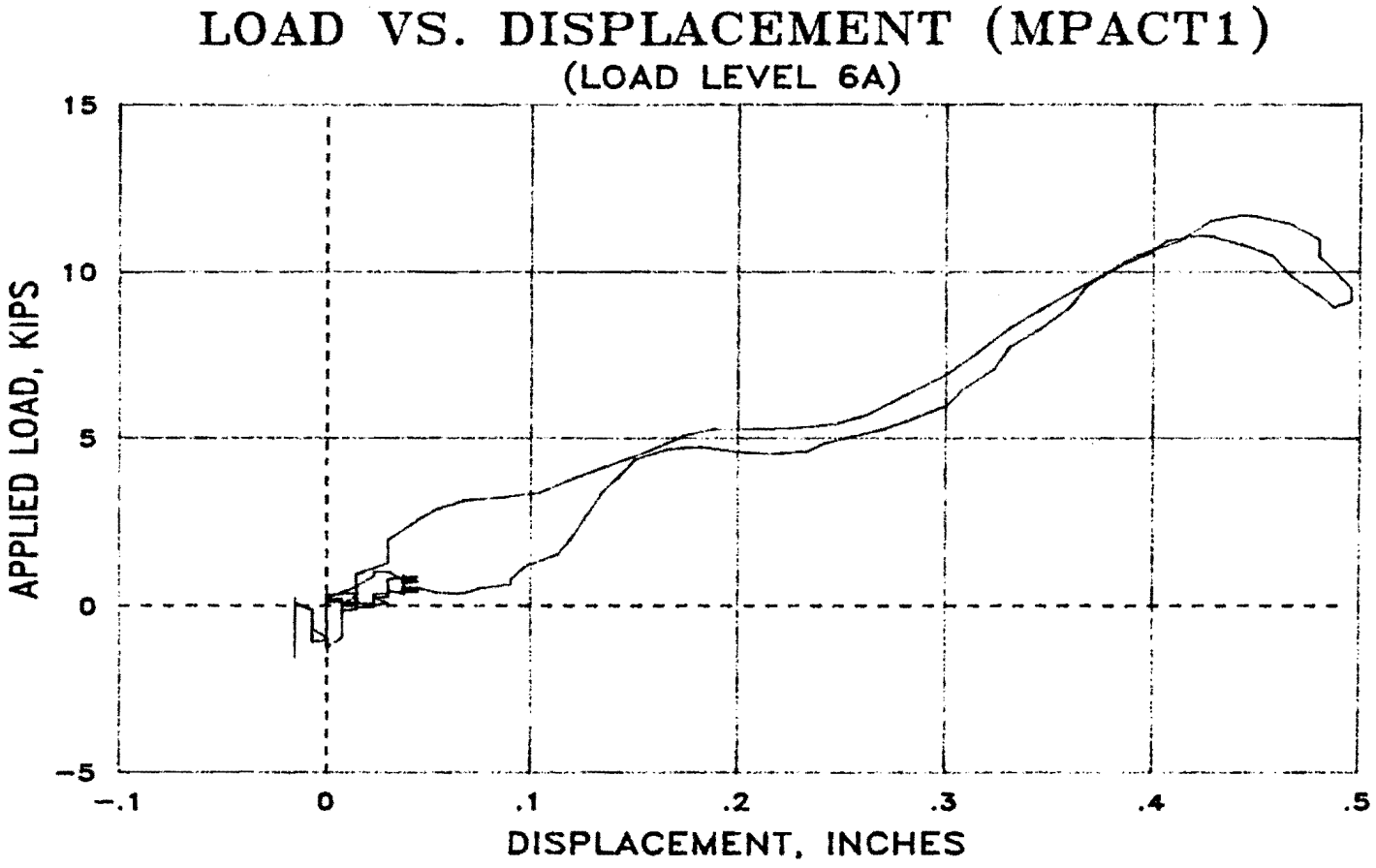

Fig. B.17 Load vs. displacement - load level 6A: MPACT1

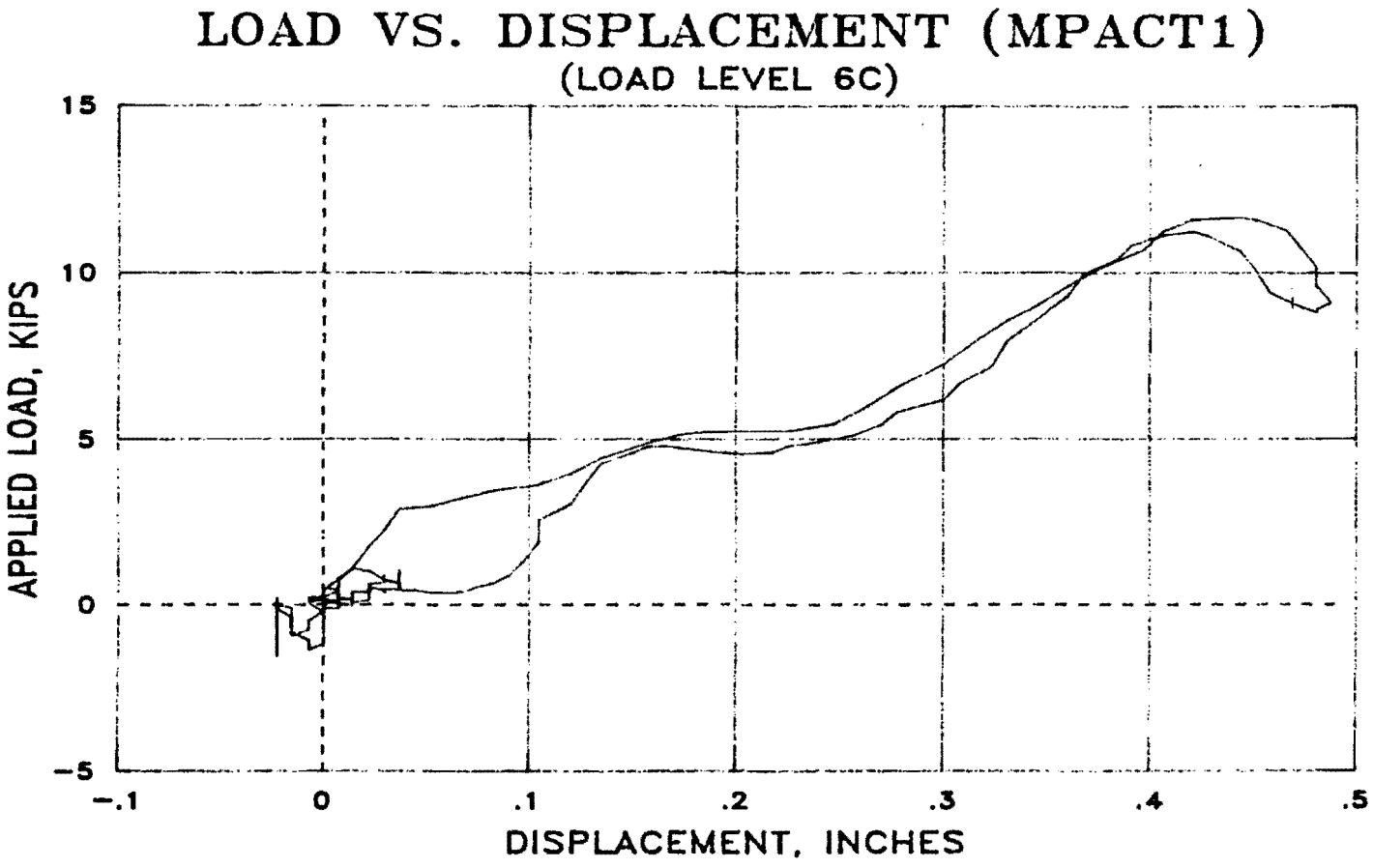

Fig. B.18 Load vs. displacement - load level 6C: MPACT1

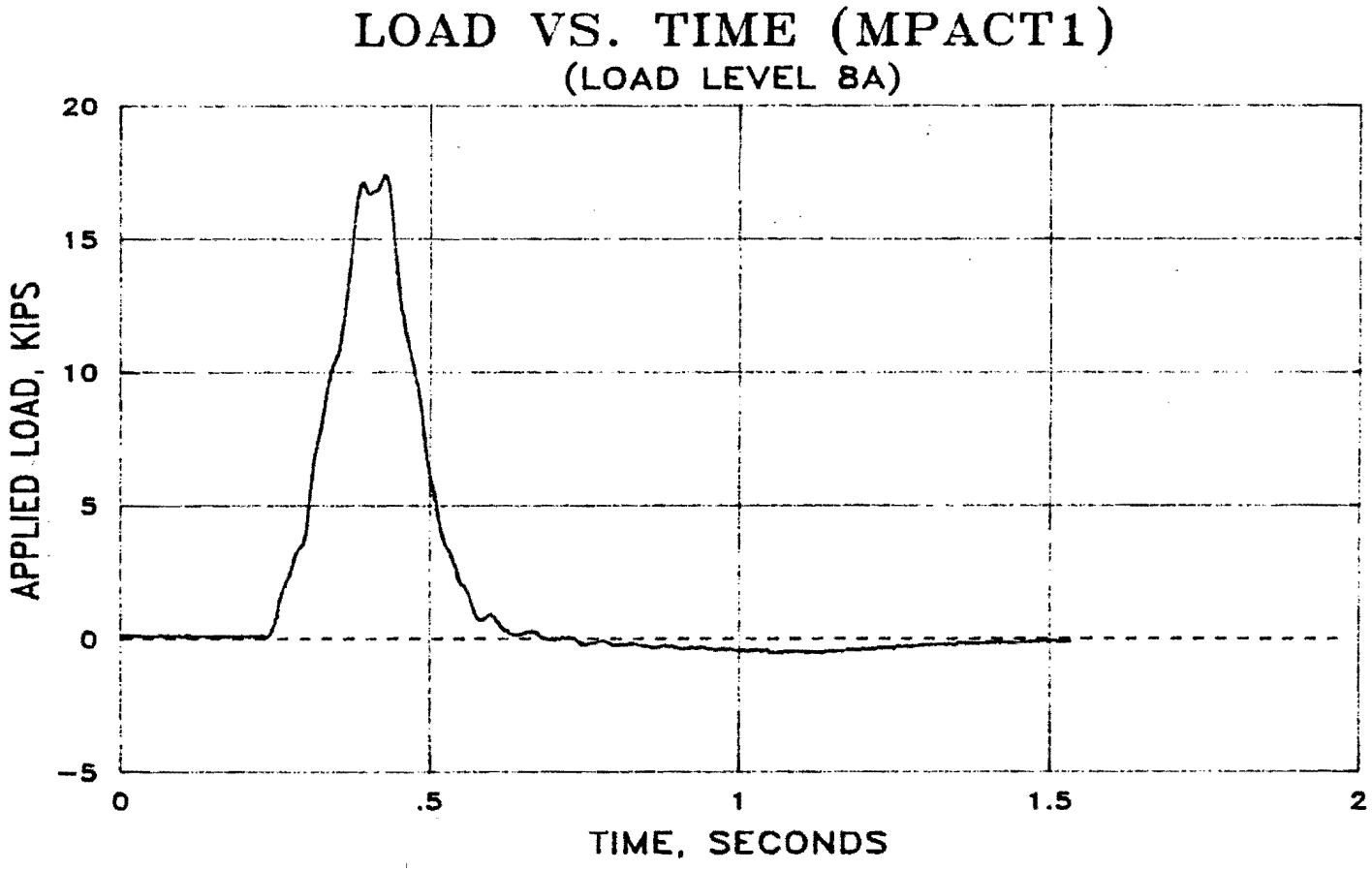

Fig. B.19 Load vs. time - load level 8A: MPACT1

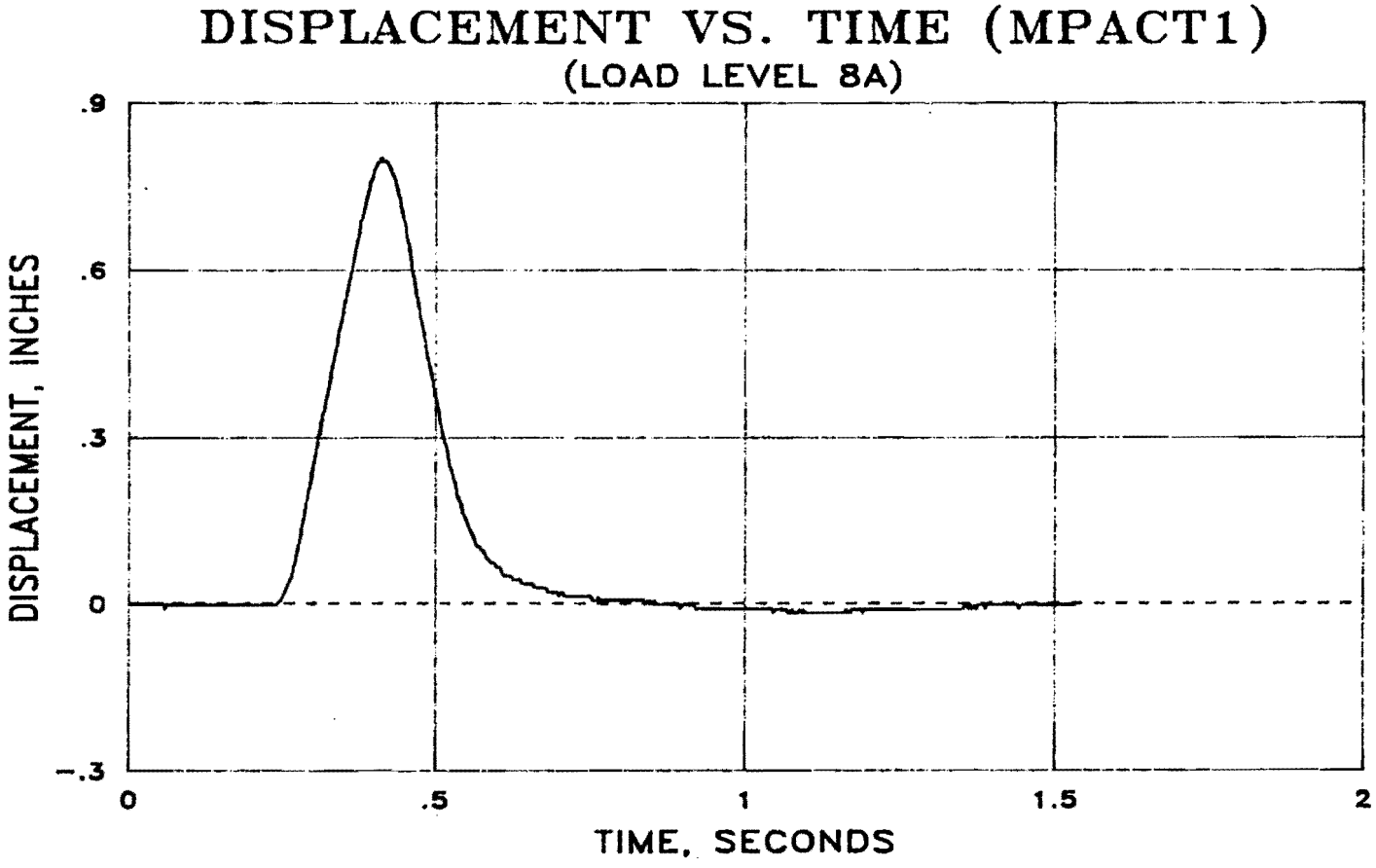

Fig. B.20 Displacement vs. time - load level 8A: MPACT1

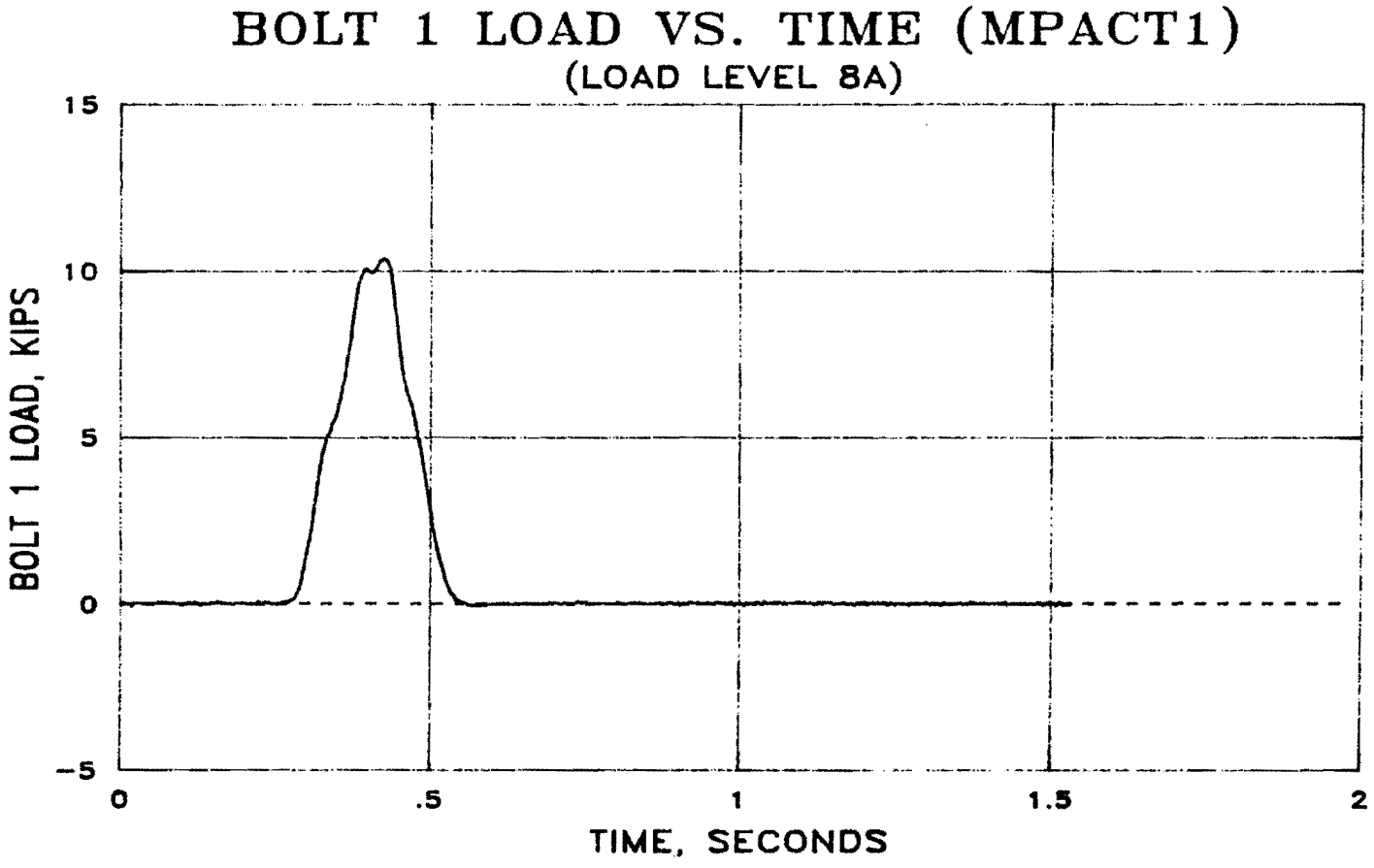

Fig. B.21 Bolt 1 load vs. time - load level 8A: MPACT1
(refer to Fig. 4.1 for anchor bolt locations)

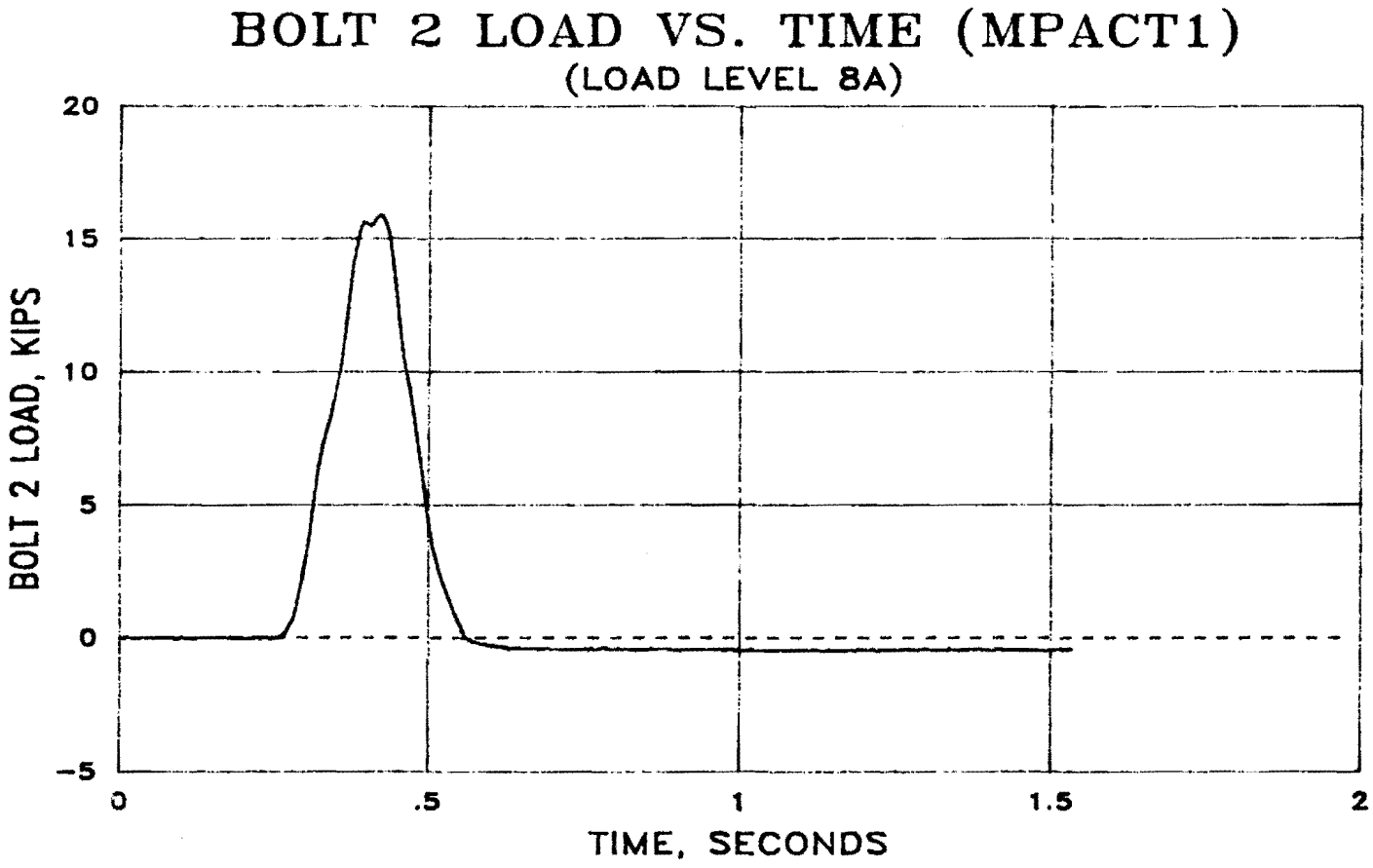

Fig. B.22 Bolt 2 load vs. time - load level 8A: MPACT1
(refer to Fig. 4.1 for anchor bolt locations)

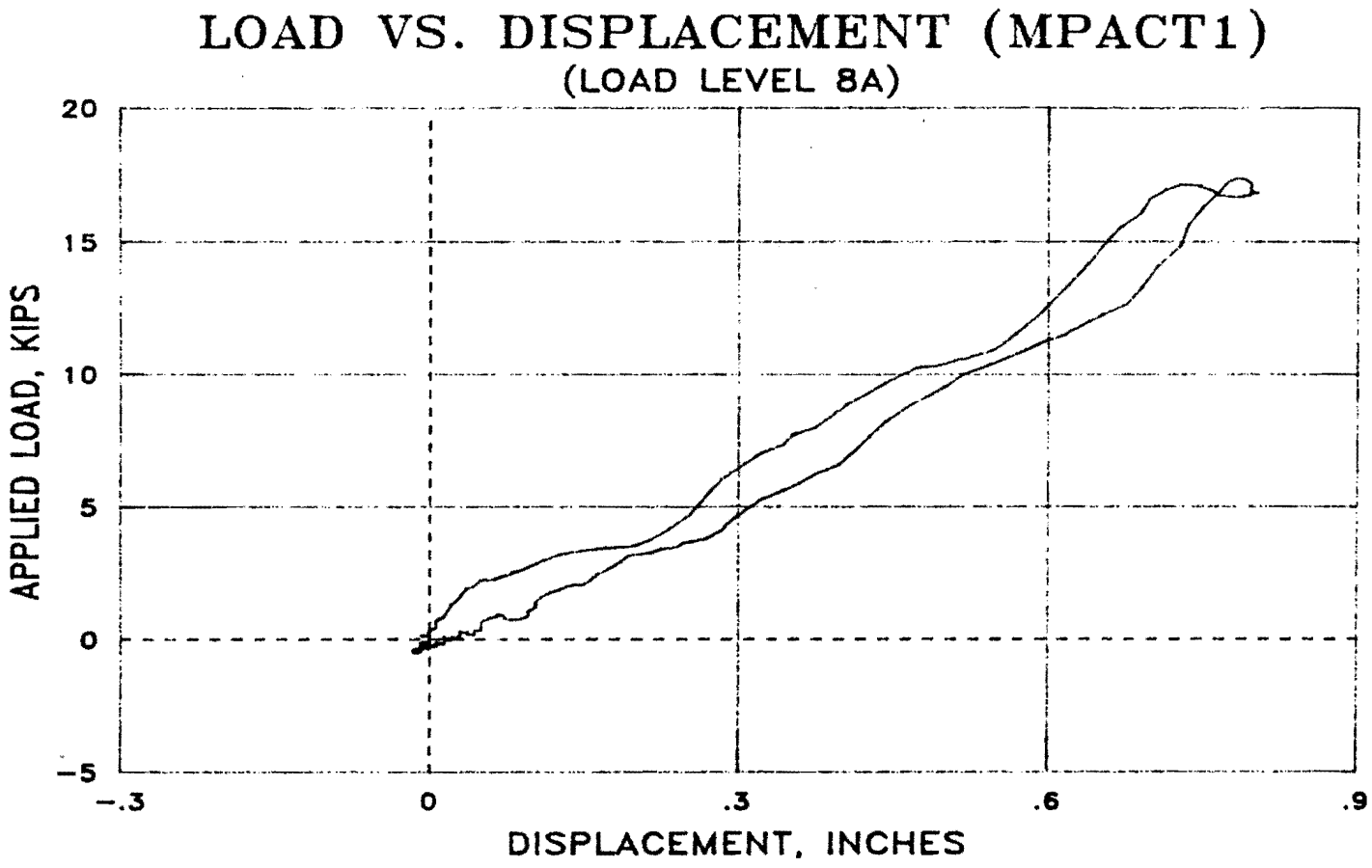

Fig. B.23 Load vs. displacement - load level 8A: MPACT1

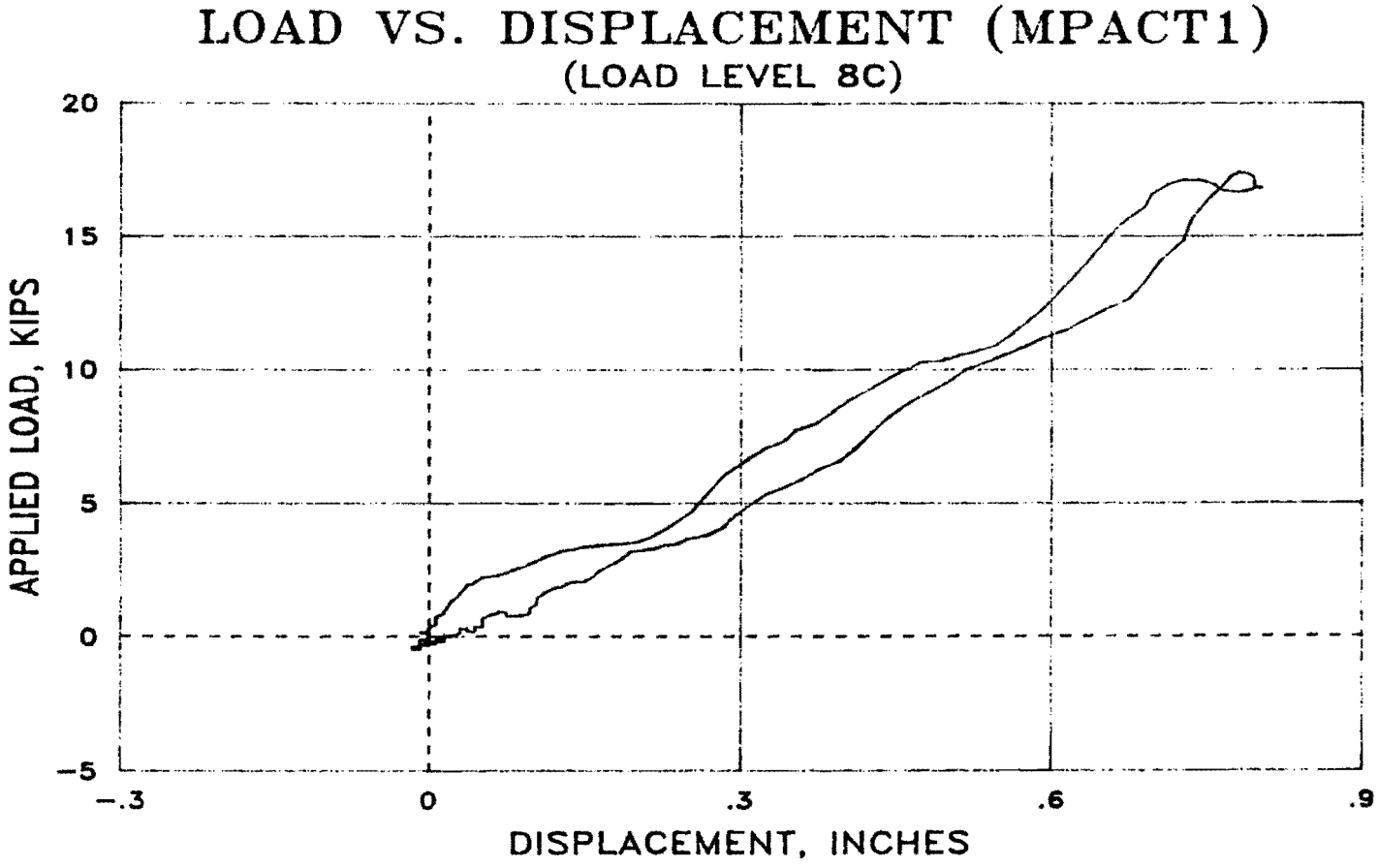

Fig. B.24 Load vs. displacement - load level 8C: MPACT1

REFERENCES

1. Arnold, A. and Hirsch, T.J., "Bridge Deck Designs for Railing Impacts," Research Report 295-IF, Texas Transportation Institute, Texas A&M University, Nov. 1983.

2. ACI Committee 318, Building Code Requirements for Reinforced Concrete (ACI 318-83), and "Commentary on Building Code Requirements for Reinforced Concrete (ACI 318-83), American Concrete Institute, Nov. 1983.

3. ACI Committee 349, "Proposed Addition to: Code Requirements for Nuclear Safety Related Structures (ACI 349-76)," and "Addition to Commentary on Code Requirements for Nuclear Safety Related Structures (ACI 349-76)," ACI Journal, Proceedings v. 75, No. 8, Aug. 1978, pp. 329-347.

4. Fisher, J.W., McMackin, P.J., and Slutter, R.G., "Headed Steel Anchor under Combined Loading," AISC Engineering Journal, v. 10, No. 2, April 1973.

5. Hawkins, N.M., Mitchell, D. and Roeder, C.W., "Moment Resisting Connections for Mixed Construction," AISC Engineering Journal, 1st Quarter, 1980.

6. Cannon, R.W., Godfrey, D.A. and Moreadith, F.L., "Guide to the Design of Anchor Bolts and Other Steel Embedments," and "Commentary on Guide to the Design of Anchor Bolts and Other Steel Embedments," Concrete International, July 1981.

7. Armstrong, K., Klingner, R.E., and Steves, M.A., "Response of Highway Barriers to Repeated Impact Loading: Steel Post Barriers," Research Report 382-1, Center for Transportation Research, The University of Texas at Austin, Nov. 1985.